Chapter 2

Synthesis, Characterization and application of Activated carbons derived from Palm Shells as adsorbents for Organic Pollutants

2.1 Introduction

Activated carbon (AC) is the carbon produced by activation of any carbonaceous material. Activation gives well-developed porous structure and surface chemistry to the carbon (Tang et al., 2012). ACs may be in powdered (PAC), granular (GAC), microcrystalline or in pelletized form. AC is widely used as an adsorbent for purification, separation and recovery processes, as a catalyst or as a catalyst support in the catalytic processes and as electrode materials in electrochemical devices and processes (Ozdemir et al., 2014). Activated carbons have been widely employed in adsorption due to its versatility, efficiency, and low operating costs. ACs have high adsorption capacity because of their internal structure which consists of a large number of interconnecting fine pores (Budinova et al., 2006). Ever since the discovery of AC by Raphael Von Ostrejko, known as the "Father of Activated Carbon", the demand for activated carbon (AC) is increasing day by day (Menéndez-Díaz and Martín-Gullón, 2006). In spite of its prolific use, AC remains expensive, since, the higher the quality of AC, the greater is its cost. Over the past few decades, commercially available AC is manufactured from non-renewable resources such as coal or petroleum based residues. However, in recent years, the increasing cost and scarcity of raw material has encouraged researchers to find other low cost alternatives from renewable resources. Wood has been the natural renewable material most often used globally to produce AC in a large scale contributing to global deforestation. This has motivated many researchers to investigate the use of agricultural waste materials as precursors as an alternative for the preparation of carbon (Selvaraju and Bakar, 2017).

Most of the activated carbons are produced by a two-stage process carbonization followed by activation. The first step is to enrich the carbon content and to create an initial porosity, the activation process then further helps in enhancing the pore structure (Singh et al., 2008). The two key activation methods that are generally used for activation of carbon include physical and chemical activation.

The physical activation methodology has been followed by many researchers. Physical activation involves carbonization of precursors (below 700 ˚C), followed by thermal activation in presence of oxidizing gas (steam, CO_2, air or their mixture) (Aworn et al., 2009; Cabal et al., 2009; Zhu et al., 2012).

In the conventional method, the heat source is located outside the sample, and the heat is transferred to the particles by convection, conduction and radiation mechanisms. So the temperature of the surface is higher than the interior of each particle (Hesas et al., 2013). Furthermore, there is a considerable risk of complete combustion of the carbon and less yield (Antonio-Cisneros and Elizalde-González, 2010). Microwave heating could overcome the thermal gradient problem for activated carbon preparation. Further it has the advantages of short time period, uniform temperature distribution, high heating rate, high yield and less energy consumption over conventional thermal methods (Cheng et al., 2016).

During steam activation, carbon reacts with steam (H_2O) to form CO, CO_2 and H_2 according the following equations (Chowdhury et al., 2013).

Char to CO and H_2

$$C + H_2O \rightarrow CO + H_2 \ldots . (Eq. 1)$$

Char to CO_2 and H_2

$$C + 2H_2O \rightarrow CO_2 + 2H_2 \ldots . (Eq. 2)$$

These reactions contribute to the development of pores in steam-gasified carbon.

Lua and Guo have developed activated carbon from palm shell by CO_2 activation process and studied its adsorption potential for SO_2 (Lua and Guo, 2001). Aworn et al, also investigated the CO_2 derived activated carbon from corncob for monoethylene glycol adsorption (Aworn et al., 2009). Another group, Sekirifa and co-workers have developed activated carbon from a variety of local date stones using CO_2 activation and investigated the adsorption of p-chlorophenol (Sekirifa et al., 2013). The ACs obtained was with surface area in the range of 502 to 604 m^2g^{-1}. Sahin and Saka have adopted a two step pretreatment of acorn shell during physical activation with H_2O– to prepare ACs having surface area and micropore volume of 1779 m^2g^{-1} and 0.927 cm^3g^{-1} respectively (Şahin and Saka, 2013).

Bouchelta et al, have prepared ACs from date stones by the use of steam activation and showed their potential for adsorption of gases (Bouchelta et al., 2008). Aworn et al., have studied the effect of steam and CO_2 during thermal activation using different agro-wastes like nut-shell, corncob, bagasse bottom ash, sawdust and rice-husks. They prepared microporous activated carbon from macadamia nut-shell by steam activation and from corn cob by CO_2 activation. They also prepared mesoporous activated carbon from bagasse bottom ash by steam activation and from sawdust fly ash by CO_2 activation. They observed that Bagasse bottom ash activated carbon and sawdust fly

ash activated carbon could be used to adsorb large molecular organic compounds due to the higher mesopore volume of these carbons than other materials including commercial activated carbon (Aworn et al., 2008). Bouchelta et al, investigated activation of date pits by pyrolysis under dry nitrogen and wet nitrogen conditions for preparation of ACs with high content of hydroxyl groups, good microporosity and high surface density of adsorption sites (Bouchelta et al., 2012) and applied the prepared ACs for Fe^{3+} and Cu^{2+} adsorption. In 2014, Jung and Kim developed ACs from oak using CO_2 activation by three different methods (N_2/CO_2 without cooling, N_2/CO_2 with cooling and direct CO_2). Their observation was that the activated carbons produced by the direct CO_2 method had a specific surface area of approximately $800 m^2 g^{-1}$ which appeared to be sufficiently high for commercial uses (Jung and Kim, 2014). Similarly, Sun and Jiang have developed ACs from rubber-seed shell by steam activation (Sun and Jiang, 2010). Tam and Antal, have used air activation to fabricate ACs from coconut shell (Tam and Antal, 1999).

ACs were also produced by CO_2 activation of date palm tree fronds (Shoaib et al, 2015), rubber wood sawdust (Mazlan et al., 2016), polyethyleneterephthalate (PET) wastes (Esfandiari et al., 2012), biomass (Kilpimaa et al., 2015) and sawdust of Algarroba (Matos et al., 2011). Zhu et al., treated anthracite by both CO_2 and steam activation for the production of ACs (Zhu et al., 2012). Steam activation of black liquor lignin (Fu et al., 2013) was carried out to produce ACs.

Table 2.1a presents the recent literature related to the development of ACs by physical activation.

Table 2.1a Literature review of Physical activation for ACs preparation

Physical Activation						
Sr. No.	Raw material	Activation	Surface area ($m^2.g^{-1}$)	Porevolume ($cm^3.g^{-1}$)	Pollutant	References
1	Palmshell	CO_2 activation	1366	-	SO_2	Lua and Guo, 2001
2	corncob	CO_2 activation	774	0.3959	Monoethylene glycol	Aworn et al., 2009
3	local date stones	CO_2 activation	604	0.34	p-Chlorophenol	Sekirifa et al., 2013
4	acorn shell	physical activation with H_2O–CO_2	1779	0.927	-	Şahin and Saka, 2013
5	date stones	steam activation	635	0.716	-	Bouchelta et al., 2008
6	Rice husk	steam activation, followed by 500°C thermal activation	74	0.0532	-	Aworn et al., 2008
	Macadamia nut-shell	steam activation, followed by 800°C thermal activation	844	0.4852		
		CO_2 activation, followed by 500°C thermal activation	487	0.2522		
	Corncob	steam activation, followed by 500°C thermal activation	675	0.359		
		CO_2 activation, followed by 500°C thermal activation	836	0.4258		
	Bagasse bottom	steam activation, followed by 300°C thermal activation	595	0.3953		
		CO_2 activation, followed by 300°C thermal activation	517	0.3059		
	Sawdust	steam activation, followed by 500°C thermal activation	613	4926		
		CO_2 activation, followed by 500°C thermal activation	816	0.5469		
7	Date pits	1 hr thermal treatment at 700˚C under 150 cm^3min^{-1} of nitrogen flow saturated with steam after passing through a water saturator heated at 80˚C.	1467	0.521	Cu^{2+} and Fe^{2+}	Bouchelta et al., 2012
	Date pits	1 hr thermal 700˚C under 100 cm^3/min of nitrogen flow	635	-		

8	Raw Oak	Intermediate pyrolysis, 800°C	249	0.1077	Proposed adsorbent for Gaseous pollutants	Jung and Kim, 2014
		N_2/ CO_2 without cooling 900 °C, 60 min	1126	0.4929		
		N_2/ CO_2 with cooling 800 °C, 60 min	724	0.2786		
		Direct CO_2 900 °C, 60 min	807	0.3349		
9	Rubber-seed shell	820 °C activation in presence of steam at 6 kg/h for 60 min	878	0.668	-	Sun and chun Jiang, 2010
		850 °C activation in presence of steam at 6 kg/h for 60 min	893	0.814		
		880 °C activation in presence of steam at 6 kg/h for 60 min	948	0.988		
10	Nut shell	air activation	1020	-	-	Tam and Antal, 1999
	Coconut shell	air activation	1028	-	-	
11	palm tree fronds	30 min activation dwell time 50 cm3 min-1 CO2 flow rate at 850 °C	1094	0.4382	-	Shoaib and Al-Swaidan, 2015
12	Rubber Wood Sawdust	CO_2 activation at 740 °C for 60 min	465	0.239	Benzene, Trichloroethylene	Mazlan et al., 2016
13	PET waste	carbonization temperature 800°C, carbonization time 60 min, activation temperature 975 °C, activation time 240 min, heating rate of carbonization and activation 10 k/min, flow rate N_2 200 ml/min and CO_2 100 ml/min.	790.3	0.4313	Phenol	Esfandiari et al., 2012
14	Carbon residue byproduct from biogasification of wood)	800 °C activation for 3 h in presence of CO_2	590	0.335	Phospahates and Nitrates	Kilpimaa et al., 2015
15	sawdust of Algarroba	Pyrolysis under CO_2 and activation at 900 °C	590	0.231	-	Matos et al., 2011
16	anthracite	CO_2 activation at 71.3 ml/min at 850 °C	1379	0.684	Sulphur dioxide	Zhu et al., 2012
		steam activation at 74.3 ml/min at 850 °C	1333	0.698		
17	black liquor lignin	Carbonization at 450 °C, 60 min, activation temperature 750 °C in presence of steam for 40 min	288.79	0.249	Methylene blue	Fu et al., 2013

Chemical activation (wet oxidation) process involves impregnation of the precursor material with reactive chemicals such as $ZnCl_2$, H_2SO_4, NaOH, KOH, K_2CO_3, $FeCl_3$, K_2HPO_4 or H_3PO_4, followed by thermal activation., the dehydrating and or oxidising effect of the used activating agents hinders the formation of tar which leads to higher AC yield and to lower activation temperatures than those reported for physical activation (Demiral et al., 2011; Marsh and Rodriguez-Reinoso, 2006; Zhu et al., 2007). Among the numerous dehydrating agents, sulphuric acid in particular is the widely used chemical agent in the preparation of activated carbon (Olivares-Marín et al., 2012). Chemical activation by H_2SO_4 improves the pore development in the carbon structure (Singh et al., 2008). Sulphuric acid treatment oxidises cellulose, hemicellulose and some lignin into organic materials with higher oxygen content (Guo et al., 2005).

$$\left[C_nH_xO_y\right] + H_2SO_4 \rightarrow H_2O + S(\text{element}) + \left[C_nH_xO_{y+3}\right] \ldots . (\text{Eq. } 3)$$

Such rich oxygen content further facilitates pyrolysis by providing more oxygen internally that initiates the thermo-chemical process at a lower temperature. In the process of preparation of the ACs using KOH (Li et al., 2016; Muniandy et al., 2014), this agent is expected to become a form of metallic potassium during the carbonization and inert gas flow. The reaction of KOH and carbon occurs as given in equation 4: (Marsh and Rodriguez-Reinoso, 2006).

$$6KOH + 2C \rightarrow 2K + 3H_2 + 2K_2CO_3 \ \ldots . (\text{Eq. } 4)$$

This mechanism proposes the formation of K_2CO_3 during the pyrolysis process and ultimately during interactions results in K, K_2O, CO and CO_2. Therefore, the pores are large and are external. Another proposed mechanism for the reaction of KOH and raw materials during pyrolysis suggests that the reaction between KOH and the carbon precursor can result in the formation of functional groups such as OK by using the oxygen of the alkali salt:

$$K_2O + C \rightarrow COK + K \ \ldots . (\text{Eq. } 5)$$

Activation has also been performed using K_2CO_3 (Tsubouchi et al., 2016).

Chemical activation by phosphoric acid as well as phosphate sources is also well known. H_3PO_4 is effective in producing mesopores, resulting in higher pore volumes and pore diameters of the carbons. Further H_3PO_4 is environment friendly and the resulting carbon can be easily recovered in high yields after just washing with water (Romero-Anaya et al., 2012; Wang et al., 2010).

Activation of Paulownia wood using H_3PO_4 was carried out by Yorgun and Yildiz, resulting in ACs with effective surface area and micropore volume of 2806-2300 m^2g^{-1}, and 1.746-1.196 cm^3g^{-1} respectively (Yorgun and Yıldız, 2015). Cherry Stones a lignocellulosic material was treated with H_3PO_4 by Olivares-Marı´n and co-workers to form ACs with surface area 1688 m^2g^{-1} and applied the ACs for the removal of liquid phase pollutants, gas storage, or vapor capture (Olivares-Marín et al., 2007). Shamsuddin and co-workers have developed ACs from kenaf core fiber by activation with H_3PO_4 with high percentage of carbon and low percentage of ash (Shamsuddin et al., 2016). Sun et al., treated biomass wastes viz. “Arundo donax Linn” and “pomelo peel”- kind of wetland plants with 85 weight % H_3PO_4, followed by thermal treatment at 450 ˚C. (Sun et al., 2016) and used the developed ACs for the removal of ciprofloxacin fluoroquinolone antibiotics. Similarly reedy grass leaves were activated by H_3PO_4 for ACs formation (Xu et al., 2014). Apart from phosphoric acid activation, $H_4P_2O_7$ activation to Arundo donax Linn (Sun et al., 2013), guanidine phosphate activation to lotus stalk (Liu et al., 2013b), trimethyl phosphate and tributyl phosphate activation to lotus stalk (Liu et al., 2013a) and ammonium polyphosphate activation to Enteromorpha, a renewable biomass (Gao Y. et al., 2016) was studied for the preparation of ACs.

Another important and widely employed chemical agent used for chemical activation is zinc chloride. Yang and Qiu have prepared ACs from herb residues using vacuum and traditional $ZnCl_2$ chemical activation with high methylene blue and iodine absorption values (Yang and Qiu, 2011). Activation of chestnut shell by $ZnCl_2$ chemical activation, followed by Ag-coating was done by Altintig and Kirkil and demonstrated their probable use for dyes and drug adsorption (Altintig and Kirkil, 2016). ACs for the removal of methylene blue and phenol was developed from fox nutshell using $ZnCl_2$ chemical activation (Kumar and Jena, 2016). $ZnCl_2$ chemical activation was also done by Angin and co-workers onto safflower seed press cake to form ACs from biochar which showed good methylene blue adsorption properties (Angin et al., 2013). GAC was prepared from oil palm shell by $ZnCl_2$ and physical activation and was investigated for its methane adsorption potential (Arami-Niya et al., 2010).

Other less popular chemical activating agents include NaOH (Muniandy et al., 2014), Organic acids (formic acid, oxalic acid, and sulfamic acid) (Tang et al., 2016),

persulphate (Karthikeyan and Sivakumar, 2012; Moreno-Castilla et al., 1995), MgO (Shahkarami et al., 2016) and $KMnO_4$ (Foroushani et al., 2016).

The modification of the surface chemistry of carbons is considered as a promising and attractive way toward new applications of carbon in many fields (Bhatnagar et al., 2013). Modification of AC involves oxidation and further grafting of functional groups (e.g., carboxylic acid, amine, etc.) and molecules such as cyclodextrin onto the AC surface by chemical, electrochemical, plasma and/or microwave method. Oxidation can be attained by chemical modification (Moreno-Castilla et al., 1995; Otake and Jenkins, 1993), air oxidation (Otake and Jenkins, 1993; Silva et al., 2001), electrochemical oxidation (Delamar et al., 1997), and plasma (García et al., 1998) or ozone treatment (Belyaeva et al., 2011). Table 2.1b, c and d present the literature for the development of ACs by chemical activation using H_3PO_4, $ZnCl_2$ and other chemical activation agents.

Table 2.1b Literature review of ACs preparation (H_3PO_4 treatment)

Chemical Activation (H_3PO_4 treatment)						
Sr. No.	Raw material	Activation	Surface area ($m^2.g^{-1}$)	Porevolume ($cm^3.g^{-1}$)	Pollutant	References
1	Paulownia wood	H_3PO_4 (4:1, w/w of wood) impregnation at 85°C, followed by carbonization at 400 °C	2806	1.746	-	Yorgun and Yıldız, 2015
2	Cherry Stones	First treatment with H_2SO_4, followed by impregnation with H_3PO_4 and finally carbonization at 500°C	1688	1.82	Probability studies related to the removal of substances from the liquid phase, gas storage, or vapour capture	Olivares-Marín et al., 2007
3	kenaf core fiber	carbonization at 400°C, H_3PO_4 impregnation (4:1 of material), pyrolysis at 500°C	299.02	0.12	-	Shamsuddin et al., 2016
4	Arundo donax Linn	Impregnation with 85% H_3PO_4 (2.5:1 of precursors, 10 h), followed by activation at 450°C for 60 min	675	0.312	ciprofloxacin	Sun et al., 2016
	Pomelo peel		1252	1.33		
5	Reedy grass leaves	Impregnation with 60% H_3PO_4 (0.88:1 of precursors, 4 h), followed by activation at 500°C for 2 h	1474	0.56	-	Xu et al., 2014
6	Arundo donax Linn	Impregnation with $H_4P_2O_7$ (0.4-2.5 ratio of precursors, 1 h at 400 °C-600°C)	1443.4	1.333	oxytetracycline	Sun et al., 2013
7	Lotus stalk	Impregnation with 85% H_3PO_4 (1.96:1 of precursors, 105 °C, 9 h), followed by activation at 450°C for 1 h	1503	1.08	Cd(II)	Liu et al., 2013b
		Impregnation with Guanidine Phosphate (1.96:1 of precursors, 105°C, 9 h), followed by activation at 450°C for 1 h	491	0.25		
8	Lotus stalk	Impregnation with Trimethyl phosphate (10 g of precursors/0.2 mol, 105°C, 9 h), followed by activation at 450°C for 1 h	345	0.166	Pb(II)	Liu et al., 2013a
		Impregnation with Trimethyl phosphate (10 g of precursors/0.2 mol, 105°C, 9 h), followed by activation at 450°C for 1 h	541	0.266		
9	Enteromorpha	5 g of Precursor was mixed with (50%) Ammonium phosphate solution, heated at	882	1.051	Acid brilliant scarlet dye	Gao Y. et al., 2016

		800 °C for 1 h				

Table 2.1c Literature review of Chemical activation for ACs preparation ($ZnCl_2$ treatment)

Chemical Activation ($ZnCl_2$ treatment)						
Sr. No.	Raw material	Activation	Surface area ($m^2.g^{-1}$)	Porevolume ($cm^3.g^{-1}$)	Pollutant	References
1	Herb Residues	Impregnated at 1.225:1 ($ZnCl_2$:Precursor), for 48 hr h, followed by heating at 474 °C, under vacuum for 60 min	1551	0.814	Methylene Blue	Yang and Qiu, 2011
2	chestnut shell	Impregnated at 1:1 ($ZnCl_2$:Precursor), for 24 hr h, followed by heating at 700°C, under vacuum for 1 h	926.7	0.496	Probabilty for treatment of Dye and Raw materail for drugs in wastwater	Altintig and Kirkil, 2016
	chestnut shell-ACs	ACs from $ZnCl_2$ activation was mixed with sodium alginate, followed by mixing with 0.01 M biammine silver nitrate solution (25% Aq ammonia+$AgNO_3$, pH-9 using HNO_3), Whole mass was mixed for 4 h, washed with ethanol, Dryed.	541.6	0.418		
3	Fox nutshell	10 g of dried precursor was mixed with 150 ml $ZnCl_2$ (20 g $ZnCl_2$), 24 h impregnation, followed by activation at 600°C for 60 min	2869	1.96	Methylene Blue , Phenol	Kumar and Jena, 2016
4	Biochar of safflower seed	Impregnated at 4:1 ($ZnCl_2$:Precursor), for 24 hr h, at 80 °C followed by heating at 900°C, under vacuum for 60 min	801.5	0.393	Methylene Blue	Angın et al., 2013
5	Oil palm shell	Impregnated at 0.65:1 ($ZnCl_2$:Precursor), for 24 hr h, at 85°C followed by heating at 500°C, under vacuum for 60 min, Followed by activation at 900°C in presence of N_2 stream	1671.6	0.99	Methane	Arami-Niya et al., 2010

Table 2.1d Literature review of Chemical activation for ACs preparation (other chemical activating agents)

Chemical Activation (Miscellaneous)						
Sr. No.	Raw material	Activation	Surface area ($m^2.g^{-1}$)	Porevolume ($cm^3.g^{-1}$)	Pollutant	References
1	Rice husks Waste (RHW)	RHW first treated with HNO_3 and NaOH respectively for the removal of metal impurities and Si impurity respectively to form RH char which was impregnated with 40% NaOH (1:2 of RHW:NaOH) for 30 min, 15 min Sonication, followed by activation at 750 °C for 60 min under N_2.	594.9	0.34	-	Muniandy et al., 2014
		RHW first treated with HNO_3 and NaOH respectively for the removal of metal impurities and Si impurity respectively to Form RH char which was impregnated with 40% KOH (1:4 of RHW:KOH) for 30 min, 15 min sonication, followed by activation at 750°C for 60 min under N_2.	1394	0.837		
2	Lignin	Lignin was mixed with urea and K_2CO_3 in ratio of 1:1:2 (Lignin: Urea : K_2CO_3), Acitvated in transperant glass furnace under ultra pure He gas (99.995% pure) at 800-900°C for 1 h	3300-3400	2.0-2.3	-	Tsubouchi et al., 2016
3	Commercial Granular activated Carbon (AC)	AC was first purified by water washing followed by DI water washing to form AC-A. AC-A was impregnated with 0.5 M Oxalate dihydrate for 1 h, washed with DI water and dried till constant weight to form AC-OA	788.07	0.424	Acetone, Isopropanol	Tang et al., 2016
		AC was first purified by water washing followed by DI water washing to Form AC-A. AC-A was impregnated with 0.5 M formic Acid for 1 h, washed with DI water and dried till constant weight to form AC-FA	813.8	0.433		
		AC was first purified by water washing followed by DI water washing to form AC-A. AC-A was impregnated with 0.5 M sulphamic acid for 1 h, washed with DI water and dried till constant weight to form AC-FA	699.87	0.367		
4	Almond shell	Pyrolysed under N_2 flow at 1173 K, and steam activated at 1123 K, The sample was further treated to oxidise with $(NH_4)_2S_2O_8$. in H_2SO_4 at 298 K for 48 h	1060	0.258	-	Moreno-Castilla et al., 1995

5	Feronia limonia (wood apple)shell	Material was treated in (1:1.8:0.1) of (material: H_2SO_4: $(NH_4)_2S_2O_8$, at 80^oC for 12 hrs. followed by $NaHCO_3$ neutralization and water washing and drying. Thermal activation was done at 750°C for 30 min.,washed with water and dried at 110°C for 6 h	309.61	0.206	Probability of its potential for both organic and inorganic effluent removal	Karthikeyan and Sivakumar, 2012
6	White wood	White wood was heated at 700°C under N_2, followed by under steam for 1.4 h to form bichar. Biochar was treated with 100 ml 3 wt% of MgO solution for 15 h, followed by calcination at 325°C for 4 h and drying at 100°C for 4 h.	760	0.56	CO2	Shahkarami et al., 2016
7	Pistachio shells	3 g of material was soaked in to $KMnO_4$ bath (9.9 wt%). followed by drying at 80 C for 20 min in oven. The sample was then stabilized under O_2 atmosphere followed by pyrolysis under N_2 atmosphere at 650°C	145	0.54	-	Foroushani et al., 2016
8	cherry stones	7 g of material was first given Physical activation treatment, by heating at 600°C for 2 h under N_2 stream to form char. 25 g of char was treated with 100 mL of Conc. H_2SO_4 for 7 days, followed by washing with water and drying at 120°C over night.	145	0.37	-	Olivares-Marín et al., 2012

Another approach that is now a days' more popular is **combinations of different activation techniques**. The combination of the chemical and physical activation processes was employed to produce activated carbons (Valizadeh et al., 2016). Different combination of chemical and activation techniques investigated by researchers is summarised in Table 2.1e.

Thermo-chemical techniques- Hydrothermal carbonization (HTC) is a thermo-chemical process used to produce a coal-like product (C~ 40-50 wt %) from an aqueous suspension of raw biomass or carbohydrates using an autoclave under moderate temperatures (180-250 °C) and self generated pressures. Subcritical water is used for the conversion of biomass to carbonaceous product. Generally a carbonization temperature of 150–350 °C is typically employed. Hydrothermal carbonization results in efficient hydrolysis generating high amount of oxygenated functional groups and dehydration of biomass making it an effective precursor for the production of chemically activated carbon (Jain et al., 2016). The resulting carbons have a regular morphology and a rich surface chemistry. HTC presents some advantages in comparison with classical pyrolysis, regarding its simplicity, low cost production, energy and CO_2 efficiency. It can be classified as a “green” process since it takes place without the use of organic solvents, surfactants or catalysts, uses moderate temperatures and has minimum CO_2 emissions. Jain et al. have critically reviewed the production of activated carbon from hydrochars (Jain et al., 2016). Mechanochemical activation of the precursors has been recently investigated for fabrication of activated carbon. Tzvetkov et al. has developed activated horse chest nut shell mechanochemically by ball milling in the presence of K_2CO_3 (Tzvetkov et al., 2016).

In all cases researchers found effective results in terms of high carbon content, high micropore volume and high specific surface area and hence high effectiveness as an adsorbent when combination of chemical and physical activation techniques were employed.

Table 2.1e Literature review of combination of Physical and Chemical Activation

Combination of Physical and Chemical activation						
Sr. No.	Raw material	Activation	Surface area ($m^2.g^{-1}$)	Porevolume ($cm^3.g^{-1}$)	Pollutant	References
1	sugarcane bagasse	Material was treated with Conc. H_2SO_4 in (4:3) ratio for 30 min followed by low temperature activation at 160 ° C, for 2 h. Char was water washed and dried. The char was heated at 900 C for 15 h under nitrogen	1433	0.91	Methane	Valix et al., 2004
2	cherry stones	Drying, followed by pyrolysis at 500 °C , followed by Chemical activation using KOH at 700 °C for 30 min in presence of CO_2	1324	0.74	H_2S,	Nowicki et al., 2015
3	leather waste	4 g of waste was impregnated with $H_4P_2O_7$ (1:1), heated at 105 ° C for 1 h, followed by heating at 450 ° C. washed and dried	494.78	0.331	Methylene blue	Kong et al., 2013
4	Residual fluid petroleum coke (RPC)	20 g of RPC was treated with 60% KOH, stirred for 2 h, followed by drying at 120 °C, First activation was done at 300 °C under N_2 for 1 h followed by further activation at 500 °C. Product was washed with 0.1 M HCl followed by water washing and drying at 110 °C for 12 h.	692.4	0.264	catalytic oxidation H_2S	Rambabu et al., 2013

Bhatnagar et al., have reviewed the different activation and modification treatments given to carbons and their precursors along with their relative advantages and disadvantages (Bhatnagar et al., 2013). The two methods have their own advantages. For example, physical activation has an advantage over chemical activation because it avoids the incorporation of additives/impurities coming from the activating agents. Microporous as well as ultramicroporous carbons are usually formed by this method. On the other hand chemical activation is more popular to prepare ACs owing to the simplicity, lower temperature, shorter activation time, higher yield, and good development of the porous structure (Guo and Rockstraw, 2007). The activating agents dissolve the cellulosic components of the precursor (Campbell et al., 2012) promoting the formation of cross links (Örkün et al., 2012). Chemical activation results in higher surface area (Budinova et al., 2006), creates well developed micro porosities (Hirunpraditkoon et al., 2011), and reduction of mineral matter content as compared to physical activation techniques (Lillo-Ródenas et al., 2003). The carbons formed by this method generally have wider micropores and higher pore volumes making them comparatively more suitable for liquid phase adsorption.

However, there are also some disadvantages in chemical activation such as, washing is needed to remove the impurities coming from the activating agents and also the corrosiveness properties of the agents (Lozano-Castelló et al., 2001).

"The adsorption property of ACs is mainly due to its porous structure".

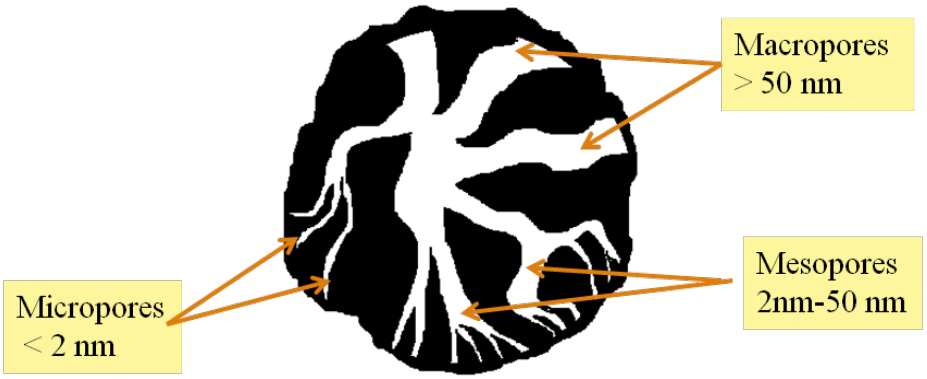

Figure 2.1 porosity distributions in ACs

The distribution of pore size is shown in Figure 2.1, wherein the pores are classified as macropores (diameter > 50 nm), mesopores (diameter 2–50 nm) and micropores (diameter < 2 nm). Carbon materials with high proportion of mesoporous structures are critical for applications as adsorbents for bulk molecules, catalyst support, gas storage and biomedical engineering. Since mesopores can serve as main transport arteries for large molecules and alleviate pore obstruction (Gao Y. et al., 2016; Liou, 2010), the presence of mesopores is necessary for maintaining a fast kinetic adsorption rate and enhancing the adsorption capacities of carbon materials. Hence, an increasing interest has been triggered for the production of mesoporous carbon materials. The macropores in ACs skeleton serve like transport pores, enabling the molecules of the adsorbate to go through the smaller pores to reach to the still smaller pores situated in inside area of ACs thus influencing the rate of diffusion into the meso and micropores (Song et al., 2015). Mesopores serve as passage between macro and micropores allowing rapid access to the micropores and also provide sites for capillary condensation to take place. Thus it is more important to develop ACs with large proportion of mesopores in order to increase the effectiveness of adsorption. The adsorption finally occurs in the micropores or mesopores depending on the size of the adsorbate. The present investigation involved the preparation of ACs using agrowaste palm shell as precursor by employing a combination of acid, chemical (oxidising agent persulfate), thermal and steam activation techniques.

Persulfate activation of carbon has been less explored (Vasu, 2008) though it has been used for regeneration of spent carbon (Huling et al., 2011; Liang et al., 2009). With proper activation, persulfate can generate highly reactive radical species, mainly sulfate radical (E^0 = 2.7 v) and hydroxyl radical (E^0 = 2.8 v) that can oxidize most

recalcitrant organic contaminants (Peng L. et al., 2016; Tsitonaki et al., 2010). Recently, persulfate salts ($S_2O_8^{2-}$), have emerged as a promising alternative owing to its advantages over other common oxidation reagents. Persulfate has high aqueous solubility with a strong redox potential (E^0 = 2.01 V). Also, persulfate is relatively stable at ambient temperature and can be activated by heat, UV light (Eq. (6)), transition metals (Eq. (7)), alkali and H_2O_2 to generate stronger oxidant, sulfate radicals (SO_4^-, E^0 = 2.60 V), which have a long life time. Thermally activated persulfate oxidation is a very promising and attractive advanced oxidation technology to decompose contaminants of concern (Gao H. et al., 2016) Chemical activation (Chiu et al., 2013; Huling et al., 2009, 2007) and thermal activation (Ghauch et al., 2012; Huang et al., 2002; Waldemer et al., 2007) of persulfate for GAC regeneration have been reported.

$$S_2O_8^{2-} + \frac{\text{heat}}{\text{UV}} \rightarrow 2SO_4^{-\cdot} \quad \ldots.(\text{Eq. } 6)$$

$$SO_4^{-\cdot} + H_2O \rightarrow .OH + SO_4^{2-} + H^+ \ldots.(\text{Eq. } 7)$$

Persulfate-driven oxidation reactions produce acid (Hutson et al., 2012). Under acidic conditions (pH < 3), activated persulfate can effectively and rapidly oxidize the surface groups like -C=O, -C≡N, -C-H to –COOH, -$CONH_2$ (An et al., 2015).

It was thus decided to treat powdered palm shell, an agrowaste obtained from coastal Andhra Pradesh with sulfuric acid to facilitate the modification of celluloses and lignin thus altering the pyrolysis and combustion characteristics of PSP to produce APSP. Thermal activation followed by steam activation (SPAC) or steam activation followed by thermal activation (PSAC) onto APSP was further investigated. Thermal treatment was for effective lignin and char decomposition at a higher temperature. Steam activation was done prior to thermal activation or afterwards to facilitate pore development. The effect of persulfate sulfuric acid mixture to facilitate rapid oxidation of the functional groups present in PSP was also investigated (PSAC).

The activated carbons thus prepared from PSP were -

PAC Acid treatment of Palm Shell Powder (PSP) followed by Thermal activation

SPAC Steam activation of PAC (14 kg pressure in autoclave)

PSAC Acid treatment of PSP followed by Steam activation (14 kg pressure in autoclave) followed by thermal activation

PCAC Chemical activation of PSP using sulphuric acid and persulfate followed by thermal activation

The prepared activated carbons were characterized by different techniques and the potential of the activated carbons as adsorbents for model pollutants such as 4CP, 4NP, DNP, TNP, BPA and MnCP was investigated. The properties of the selected model pollutants are given in Table 2.2.

Table 2.2 Properties of selected model pollutants

Sr. No.	Pollutant	Structure	M.W. ($g.mol^{-1}$)	pKa Value	Log k_{OW}
1	4-Chlorophenol (4-CP)	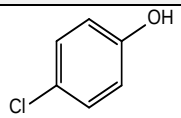	128.56	9.41	2.39
2	4-Nitrophenol (4-NP)	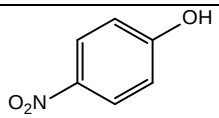	139.11	7.16	1.91
3	2,4-Dinitrophenol (DNP)	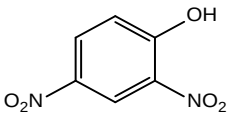	184.11	4.09	1.67
4	2,4,6-Trinitrophenol (TNP)	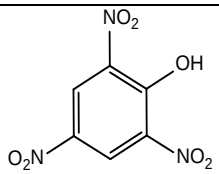	229.10	0.4	1.6
5	Bisphenol-A (BPA)	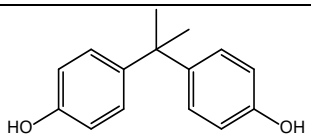	228.29	9.6-10.2	3.32
6	Monocrotophos (MnCP)	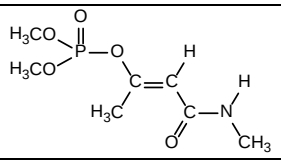	223.16	4.4	-0.20

(Part-A)

Synthesis and characterization of Activated carbons from palm shell

2.2 Experimental

2.2.1 Chemicals and reagents

Sulphuric Acid (H_2SO_4, LR, Spectrochem, India), Sodium bicarbonate (Na_2CO_3, AR, Spectrochem, India), NaOH (Sodium Hydroxide, LR, Spectrochem, India), HCl (Hydrochloric Acid, AR, Spectrochem, India), deionised water.

2.2.2 Pretreatment and modification of Palm shell powder

Palm shells obtained from the coastal areas of Andhra Pradesh, India; were washed, sun dried for 24 h, further dried at 110 °C in a hot air oven and ground using a jaw crusher to obtain PSP of 40 mesh size. PSP was then subjected to different combinations of thermal, chemical and physical treatments. The following flow chart (Figure2.2) shows the methodologies adopted for conversion of PSP to activated carbons (ACs).

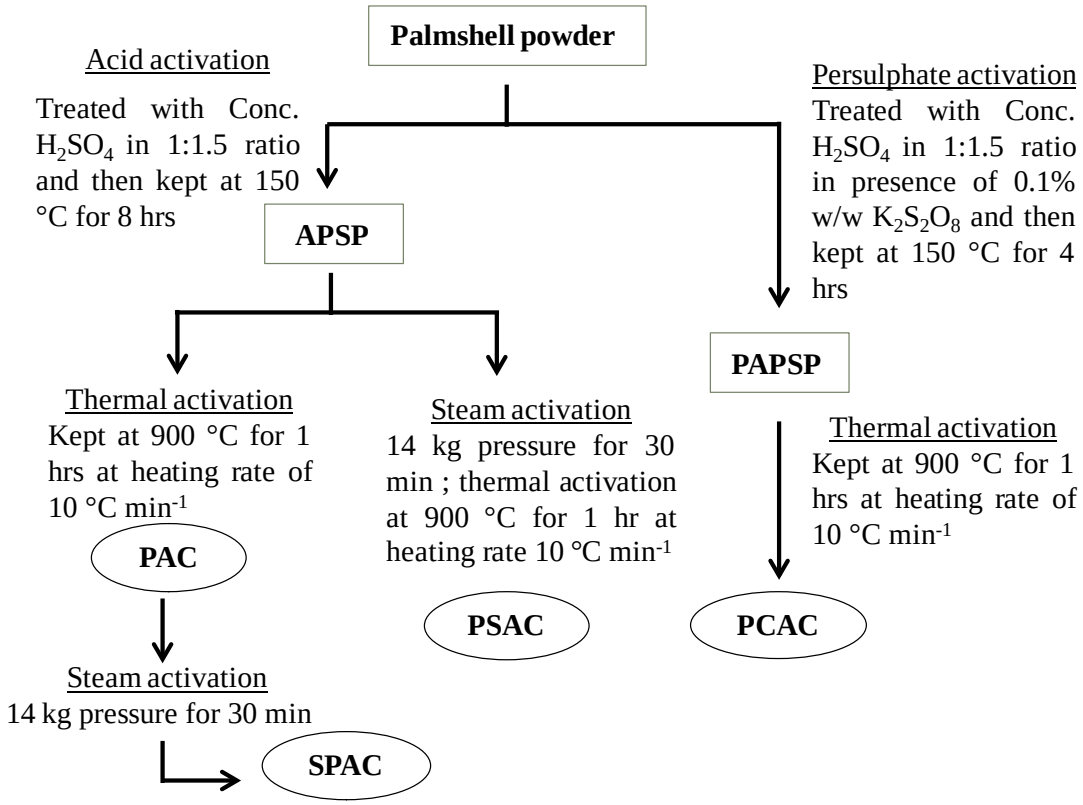

Figure 2.2 Modification of Palm shell powder to activated carbon

For drying of PSP to less than 120 ˚C, a hot air oven was used. The thermal activation was carried out in a box type muffle furnace. The heating rate was kept 10˚C min^{-1} in all the cases. The maximum heating temperature of muffle furnace was 1100 ˚C.

2.2.3 Method of analysis and Characterizations of activated carbons

The prepared activated carbons were analyzed for their physical properties like moisture content, solubility in water, solubility in acid (0.25 N HCl), Bulk density and chemical properties like pH, Iodine value, Ion exchange capacity, Boehm titration and zeta-potential.

Moisture content was determined by heating a known weight of AC sample in a hot air oven at 105±5°C for 4 hrs. Heating, cooling and weighing were repeated till constant weight was obtained with less than 5 mg variation. The final weight and initial weight difference gave moisture content value.

Solubility in water/ acid (0.25 N HCl) was determined by taking 10 g of AC sample in a one liter beaker and boiling by adding 300 mL water or acid. The solution was digested for 30 min followed by filtration. The filtrate was collected in a 100 mL volumetric flask. The AC residue was washed several times and washing was collected along with filtrate. The solution was allowed to cool and after cooling it was made up to 100 mL with water. Exactly 50 mL aliquot was evaporated to almost dryness in an evaporating dish, and kept in an oven at 105±5°C for 4 hrs, cooled and weighed till constant weight was obtained. The weight of residue in dish gave solubility in water or acid.

Bulk density was determined by using a previously weighed 100 mL graduated cylinder. The AC sample was filled to 50 mL and weight of cylinder was again noted. Bulk density was determined by dividing the difference in weight by volume i.e. 50.

pH was measured by heating 10 g of AC sample in 300 mL water to boiling with constant stirring. The solution was then digested for 30 min. The solution was filtered, cooled to room temperature and pH of the resulting solution was measured.

Iodine value gives information about surface area and porosity .In a typical procedure 0.2 g of AC under study was equilibrated with 40 mL of iodine solution for 4 min, followed by filtration through whatman 42 filter paper. A 10 mL aliquot of the filtrate was immediately titrated against standardised 0.1 N sodium thiosulphate solution.

$$\text{Iodine value} = (\text{blank reading} - \text{sample reading}) \times \text{Conversion factor} \quad \ldots . (\text{Eq. } 8)$$

$$\text{Conversion factor} = \frac{\text{Eq. weight of Iodine (127)} \times 40 \times \text{N}_{\text{Na}_2\text{S}_2\text{O}_3}}{\text{wt. of carbon} \times 10} \quad \ldots . (\text{Eq. 9})$$

Ion exchange capacity (IEC) generally gives idea about exchangeable protons of the adsorbent. For determination of IEC, 0.5 g of AC sample was equilibrated with 100 mL of 0.25 M sodium sulphate in a glass stoppered conical flask on thermally regulated shaker for 5 h. The content was filtered and was titrated against 0.1 N NaOH solution using phenolphthalein as an indicator. The IEC was calculated using equation 10.

$$\text{Ion Exchange capacity } \left(\frac{\text{meq}}{\text{g}}\right) = \frac{\text{aW}}{\text{V}} \quad \ldots . (\text{Eq. 10})$$

Where, a=Normality of NaOH, V=volume of NaOH, W=Weight of ACs in g.

Boehm titration was originally developed in 1994 by Hans Peter Boehm for quantifying the oxygen-containing surface functional groups of carbon blacks (Boehm, 1994). The titration's underlying principle is that strong acids and bases can react with all respective bases and acids, whereas weak acids will only donate protons to the conjugate bases of acids with higher pKa values.

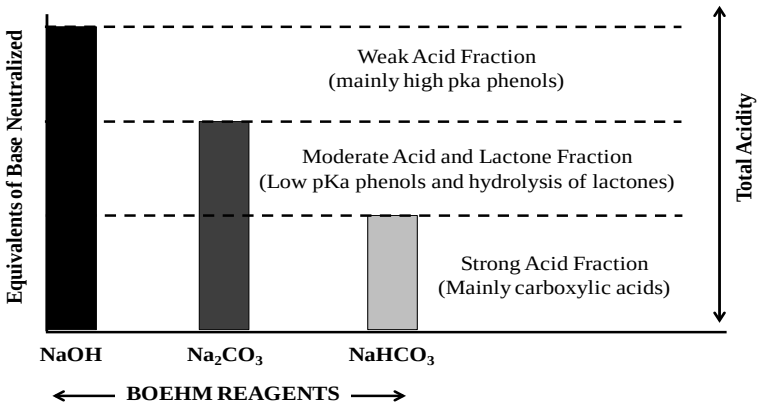

Figure 2.3 Boehm reagents for different regions

The conventional procedure followed was equilibration of 0.05 M solutions of $NaHCO_3$, Na_2CO_3, and NaOH with separate samples of ACs (Figure 2.3). The ACs were then separated from the solution, and the solution was acidified and boiled to remove CO_2. Finally, aliquots of the resulting solutions were back-titrated with NaOH to determine the quantity of the reactants that had been reacted during equilibration. Basic sites were determined by reacting ACs with 0.05 M HCl and solution was filtered and titrated against NaOH.

$$n_{COOH} = \text{Carboxylic sites} = n_{FG,NaHCO_3} \ldots . (\text{Eq. } 11)$$

$$n_{Lactonic} = \text{Lactonic sites} = n_{FG,Na_2CO_3} - n_{FG,NaHCO_3} \ldots . (\text{Eq. } 12)$$

$$n_{Phenolic} = \text{Phenolic sites} = n_{FG,NaOH} - n_{FG,Na_2CO_3} \ldots . (\text{Eq. } 13)$$

$$n_{FG,NaHCO_3} = \frac{eq_{NaHCO_3,Initial} - eq_{NaHCO_3,Final}}{m_{AC}} \ldots . (\text{Eq. } 14)$$

$$n_{FG,Na_2CO_3} = \frac{eq_{Na_2CO_3,Initial} - eq_{Na_2CO_3,Final}}{m_{AC}} \ldots . (\text{Eq. } 15)$$

$$n_{FG,NaOH} = \frac{eq_{NaOH,Initial} - eq_{NaOH,Final}}{m_{AC}} \ldots . (\text{Eq. } 16)$$

$$n_{FG,HCl} = \frac{eq_{HCl,Initial} - eq_{HCl,Final}}{m_{AC}} \ldots . (\text{Eq. } 17)$$

Zeta Potential is a very important parameter for characterisation of the surface of activated carbon. The chemical affinity between adsorbent and adsorbate can be assessed by investigating the zeta potential of the adsorbent over a wide pH range. Zeta potential of suspension of ACs in water in pH range of 1.0-11.0 was measured using particle size analyser equipped with zeta potential measurement (90Plus/BI-MAS model, Brookhaven Instruments Corporation).

- ***Fourier Transform Infrared Spectroscopy (FT-IR)***

FT-IR was used to determine the vibrational frequencies of the functional groups in the adsorbents. The spectra were collected using Perkin-Elmer RX1 model in the wavenumber range 400 to 4000 cm^{-1}. Specimens of samples were first mixed with KBr at an appropriate ratio of 1/100 and then ground in an agate mortar. The resulting mixture was pressed at 10 tons for 5 min. for the preparation of pellets. The spectra were recorded after sixteen scans and 8 cm^{-1} resolution. The background obtained from the scan of pure KBr was automatically subtracted from the sample spectra.

- ***Scanning Electron Microscopy (SEM)***

The topography of PSP and ACs was visualized by using a SEM microscope (LEO 1430 VP). Sample was mounted onto metal holders using a conducting substrate. The

SEM analysis enables the direct observation of the changes in the surface microstructures of the adsorbent due to the chemical surface modifications and the elemental composition.

- ***BET Surface area (BET)***

The surface area measurements ($m^2 \cdot g^{-1}$) of ACs were performed using Micromeritics ASAP 2020 operated at 77 K with the help of BET equation.

$$\frac{1}{v\left[\left(\frac{P_0}{P}\right)-1\right]} = \frac{C-1}{v_m C}\left(\frac{P}{P_0}\right) + \frac{1}{v_m C} \quad \ldots.(Eq.18)$$

P and P_0 are the equilibrium and the saturation pressure of adsorbates at the temperature of adsorption, v is the adsorbed gas quantity (for example, in volume units), and v_m is the monolayer adsorbed gas quantity; C is the BET constant, which is expressed by:

$$C = exp\left(\frac{E_1 - E_L}{RT}\right) \ldots.(Eq.19)$$

E_1 is the heat of adsorption for the first layer, and E_L is that for the second and higher layers and is equal to the heat of liquefaction.

- ***X-ray diffraction Analysis (XRD)***

X-ray diffraction (XRD) measurements were performed on a Philips X'pert MPD X-ray diffractometer to determine the phases formed in ACs. The X-ray source used was Philips high intensity ceramic sealed tube (3kW) with Wavelength Cu-Kα radiation (1.5405 Å).

- ***Thermogravimetric Analysis (TGA)***

The temperature effect on the prepared activated carbons was investigated by thermogravimetric analysis using TGA/DTA-6300 EXSTAR, INKARP at a heating rate of $10°C \cdot min^{-1}$. Sample of approximately 100mg was heated from 30°C to 1000°C in a platinum pan. The instrument was purged with nitrogen at a flow rate of 10.00 $mL \cdot min^{-1}$ during analysis.

- ***X-ray Photoelectron Spectroscopy (XPS)***

X-ray Photoelectron Spectroscopy (XPS) also known as Electron Spectroscopy for Chemical Analysis (ESCA) was used to obtain quantitative and chemical state information about the surface of the ACs under study. XPS measurements were performed using a photoelectron spectrometer equipped with an Omicron electron analyzer model EA 125D using Al Kα radiation. The average depth of analysis is

approximately 5 nm. All spectra are presented charge balanced and energy referenced to C 1s at 284.6 eV. Chemical states of O, N and C species were determined from the charge corrected hi-resolution scans.

2.3 Results and discussion

2.3.1 Physical and chemical properties of ACs

The physical and chemical characteristics of activated carbons under study SPAC, PSAC, PCAC and PAC are listed in Table 2.3

Table 2.3 Physical and chemical properties of ACs

Sample	Moisture (%)	Solubility (%)		Bulk density ($g.ml^{-1}$)	pH	Iodine number $mg.g^{-1}$	IEC ($meq.g^{-1}$)
		Water	HCl				
PSP	8.37	3.44	4.04	0.351	6.0	146.82	0.004
SPAC	8.65	0.49	0.88	0.669	4.9	1476.27	0.067
PSAC	12.52	0.46	0.85	0.560	5.9	1889.14	0.100
PCAC	8.85	0.44	0.82	0.605	6.8	1737.69	0.200
PAC	8.26	0.51	0.93	0.704	8.3	1828.98	0.067

The activated carbons had pH in the range of 4.9-8.3 indicating the potential applicability of the prepared ACs as adsorbents for waste water treatment. The moisture content of the ACs was due to their contact with atmosphere after the activation process. Low solubility in both water (<0.52 %) and acid (0.25 N HCl) (<1.0 %) support their stability even in acidic conditions. The bulk density indicates the applicability of the adsorbents in columns. The ion exchange capacity was highest in PSAC and PCAC followed by SPAC, PAC and PSP, suggesting that after activation the amount of exchangeable protons had increased. The iodine value was in the order PSAC>PAC>PCAC>SPAC indicating significant porosity of the ACs.

Table 2.4 Surface functional group study using Boehm titration

Sample	$Eq.gm^{-1}.L^{-1}$			
	Phenol	Lactone	Carboxylic	Basic
SPAC	0.8802	2.1516	1.7604	0.1860
PSAC	1.3692	2.3472	3.5208	1.7271
PCAC	3.9120	1.9560	3.3252	0.4545
PAC	0.9780	1.9560	2.1516	0.1860

Table 2.4 summarizes the results of Boehm titrations. Carboxylic groups increased on thermal activation followed by steam activation (PSAC) rather than steam activation

followed by thermal activation (SPAC). Carbon prepared by persulfate treatment followed by thermal activation also had reasonable amount of carboxylic groups (PCAC). On the other hand lactonic groups were less in PAC as well as PCAC and had increased on activation of PAC to SPAC and PSAC. Phenolic groups decreased as PAC was converted to SPAC while the number of phenolic groups increased in PSAC and PCAC. Basic sites (quinone and carbonyl) decreased in the order PSAC<PCAC<PAC<SPAC. The total oxygen containing functional groups are in the order of PCAC<PSAC<PAC<SPAC. Acidic functional groups were found to be higher than basic functional groups in all the activated carbons under study.

2.3.2 FTIR analysis of ACs

The obtained FTIR spectrum of ACs revealed major peaks at 3365, 3150 cm^{-1} which can be assigned to O-H stretching vibrations, and ~1567 cm^{-1} can be attributed to C=C double bonds in quinone like structures/large aromatic skeletons in activated carbons derived from agricultural wastes. The peaks at ~2000 and 1500 cm^{-1} indicated carboxylic acid and/or a lactone group, and 1123 cm^{-1} can be attributed to C-O stretching peak in heterocyclic rings and -OH bending mode of alcoholic, phenolic and carboxylic groups (Jaouadi et al., 2016; Juan and Ke-Qiang, 2009; Shin et al., 1997). The band at 2325 cm^{-1} is the C≡C stretching vibrations in alkyne groups (Saka, 2012).

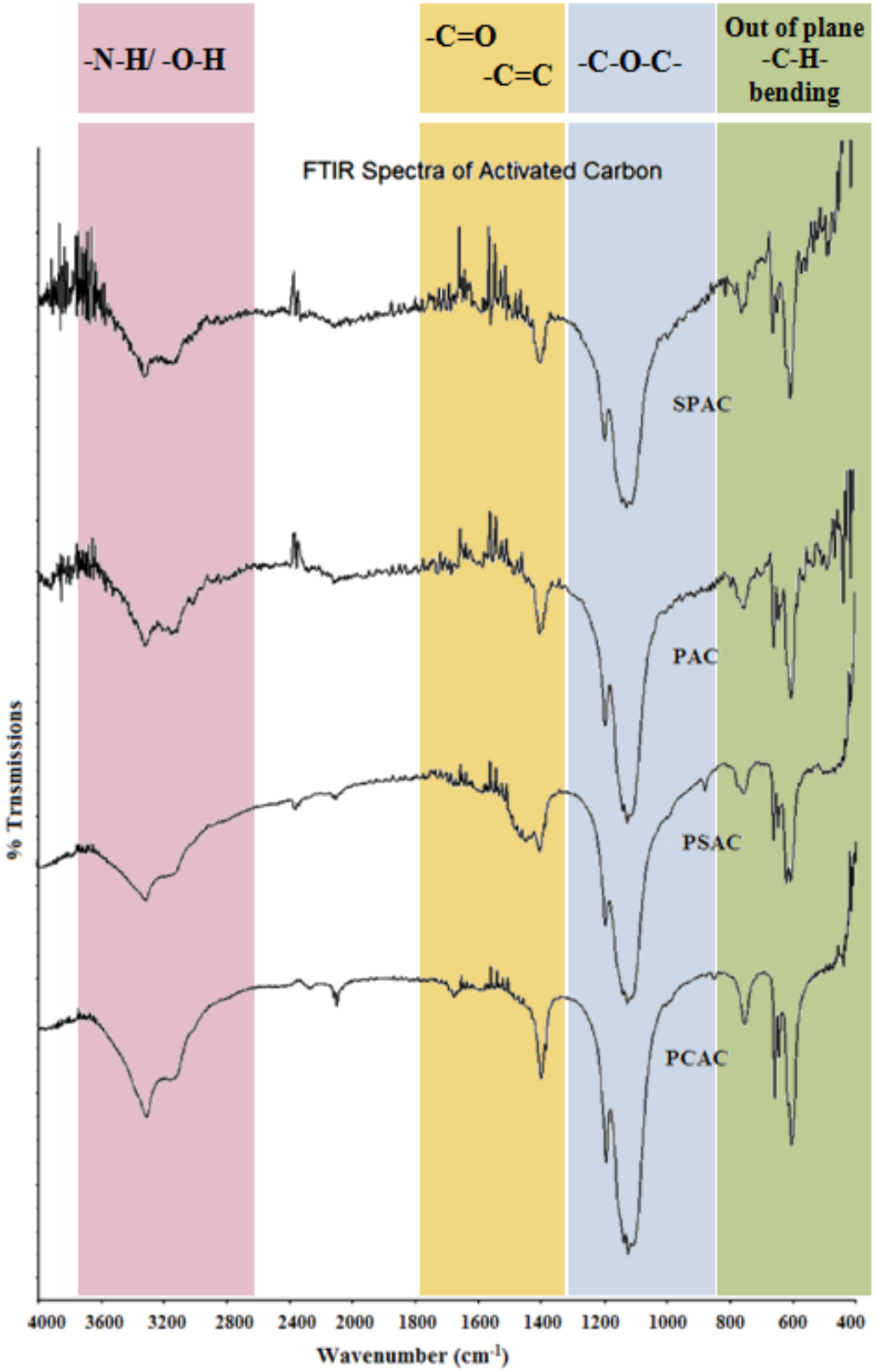

Figure 2.4 FTIR spectra of ACs

Furthermore, the IR signals at 698 and 740 cm^{-1} can be assigned to C–H out of plane bending vibrations of the aromatic ring. The peak at 668 cm^{-1} corresponds to -C≡N stretching, while the peak observed at 564 cm^{-1} corresponds to S–O stretching (Bello

et al., 2015). The peak at ~1433 cm^{-1} is assigned to the skeletal C=C vibration of aromatic rings. The low intensity peak at ~ 1750 cm^{-1} for PCAC can be attributed to carbonyl functional group.

2.3.3 SEM analysis of ACs

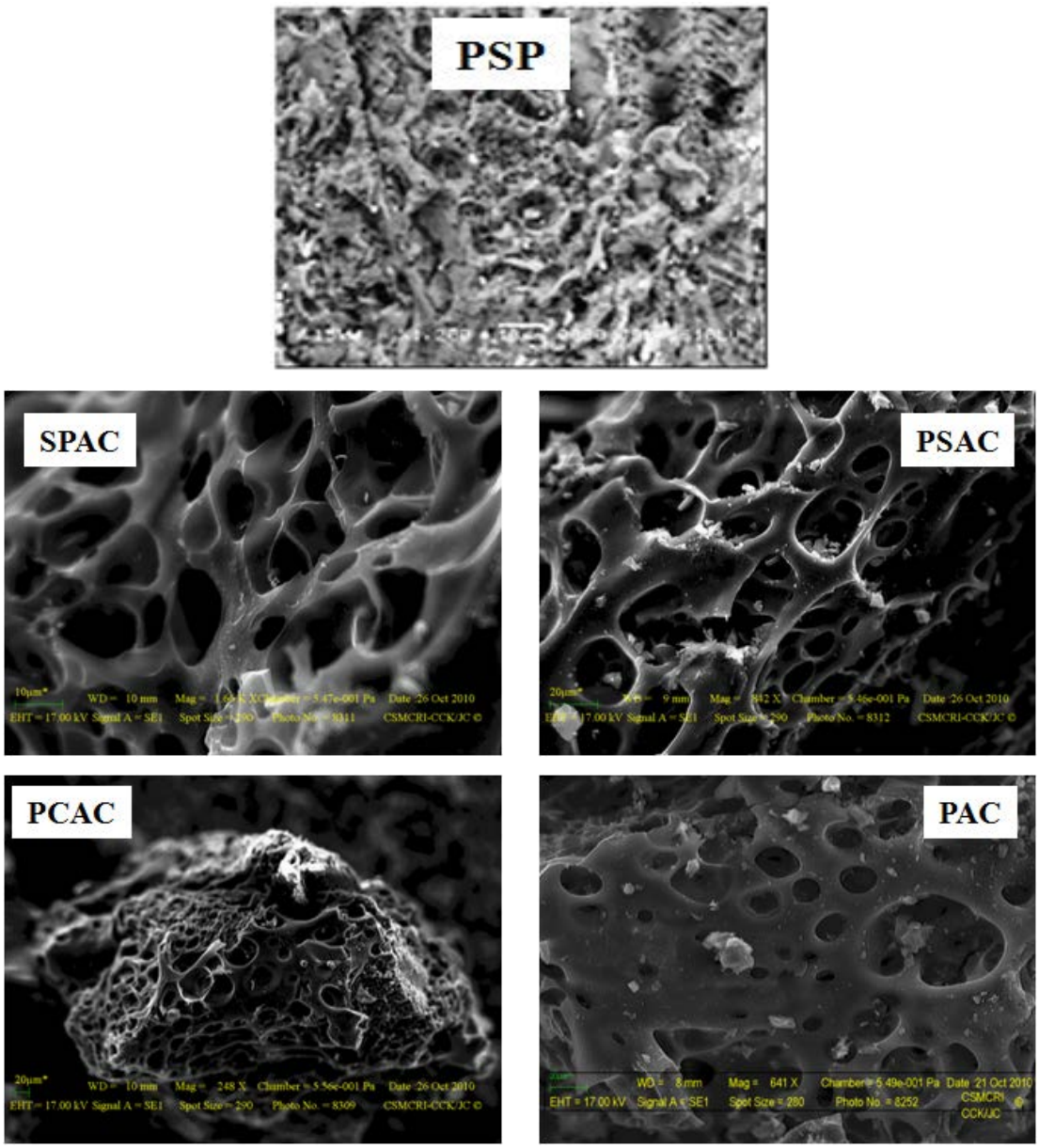

Figure 2.5 SEM images of ACs and PSP

The SEM images of the ACs are presented in Figure 2.5. The SEM images of all four ACs showed the irregular, rough and porous nature with identifiable micropores and mesopores as compared to pristine PSP.

2.3.4 BET-Surface area analysis of ACs

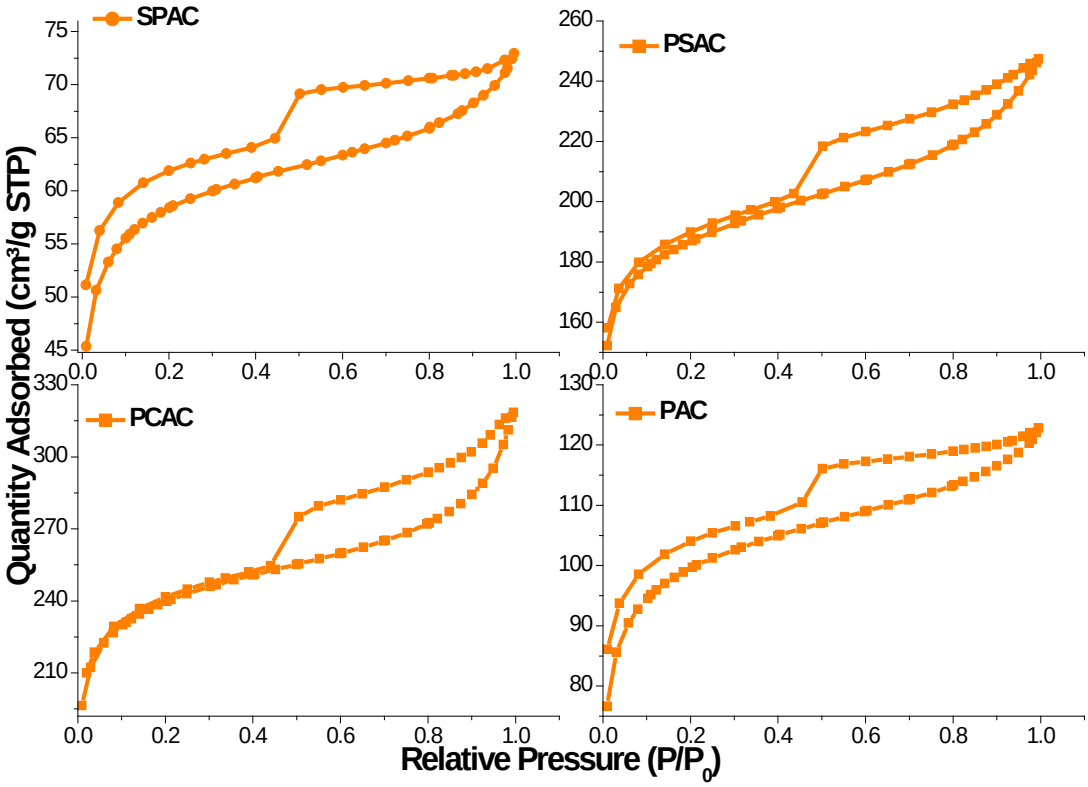

Figure 2.6 BET surface area analysis of ACs.

The N_2 adsorption and desorption isotherms (Figure 2.5) of PSAC and PCAC belong to a mixed type in the IUPAC classification, type I at low relative pressures (P/P_0) and type IV at intermediate and high relative pressures. In their initial part both PSAC and PCAC are of type-I with a significant uptake at low relative pressures, characteristic of microporous materials (Passe-Coutrin et al., 2008) while PAC and SPAC exhibit type IV isotherm. A hysteresis loop can be observed at intermediate and high relative pressures, indicating the presence of large number of micropores and mesopores (type IV) with average pore size varying between 23 to 26 Å for SPAC, PSAC, PCAC and PAC respectively (Table 2.6). The hysteresis loops are caused by the capillary condensation of adsorbate in mesopores.

The hysteresis loop closes only for PCAC and PSAC, whereas for SPAC and PAC, desorption is not complete at low pressures. This can be attributed to the blocking of pores, caused by narrow inlets and wide interiors (Oleszczuk et al., 2016). According to the IUPAC classification H_3 hysteresis does not exhibit a limiting adsorption at high values of P/P_0 and is related to the presence of assemblages of slit-shaped pores (Lowell et al., 2004; Thommes, 2010). The greater amount of N_2 adsorption at low

relative pressure ($P/P_0 < 0.1$) for PSAC and PCAC indicates the creation of large amount of new micropores. However, for higher relative pressures (P/P0 > 0.2), the nitrogen adsorption increased gradually, indicating a higher volume of wide micropores and the presence of small mesopores. Further, typical H_2 hysteresis behavior was also observed in PAC and SPAC where the main hysteresis loop has a prominent triangular shape especially at high pressures (Cimino et al., 2013).

The pore size distributions of the ACs were evaluated by Barrett-Joyner-Halenda (BJH) method (Figure 2.7). It can be seen that all the samples showed a distribution centered at 4 nm affirming the presence of mesoporosity in the materials. The micropore volume of the PCAC is significantly larger followed by PSAC, which probably explains the differences of the SSA and N_2 BET values.

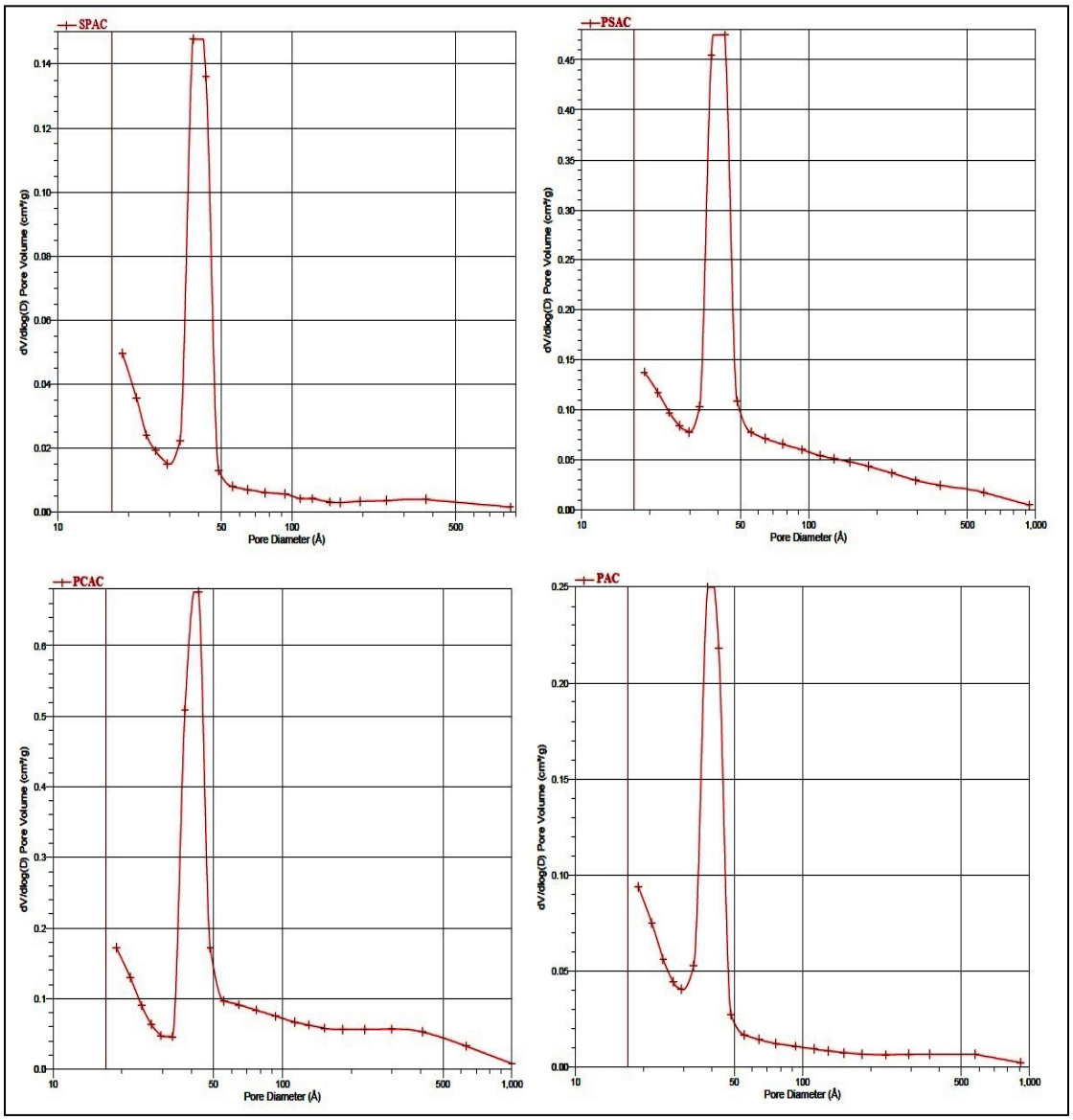

Figure 2.7 BJH pore volume plot

Table 2.5 BET surface area analysis

Adsorbent (ACs)	**BET surface area results (m^2/g)**			
	S_{BET}	**S_{micro}** (from t- plot)	**S_{ext}** (from t- plot)	**Langmuir Surface area S_L**
SPAC	191.1321	129.2671	61.8650	265.2412
PSAC	604.0306	418.2395	185.7910	848.1240
PCAC	770.8442	555.9275	214.9167	1082.3319
PAC	322.2221	211.5898	110.6323	453.5825

Table 2.6 Porosity analysis of the ACs

Adsorbent (ACs)	**Porosity results**			
	Pore Volume ($cm^3.g^{-1}$)			**Pore size (Å)**
	V_{total}	V_{micro}	V_{meso}	
SPAC	0.1128	0.0632	0.0496	23.61
PSAC	0.3828	0.2077	0.1751	25.35
PCAC	0.4926	0.2765	0.2161	25.56
PAC	0.1899	0.1055	0.0844	23.58

The pore volume and surface area both were maximum when treated with persulfate (Table 2.5 and 2.6) probably due to the action of sulfate and hydroxyl radicals. The micropores accounted for around 55% of the activated carbons. All the carbons had almost equal number of mesopores and micropores to facilitate efficient adsorption

2.3.5 TGA analysis of ACs

TGA analysis was performed by heating the sample from 30°C to 900°C under nitrogen atmosphere at a heating rate of 10°C/min.

TGA of the ACs was performed to test the thermal stability and was compared with that of pristine PSP (Figure 2.8). The weight loss during thermogravimetric decomposition of the adsorbents can be divided into different stages and is tabulated in Table 2.7

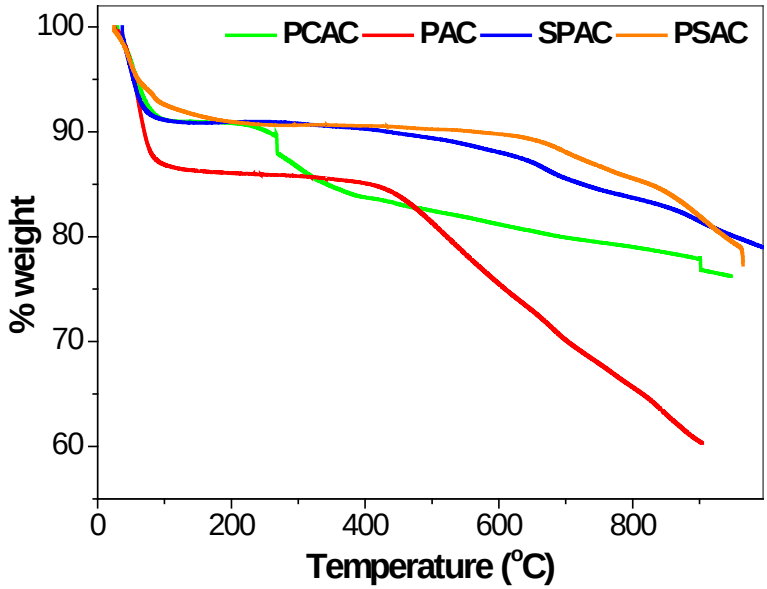

Figure 2.8 TGA analysis of ACs

Table 2.7 Thermogravimetric analysis of ACs

% Weight Loss						
Sample	1st stage	Temperature range (°C)	2nd stage	Temperature range (°C)	3rd stage	Temperature range (°C)
PSP	5.61	26.1-99.0	89.21	207.3-493.7	1.91	493.7-858.3
SPAC	8.84	37.9-127.4	3.59	244.1-642.6	7.18	675.2-899.8
PSAC	6.93	29.9-104.9	1.72	113.9-273.0	11.35	580.1-965.3
PCAC	8.32	27.5-105.9	3.25	184.2-268.4	11.24	471.8-897.4
PAC	13.35	26.4-118.4	1.22	138.6-386.2	24.59	391.7-898.9

PSP exhibited a total weight loss of ~95% upto 900 ˚C while PAC exhibited 37% weight loss. On the other hand SPAC, PCAC and PSAC underwent ~19-22% weight loss when heated to 900 ˚C.

The TGA curves of the ACs under study showed a first stage weight loss of about 4-16% at temperatures below 105°C corresponding to the loss of water molecules. The second stage (115°C<T<350°C), which corresponds to the primary carbonization(decomposition of hemicellulose (180–285 °C) and of cellulose in the range 275–365 °C (Uslu et al., 2008), is seen as a large weight loss for PSP (89.21%) suggesting the elimination of volatile matters and tars, while it is very less (~1-4%) in other carbons under study suggesting that the volatiles have been removed in the prior treatment process. The weight loss above 400°C was indicative of their transformation to a structure with higher stability by decomposition of lignin and loss of those

species which are anchored strongly with the materials via covalent linkages (Mewada et al., 2013). The TGA curves indicated that thermal stability was in order of SPAC<PSAC<PCAC<PAC.

2.3.6 X-ray Diffraction analysis of ACs

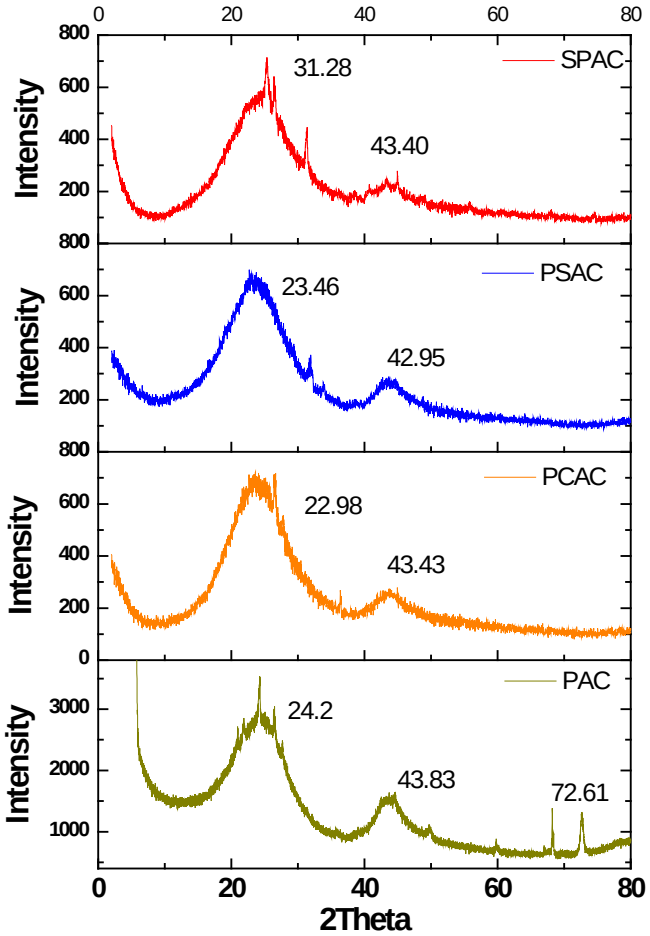

Figure 2.9 XRD analysis of ACs

The XRD analysis of the ACs under study (Figure2.9) mainly exhibited two broad peaks at~23˚ and~43˚ 2θ values associated with diffraction from the 002 and 100/101 set of planes respectively in graphite. These correspond to the interlayer spacing, Lc, and microcrystallite lateral dimensions, La, of the turbostratic (fully disordered) graphene layers (Manoj and Kunjomana, 2012). A peak located at ~24˚ scattering angle can be attributed to (002) diffraction with d-spacing value of 3.79, 3.867 and 3.676 Å in case of PSAC, PCAC and PAC respectively. The (100) and (101) reflections have probably merged into a single (10) peak. A less intense (11) peak is manifested at ~72.6˚ in PAC which is very weak or almost insignificant in SPAC, PCAC and PSAC (Bonarowska et al., 2011). An additional peak appears at 26.5˚ on top of that for the 24˚ for all the adsorbents under study except for PSAC. This peak is

well known to be due to the graphitic structure. The much weaker and broader (002) peaks in all carbons except PAC also suggests a random combination of graphitic and turbostratic stacking. In addition, the peak at 43.7˚ further suggests the presence of graphitic structure in PSAC as well as other carbons. The broad weak peaks suggested the amorphous nature of carbons that consists of small domains assembled by disordered graphene sheets (Tian et al., 2016). In addition, XRD analysis also revealed that mineral crystals were present which are more prominent in PAC and SPAC while only two sharp peaks were visible in PCAC and PSAC. These peaks could be attributed to the formation of potassium compounds such as K_2CO_3 and K_2O during persulfate and steam activation.

2.3.7 XPS analysis of ACs

XPS spectra of the ACs under study are shown in Figures2.10 (a), (b) and (c), and the assignments for the binding energies are tabulated in Table 2.8.

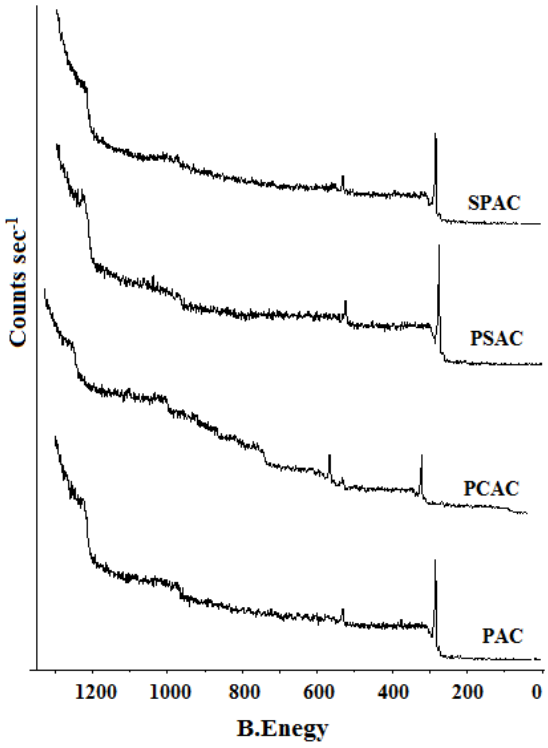

Figure 2.10a XPS survey scan of ACs

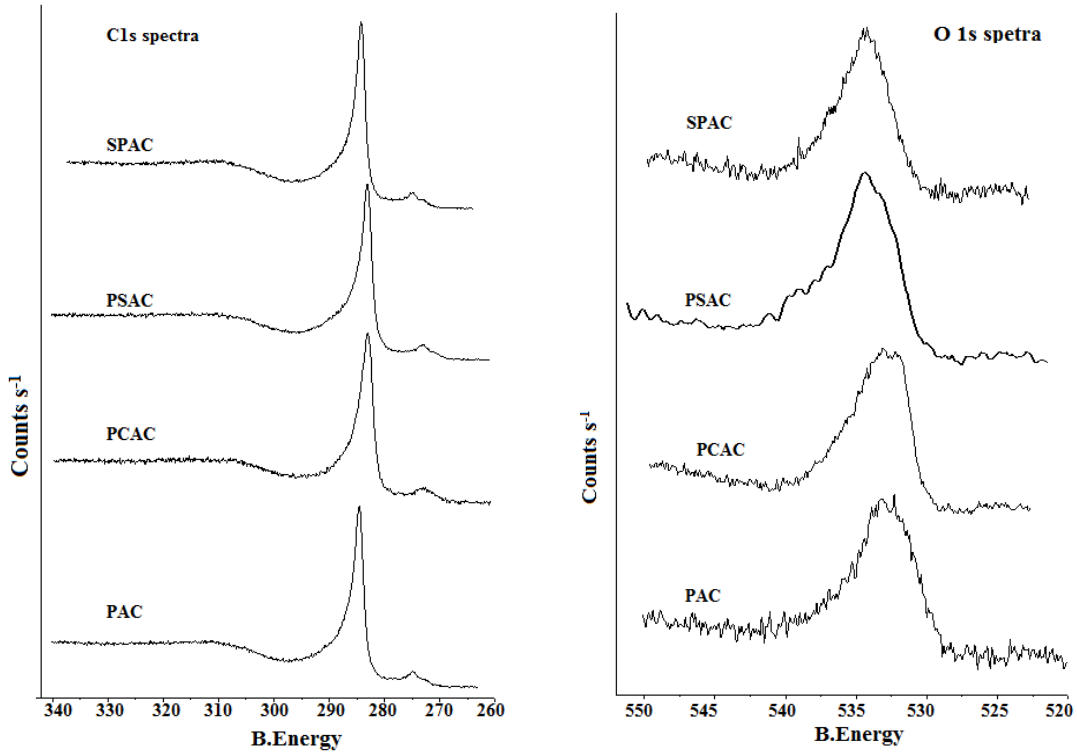

Figure 2.10b C1s and O1s core level spectra for ACs

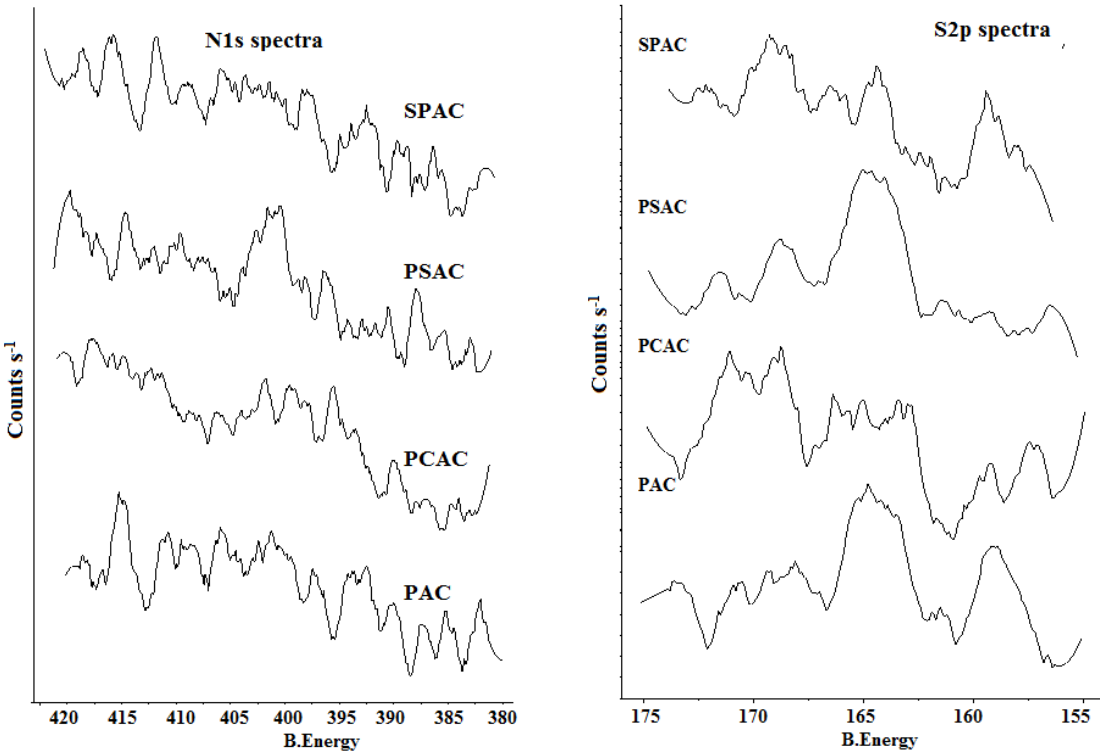

Figure 2.10c N1s and S2p core level spectra for ACs

Table 2.8 XPS characteristic binding energies and their assignments for ACs

	C1s							
	SPAC		**PSAC**		**PCAC**		**PAC**	
	B.Energy	Counts	B.Energy	Counts	B.Energy	Counts	B.Energy	Counts
C-C	284.56	6453.53	284.61	6410.22	284.56	5304.68	284.51	7489.62
C-O-C	286.06	3547.05	286.00	4012.28	286.06	3675.12	286.01	4332.43
O-C=O	288.86	2055.49	288.50	2278.64	288.46	2443.73	288.71	2432.59
Carbonate	290.36	1784.41	290.30	1932.96	290.26	2096.46	290.30	2038.79
	O1s							
	SPAC		**PSAC**		**PCAC**		**PAC**	
	B.Energy	Counts	B.Energy	Counts	B.Energy	Counts	B.Energy	Counts
C=O(carbonyl oxygen)	532.06	3193.44	531.90	3285.39	531.86	5305.10	532.01	3467.30
C-O(hydroxyl oxygen or ether oxygenC-O-C)	533.16	3347.67	533.00	3428.31	533.06	4907.98	533.11	3572.34
	N1s							
	SPAC		**PSAC**		**PCAC**		**PAC**	
	B.Energy	Counts	B.Energy	Counts	B.Energy	Counts	B.Energy	Counts
$C\text{-}NH_{2\ amine}$	399.56	2002.08	399.61	2067.76	399.46	2296.69	399.41	2292.22
C-N-C (pyrolic nitrogen)	400.66	1999.34	400.71	2067.04	400.56	2331.54	400.61	2298.14
Oxidised Nitrogen functionalitie or pyridine N-Oxide	402.36	2011.12	402.31	2043.92	402.66	2298.92	402.41	2301.22
	S2p							
	SPAC		**PSAC**		**PCAC**		**PAC**	
	B.Energy	Counts	B.Energy	Counts	B.Energy	Counts	B.Energy	Counts
S2p	163.96	272.09808	163.9	274.93621	163.9	893.10435	163.91	300.98919

The C 1S peak was deconvoluted into four different carbon species (López et al., 1991; Mérel et al., 1998; Wollbrink et al., 2016) while the N1s peak was deconvoluted into three different types of N-containing species as indicated in Table2.9. A weak sulfur peak is observed with binding energy of 163.96 eV which can be attributed to sulphur bonded directly to the graphitic ring structure or as an inclusion in the ring structure (Chin, 1981). It can be seen that more carboxyl groups are generated in PCAC as evidenced by IR spectral analysis

2.3.8 Zeta-potential analysis of ACs

Zeta-potentials of ACs at different pH conditions are shown in Figure2.11. All the ACs under study exhibited acidic zpc values (2.0, 1.9, 3.6 and 2.1 for SPAC, PSAC, PCAC and PAC respectively). The surfaces of the carbons were observed to be negatively charged from pH 3. A negative charge results from the dissociation of surface oxygen complexes of acid character such as carboxyl and phenolic groups (Bronsted acid sites). The origin of the positive surface charge, in carbons with less nitrogen functionalities could be due to the presence of surface oxygen complexes of basic character like pyrones or chromenes, or electron-rich regions within the graphene layers, which accept protons from the aqueous solution (Lewis basic centers) (Marsh and Rodriguez-Reinoso, 2006).

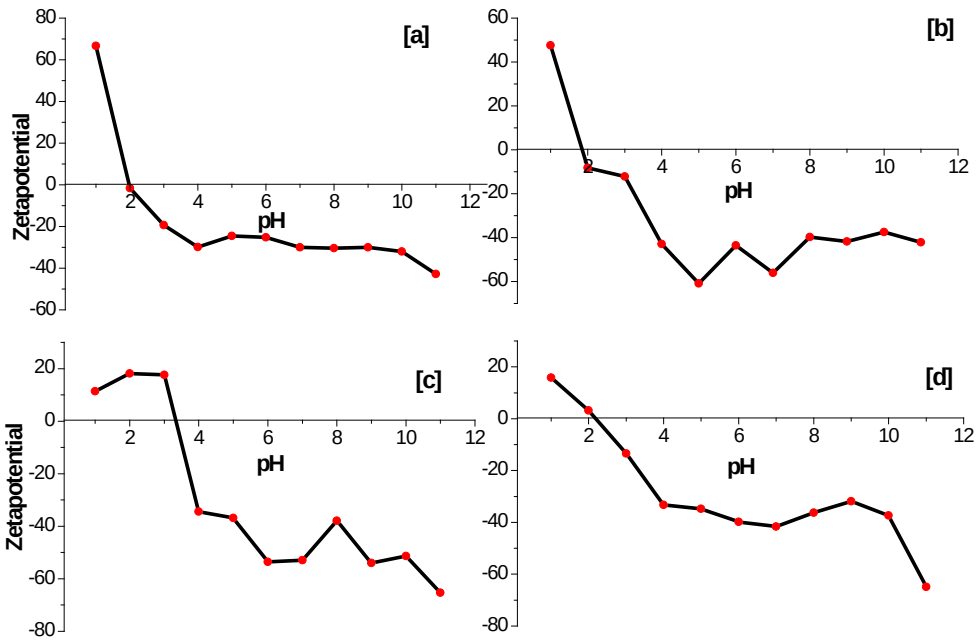

Figure 2.11 Zeta potential analysis of ACs

[a] SPAC, [b] PSAC, [c] PCAC and [d] PAC

(Part-B)

Investigation of adsorption potential of SPAC, PSAC, PCAC and PAC towards 4CP, 4NP, DNP, TNP, BPA and MnCP

2.4 Experimental

2.4.1 Chemicals and reagents

All the chemicals including model organic pollutants Bisphenol A ((4,4'-(propane-2,2-diyl)diphenol, BPA, spectrochem India), 4-Chlorophenol (4-CP, spectrochem India), Nitrophenols (4-Nitrophenol (4-NP, $C_6H_5NO_3$), 2,4-Dinitrophenol (DNP, $C_6H_4N_2O_5$), 2,4,6-Trinitrphenol (TNP, $C_6H_3N_3O_7$); LR, Spectrochem, india), Monocrotophos (70% suspension a gift sample from Gujarat Insecticides limited, ankleshwar, India) were used

2.4.2 Preparation of working solutions

A 1000 ppm solution of the adsorbate was prepared by dissolving 1000 mg of the respective compound in water and making up to 1L. BPA, 4-CP, MnCP and TNP were first dissolved in minimum quantity of methanol and further diluted to 1L using water. Working solutions of required concentrations were prepared by appropriate dilutions.

The adsorption study of the model pollutants were studied by batch technique.

2.4.3 Batch Adsorption study

Batch adsorption studies were done to evaluate the efficiency of ACs for the removal of model pollutants. The effect of adsorption parameters such as pH, amount of adsorbent (dose), time, temperature and concentration on the adsorption process were studied. The obtained results were tested using different kinetics and isotherm models to understand mechanism and order of reaction. Thermodynamic studies were also performed. In a typical experiment, 25 mL of desired concentration of adsorbate solutions were taken in 150 mL stoppered Durasil conical flasks and were equilibrated with required dose of adsorbent at 180 rpm on a thermally regulated orbital shaker. Table 2.9 summarizes the experimental conditions used for the various adsorption studies performed.

Table 2.9 Conditions for optimizing adsorption parameters

Study	**Condition**
pH study	25 ml, 50 ppm solution, Time 3 hrs, pH 2-11, 10-20 mg dose, at RT
Dose study	Optimum pH, 25 ml 50 ppm solution, Time 3 hrs at RT
Time study	Optimum pH, 25 ml 50 ppm solution, Time 10-60 min &60-720 min (saturation time), Dose 10-20 mg at RT
Concentration Study	Optimum pH, optimum Dose, Optimum Time, 25 ml solution (50-250 ppm) at RT
Temperature Study	Optimum pH, optimum Dose, Optimum Time, 25 ml solution (150-250 ppm) at 303, 313, 323, 333 ˚K

The pH of the solutions was adjusted using 0.1 N HCl or 0.1 N NaOH**.** After considerable time period, the contents in the flask were filtered and the unadsorbed pollutant concentration in the filtrate was determined by measuring absorbance at 276 nm, 279 nm, 317 nm, 261 nm, 357 nm, 294 nm for BPA, 4-CP, 4-NP, DNP, TNP, MnCP respectively using a Jasco, (Japan) V-603 UV-Visible spectrophotometer

The percentage removal of pollutant and the amount adsorbed ($mg \cdot g^{-1}$) were calculated by the following relationship (Kushwaha et al., 2011).

$$\% \, Removal = \frac{(C_i - C_e)}{C_i} \times 100 \text{ ..... Eq. (19)}$$

$$q_e = \frac{(C_i - C_e)}{m} \text{ ..... Eq. (20)}$$

Where, C_i is the initial concentration of pollutant in mg/L, C_e is the equilibrium concentration of pollutant in $mg \cdot L^{-1}$, m is the mass of adsorbent in $g \cdot L^{-1}$ and q_e is the amount of pollutant adsorbed per gram of adsorbent. The adsorption mechanism of pollutant onto ACs was investigated using pseudo-first order, pseudo-second-order, intra-particle diffusion, Elovich and liquid film diffusion kinetic models by fitting the sorption data in the respective models. Table 2.10 and Table 2.11 summarize the assumptions and equations involved in the kinetic and isotherm models studied.

Table2.11 Kinetic models with their significance

Kinetics (Dynamic models)	**Equation**	**Description**	**Description**	**Reference**
Pseudo first-order	$\log(q_e - q_t) = logq_e - \frac{K_1 \mathrm{t}}{2.303}$	q_t = uptake at time t, q_e = uptake at equilibrium, k_1 = rate constant;	The kinetic model generally do not fit throughout the whole adsorption cycle, it generally at the initial stage. The amount of uptake capacities generally increases with increase in time and concentration.	Lagergren, 1898.
Pseudo-second-order	$\frac{t}{q_t} = \frac{1}{(K_2 {q_e}^2)} + \frac{t}{q_e}$	k_2 = the rate constant	The kinetic model generally supports the chemisorption of adsorbate during adsorption process..	Ho, 2006.
Intraparticle diffusion	$q_t = K_i t^{0.5}$	k_i = rate constant	Intra-particle diffusion model is of major interest because the internal diffusion determines the adsorption rate in most of the liquid systems. It is generally used for identifying the number of steps involving in adsorption process. If the Linear graph between qt and t0.5 passes through origin, shows intraparticle model applicability. If the intercept is there, it shows the boundary layer effect, gives thickness of boundary layer.	Weber J. and Morris, 1963.
Elovich	$q_t = \frac{1}{\beta}\mathrm{Ln}(\alpha\beta) + \frac{1}{\beta}\mathrm{Ln}t$	α (mg/g min) = the initial sorption rate and the β parameter (g/mg) is related to the extent of surface coverage	It generally describes the chemisorption mechanism for the adsorption process. Elovich equation is also used successfully to describe second order kinetic assuming that the actual solid surfaces are energetically heterogeneous, but the equation does not propose any definite mechanism for adsorbate–adsorbent. It has extensively been accepted that the chemisorption process can be described by this semi-empirical equation.	Rudzinski and Panczyk, 2002
Liquid film diffusion	$\mathrm{Ln}\left(1 - \frac{\mathrm{q_t}}{\mathrm{q_e}}\right) = -K_{FD}t$	k_{FD} = rate constant	Determines whether the main resistance to mass transfer is in the thin film (boundary layer) surrounding the adsorbent particle, or in the resistance to diffusion inside the pores. Applicable when flow of the reaction from the bulk liquid to the surface of the adsorbent determines the rate constant.	Boyd et al., 1947

Table 2.12 Isotherm model with their significance

Isotherm	Equation	Description	Description	Reference
Langmuir	$\frac{q_e}{q_m} = \frac{k_L C_e}{1 + k_L C_e}$ is Linearised to $\frac{C_e}{q_e} = \frac{1}{q_m} C_e + \frac{1}{k_L q_m}$	C_e = Concentration at equilibrium q_e = Uptake at equilibrium q_m = Maximum adsorption Capacity k_L = Energy of adsorption	Langmuir model is based on the assumption of a homogeneous adsorbent surface with identical adsorption sites.. The model assumes uniform energies of adsorption onto the surface and no transmigration of adsorbate in the plane of the surface. This describes quantitatively the formation of a monolayer adsorbate on the outer surface of the adsorbent, and after that no further adsorption takes place.	Langmuir, 1916
Freundlich	$log q_e = \log k_F + \frac{1}{n} log c_e$	k_F = sorption capacity n = intensity of adsoption; 1/n = 0 irreversible 1/n >1 unfavourable 0 < 1/n < 1 favourable	The constant K_f is an approximate indicator of adsorption capacity, while 1/n is a function of the strength of adsorption in the adsorption process High values for K_f shows high adsorption capacity; Heterogeneous adsorbent and multilayer adsorption and the adsorption capacity is related to the concentration of adsorbate at equilibrium. The constant n is the empirical parameter related to the intensity of adsorption, which varies with the heterogeneity of the material. The adsorption process occurs on the heterogeneous surfaces. If the n is below one, then the adsorption is chemical process; otherwise, the adsorption is physical process.	Freundlich, 1906
Temkin	$q_e = \frac{RT}{\Delta Q} \ln (K_T C_e)$	ΔQ = heat of Adsorption k_T = equilibrium constant $B = \frac{RT}{\Delta Q}$	This isotherm takes into the account adsorbent–adsorbate interactions. By ignoring the extremely low and large value of concentrations, the model assumes that heat of adsorption (function of temperature) of all molecules in the layer would decrease linearly rather than logarithmic with coverage KT equilibrium constant corresponds to maximum binding energy and B is related to heat of adsorption.	Temkiin and Pyzhev, 1939

D-R	$\frac{q_e}{q_m} = \exp(-\beta\varepsilon^2)$ $\beta = \frac{1}{E^2}$ and ε $= RT\text{Ln}\frac{C_s}{C_e}$	β = constant related to sorption energy which is related to mean adsorption energy (E) ε = Polanyi potential is defined as $\varepsilon = RTln\left(1+\frac{1}{C_e}\right)$	Dubinin–Radushkevich isotherm is generally applied to express the adsorption mechanism with a Gaussian energy distribution onto a heterogeneous surface. The model can be successfully fitted to high as well as intermediate range of concentration of solute.. Dubinin and his co-workers conceived this equation for subcritical vapors in micropore solids where the adsorption process follows a pore filling mechanism onto energetically non-uniform surface.	Dubinin and Radushkevich, 1947
Elovich	$\frac{q_e}{q_m}$ $= K_E C_e \exp -\left(\frac{q_e}{q_m}\right)$	k_E = sorption constant	The Elovich model is based on a kinetic development according to the hypothesis that the adsorption sites increase exponentially with adsorption, involving multi-layered adsorption.	Elovich and Larionov, 1962
Halsey	$q_e = (K_H/C_e)^{1/n_H}$	k_H = the Halsey constant	Halsey proposed an expression for condensation of a multilayer at a relatively large distance from the surface.	Halsey, 1948

2.4.4 Thermodynamic study

In any adsorption process, both energy and entropy considerations must be taken into account in order to ascertain the spontaneity of the process. The thermodynamic parameters, change in free energy (ΔG), enthalpy (ΔH), and entropy (ΔS) were determined by using following equations

$$\Delta G^0 = \Delta H - T\Delta S \ldots Eq.(21)$$

$$\Delta G^0 = -RTlnk_d \ldots Eq.(22)$$

$$lnk_d = \frac{\Delta S}{R} - \frac{\Delta H}{RT} \ldots Eq.(23)$$

2.4.5 Effect of ionic strength of the medium

Industrial effluent may contain large amount of salts and other inorganic impurities. The effect of such salt on the adsorption process was investigated by investigating the adsorption of 100 ppm of each of the adsorbate in 0.1 to 0.5 N NaCl solutions under optimized adsorption conditions.

2.4.6 Desorption study

Desorption studies are important to investigate the possibility for the recovery of pollutants adsorbed on the adsorbent surface, as well as for the regeneration of the adsorbent for subsequent reuse. A 100 ppm of the respective adsorbate solution was equilibrated with adsorbent under study using optimized adsorption conditions. After adsorption, the adsorbent was recovered by filtration, washed with water and dried. The adsorbent loaded with adsorbate was used for desorption by equilibrating with eluting solvent for 6 hrs. The adsorbent was then separated by filtration and concentration of the adsorbate in the filtrate was measured. The recovered adsorbate was washed, dried and used for the next adsorption cycle. The recovered adsorbent was further used for three adsorption-desorption cycles. 0.1 N HCl, 0.1 N NaOH, methanol, ethanol and acetonitrile were investigated for desorption.

2.5 Results and discussion

Preliminary adsorption studies for all the adsorbates under study were carried out using all four carbons. The % adsorption in case of SPAC, PAC was not significant enough to warrant further studies while PSAC and PCAC exhibited significant adsorption for all the adsorbates under study. So the adsorption potential of PSAC and PCAC as adsorbents for the model pollutants under study was investigated further.

2.5.1 Effect of pH

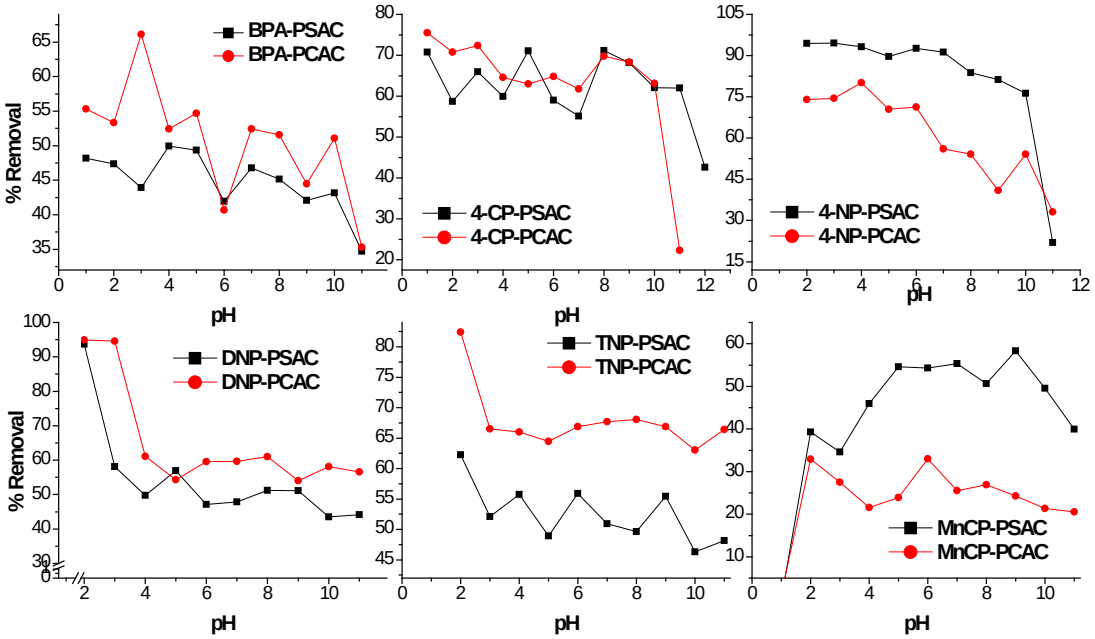

Figure 2.12 Effect of pH on adsorption using PSAC and PCAC

pH of the medium is an important parameter to be investigated as H^+ and OH^- ions compete with the adsorbate molecules for active sites on adsorbents depending on pH of the medium. Five of the selected organic pollutants were phenolics, which ionized and formed phenolate ions when pH of the solution was equal to or more than pKa (pKa of BPA, 4-CP, 4-NP, DNP and TNP are 9.6, 9.41, 7.16, 4.06 and 0.4 respectively). Below their respective pka values the phenols exist in their molecular form (Ahmaruzzaman and Gayatri, 2011). The zeta potential of the adsorbent PCAC was negative at pH >3.3 and PSAC at pH >1.8 indicating that there is a negative surface charge on the adsorbents over a wide pH range (Figure 2.12). The optimum pH was 5.0, 5.0, 3.0, 2.0, 2.0 and 7.0 for BPA, 4-CP, 4-NP, DNP, TNP and MnCP respectively for maximum adsorption onto PSAC and 5.0, 5.0, 3.0, 2.0, 2.0 and 6.0 for BPA, 4-CP, 4-NP, DNP, TNP and MnCP respectively for PCAC (Figure 2.12). The initial high adsorption for all phenolic adsorbates except for monocrotophos is due to electrostatic attraction between adsorbent and adsorbates. However there was considerable amount of adsorption beyond zpc value of PSAC and PCAC till a pH of about 7 to 8 especially in the case of BPA, 4CP and 4 NP. This could be due to hydrogen bonding till ~pH 5 after which the effect of hydrogen bond is negligible (Marzbali et al., 2016). Intermolecular π-π electron donor–acceptor interaction could be the cause of adsorption beyond pH 5 which is predominant in the case of monocrotophos (Bağda et al., 2013).

This suggested that adsorption of the adsorbates in molecular form was higher than in ionic state and these could be due to H-bonding, π-π interactions between aromatic ring and graphitic plane of PSAC as well as vander waals forces (Bautista-Toledo et al., 2005).

It is seen that CP uptake is not affected upto ~pH 9 (varies within 10%) when 4-CP is in the nonionic form (pKa= 9.38) indicating that the adsorption must be governed more by non-electrostatic interactions between the solute molecule and adsorbent surface, i.e., the dispersive interactions between the π-electrons of the aromatic ring of the adsorbate and the adsorbent (Monsalvo et al., 2011).

In case of monocrotophos, the maximum adsorption was in the pH range of 5/6-9 for PSAC and PCAC respectively. The optimum pH range was higher than the pKa value of monocrotophos (4.4). Further, the point of zero charge for PSAC and PCAC as well as adsorbate would be negatively charged at this pH. Intermolecular, π-π electron donor–acceptor interactions could be the predominant forces responsible for adsorption of monocrotophos.

2.5.2 Effect of Dose

The effect of varying doses of PSAC and PCAC on the adsorption of the pollutants under study was investigated.

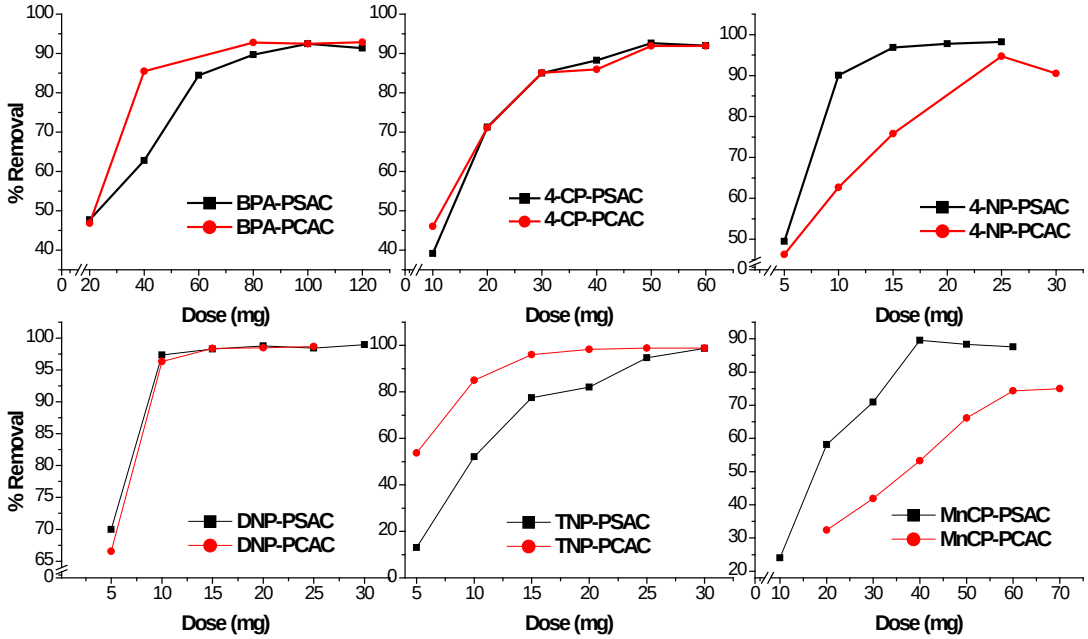

Figure 2.13 Effect of Dose on adsorption using PSAC and PCAC

The percent removal of adsorbates increased (Figure 2.13) with increase in amount of adsorbent which may be attributed to increase in adsorbent surface area and

availability of more adsorption sites initially and then saturation when a fixed concentration of adsorbate had sufficient adsorption sites.

2.5.3 Effect of Time

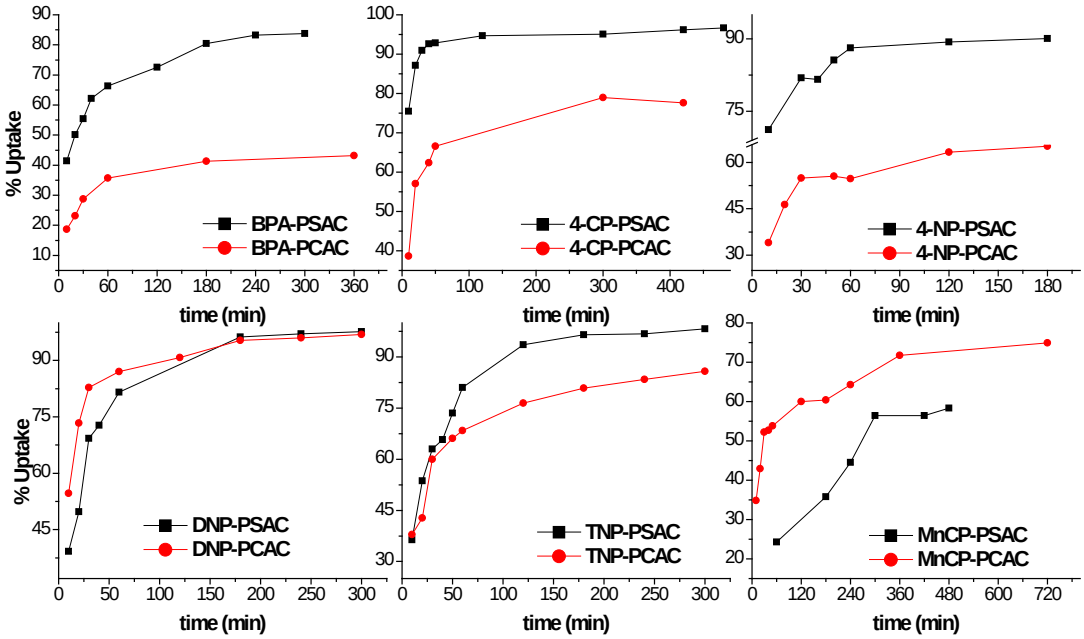

Figure 2.14 Effect of time on adsorption using PSAC and PCAC

The effect of contact time was determined by agitating 25 mL solutions containing 50 ppm of adsorbate under study and optimum dose of PSAC/ PCAC for varying time intervals. The results are shown in Figure 2.14. The rate of adsorption was faster during initial period of 40-60 minutes of contact for all adsorbates except for MnCP when PSAC and PCAC were used as adsorbents. The initial rapid adsorption may be attributed to large number of adsorbent sites that were available for adsorbate molecules. However, the adsorption slowed down in later stages due to the saturation of adsorption sites. The rate of uptake of MnCP was relatively slow.

Equilibrium was achieved at about 240 min, 150 min, 90 min, 180 min, 180 min and 240 min for BPA, 4-CP, 4-NP, DNP, TNP and MnCP respectively while the time required to achieve equilibrium for PCAC was 240 min, 150 min, 120 min, 180 min, 180 min and 300 min for BPA, 4-CP, 4-NP, DNP, TNP and MnCP respectively.

2.5.4 Temperature variation study

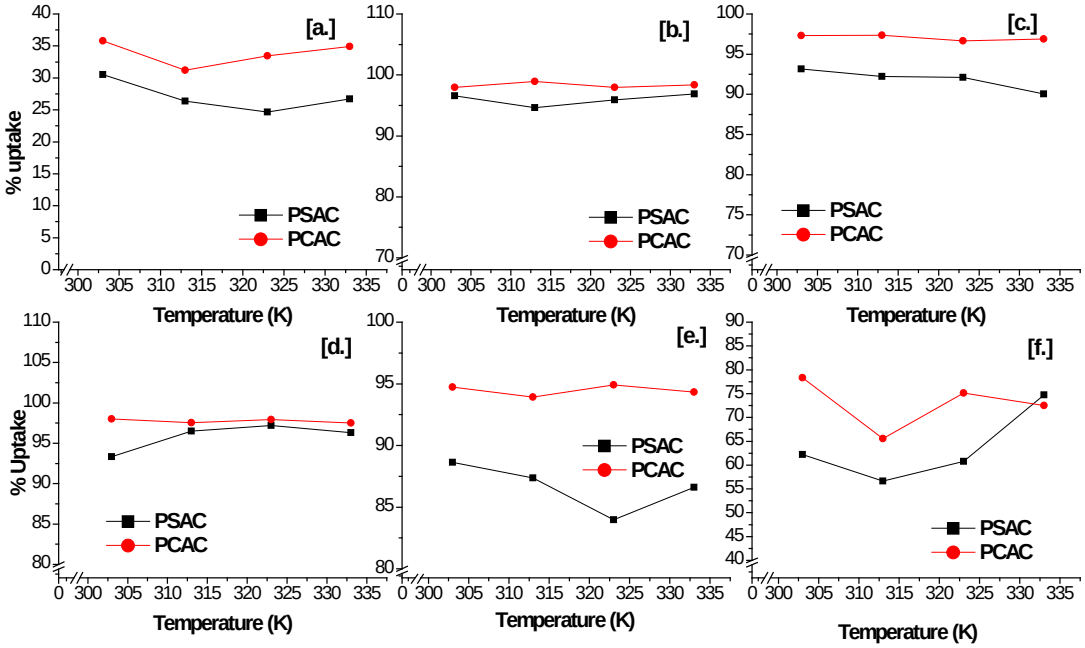

Figure 2.15 Temperature optimization study:

(a) BPA (b) 4-CP (c) 4-NP (d) DNP (e) TNP (f) MnCP

The effect of temperature was studied at optimized pH, time and dose. The adsorption was carried out at four different temperatures -Room Temperature (RT) (303 K), 313 K, 323 K and 333 K. It can be seen from Figure 2.15 that the adsorption was higher at RT and that the adsorption was an exothermic process.

2.5.5 Kinetic study

The results and data obtained from the time study were applied to evaluate the dynamics of the adsorption process for all the adsorbates under study using PSAC and PCAC as adsorbents. The different kinetic models listed in Table 2.11 were applied to the data and the kinetic constants for the different models studied are tabulated in Table 2.13 and 2.14 for PCAC and PSAC respectively. The applicability of the models was determined based on the correlation coefficient values as well as the curve fitting of the kinetic models with experimental results.

The linear fit graphs for the kinetic models are presented in Figures 2.16 to 2.21 and the same for intraparticle diffusion model are given in 2.22 (a) and (b).

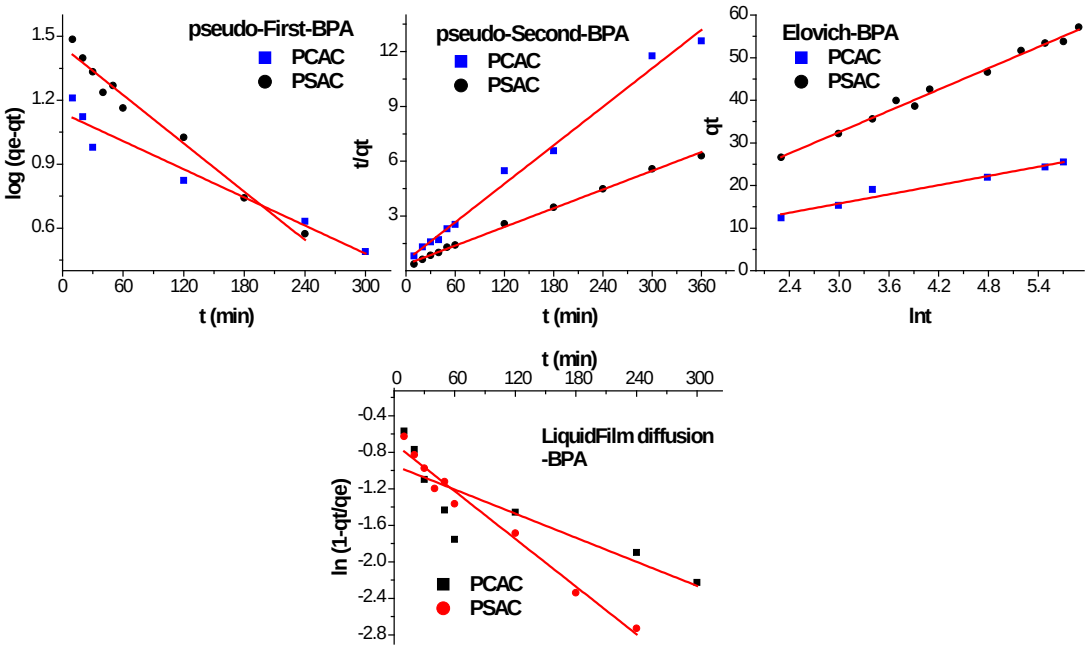

Figure 2.16 Linear plots of kinetic models for BPA adsorption study

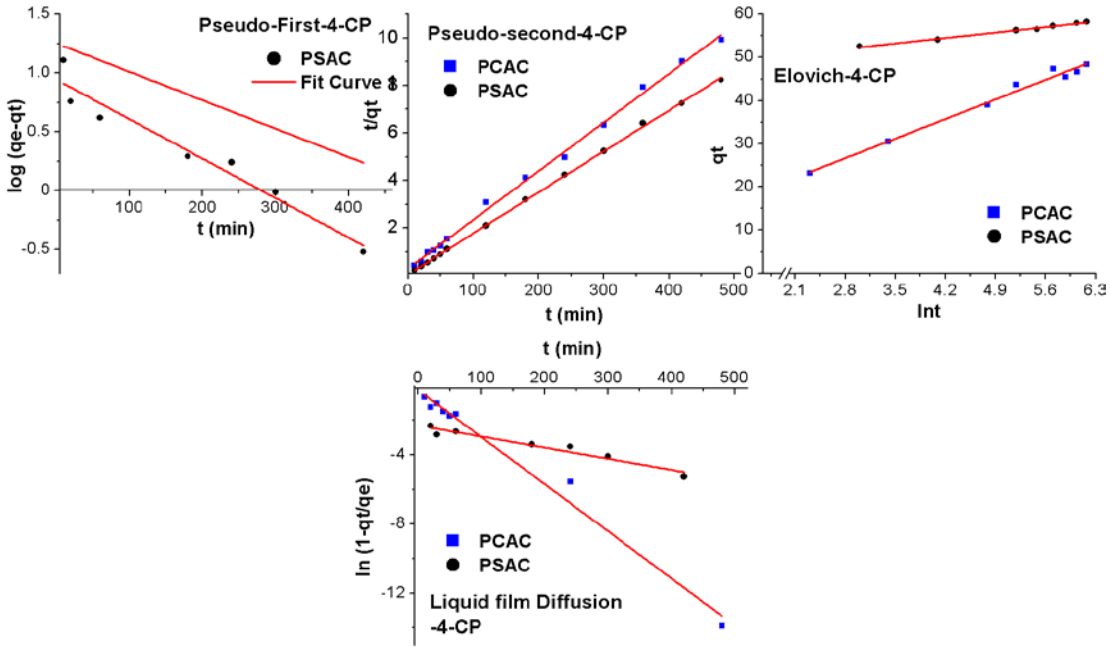

Figure 2.17 Linear plots of kinetic models for 4-CP adsorption study

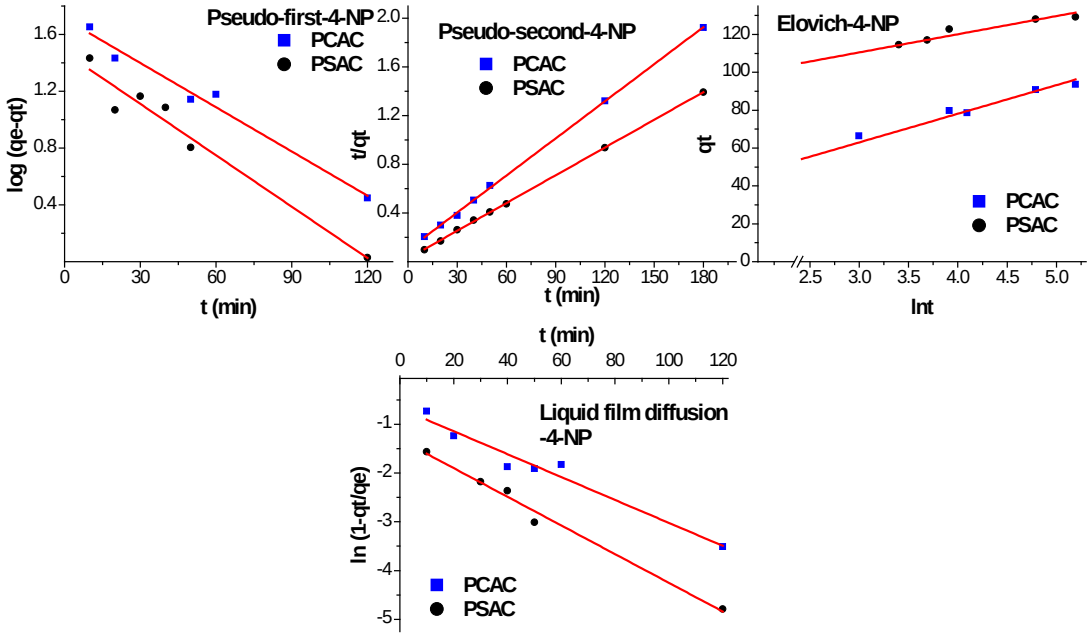

Figure 2.18 Linear plots of kinetic models for 4-NP adsorption study

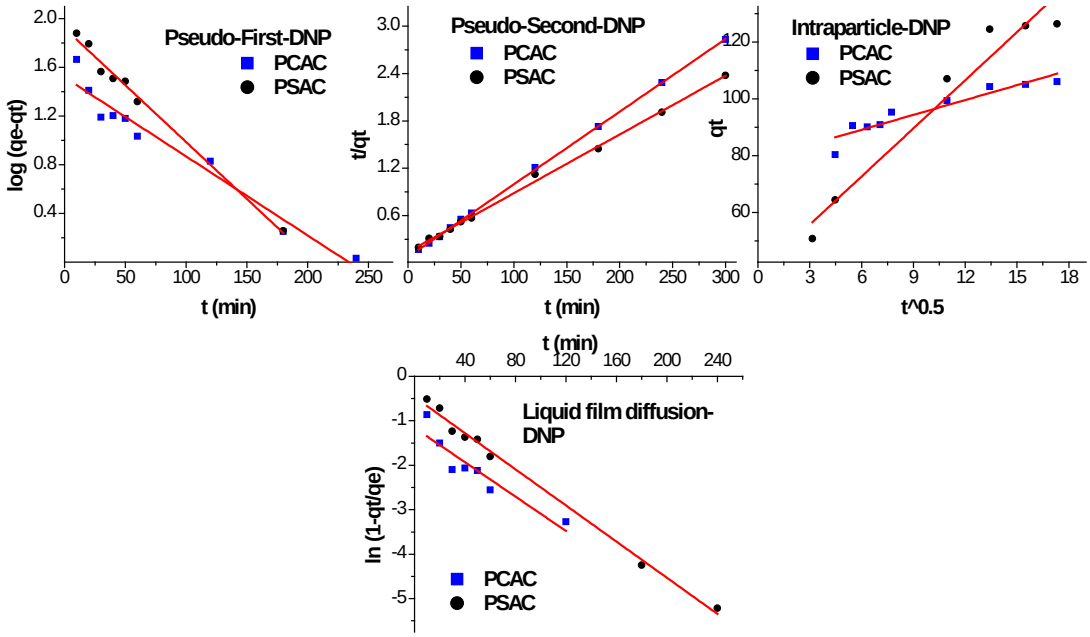

Figure 2.19 Linear plots of kinetic models for DNP adsorption study

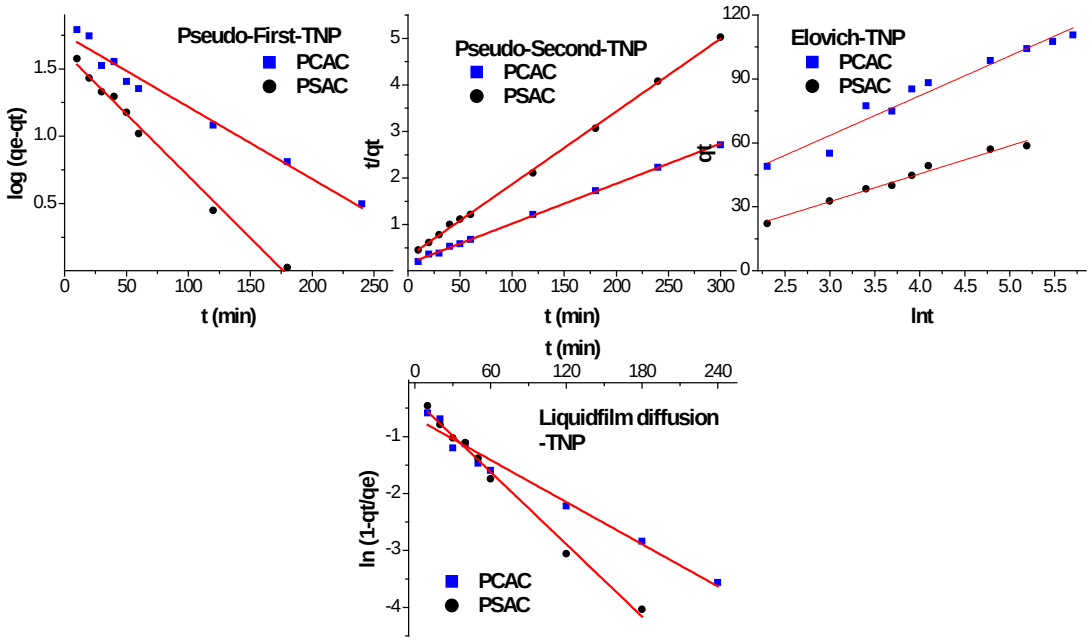

Figure 2.20 Linear plots of kinetic models for TNP adsorption study

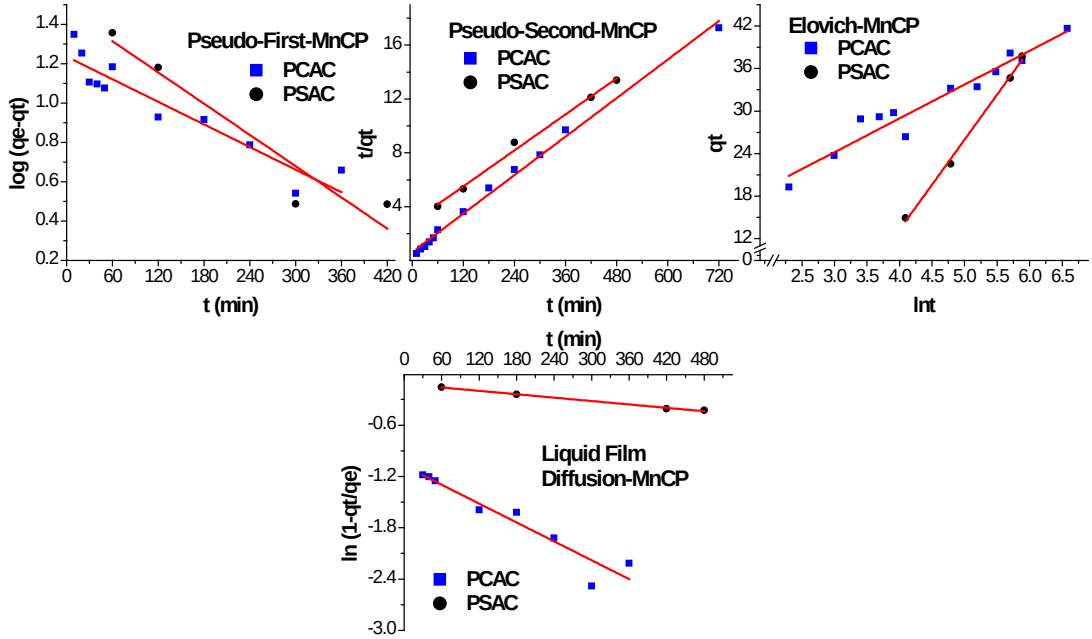

Figure 2.21 Linear plots of kinetic models for MnCP adsorption study

. It can be deduced from Tables 2.12 and 2.13 that although the r^2 value for pseudo-first order were 0.96-0.99, the q_e values did not match with the experimental q_e value probably because apart from physisorption, other interactions were also playing a role in the adsorption process.

Table 2.12 kinetic parameters for adsorption using PSAC

	BPA	pCP	pNP	24 DNP	246 TNP	MnCP
Experimental						
q_e (mg.g^{-1})	57.1643	58.2498	129.19	126.33	59.7347	37.736
Pseudo-First Order Model						
k_1(min^{-1})	0.0038	0.0034	0.0121	0.0093	0.0092	0.0026
q_e (mg.g^{-1})	28.2553	8.81658	29.7577	83.3681	42.0824	29.7646
r^2	0.9788	0.9501	0.9582	0.9907	0.9925	0.9123
Pseudo-Second Order Model						
q_e (mg.g^{-1})	58.4795	57.8035	131.579	135.135	64.1026	44.843
k_2(g.mg^{-1}.min^{-1})	0.0008	0.0057	0.0022	0.0004	0.0008	0.0002
k_o	2.8066	18.9753	38.0228	7.16846	3.26797	0.3525
r^2	0.9972	0.9996	0.9998	0.9978	0.9993	0.9936
Elovich Model						
α (mg.g^{-1}.min^{-1})	20.4519	3E+11	47846.3	19.5098	7.7580	0.6611
β (g.mg^{-1})	0.1199	0.5513	0.1042	0.0411	0.07645	0.0787
r^2	0.9903	0.9913	0.9582	0.9834	0.9832	0.9968
ln(αβ)	0.8969	25.8443	8.5141	-0.221	-0.5224	-2.956
Intra-Particle diffusion Model						
k_{IP1} (mg.g^{-1}.min$^{-1/2}$)	3.5767	3.2701	5.2986	12.555	5.5627	2.0378
r_1^2	0.9717	0.9676	0.9998	0.9267	0.9708	0.9959
k_{IP2} (mg.g^{-1}.min$^{-1/2}$)	1.2603	0.1708	0.4898	2.2904	1.0175	0.9038
r_2^2	0.9344	0.8948	0.9942	0.8512	0.8423	0.8716
Liquid Film Diffusion Model						
K_{FD}	0.0087	0.0064	0.0294	0.0203	0.0212	0.0007
r^2	0.9789	0.9462	0.9884	0.9936	0.9925	0.995

However for pseudo-second order model the r^2 values were >0.99 and the kinetic results correlated with experimental results for all the adsorbates under study with both PSAC and PCAC suggesting the applicability of the kinetic model. The applicability of pseudo second order model suggested that chemisorption which includes H-bonding, electrovalent forces and van der waals forces was predominant rather than physisorption.

The Elovich model does not predict any definite mechanism but has been found useful in describing predominantly chemical adsorption on highly heterogeneous adsorbents (Gupta and Bhattacharyya, 2006). The r^2 values were in range of 0.96-0.99 (Tables 2.12 and 2.13). The constant α is related to the rate of chemisorption while b is related to the surface coverage (Teng and Hsieh, 1999). A higher value of "α" for PSAC and PCAC during adsorption indicated chemisorption to be the predominant adsorption process. Similar results were also obtained by Ho and McKay for

adsorption of Cu (II) on peat (Ho and Mckay, 1998) and by Aroua et al., during adsorption of lead onto palm shell based activated carbon (Aroua et al., 2008)

Table2.13 Kinetic parameters for adsorption using PCAC

	BPA	**pCP**	**pNP**	**DNP**	**TNP**	**MnCP**
Experimental						
q_e ($mg.g^{-1}$)	28.6	48.32	93.6385	106.048	110.689	41.6683
Pseudo 1st order Model						
K_1 (min-1)	0.0022	0.0024	0.0096	0.0065	0.0054	0.0019
q_e ($mg.g^{-1}$)	13.8166	17.9267	47.7529	32.961	56.5979	17.2266
r^2	0.9459	0.9296	0.9872	0.9564	0.9747	0.8865
Pseudo 2nd order Model						
q_e ($mg.g^{-1}$)	0.00222	0.0014	0.0011	0.00112	0.00045	0.00091
k_2($g.mg.min^{-1}$)	1.7986	3.3245	10.101	13.245	6.14251	1.59744
k_o	28.490	48.7805	98.039	108.696	116.279	41.841
r^2	0.9913	0.9976	0.9996	0.9998	0.9991	0.9952
Elovich Model						
α ($mg.g^{-1}.min^{-1}$)	14.2024	24.032	48.399	6398.34	27.936	37.953
β ($g.mg^{-1}$)	0.2775	0.1542	0.0661	0.1145	0.0536	0.2097
r^2	0.9656	0.9845	0.9686	0.948	0.9577	0.9398
ln(αβ)	1.3716	1.3097	1.1626	6.5963	0.4037	2.0742
Intra- particle Diffusion Model						
kIP_1 ($mg.g^{-1}.min^{-1/2}$)	2.4979	6.2121	7.9443	13.3889	9.5071	3.3629
r_1^2	0.9811	0.9285	0.8989	0.9750	0.9151	0.9200
kIP_2 (mg.g-1.$min^{-1/2}$)	0.4416	0.8353	2.1986	1.3315	2.7395	0.6312
r_2^2	0.8495	0.8669	0.9594	0.9502	0.9605	0.9634
Liquid Film diffusion Model						
k_{FD}	0.0025	0.0273	0.0235	0.0193	0.0123	0.0037
r^2	0.7277	0.9847	0.9594	0.8597	0.9747	0.9108

The adsorption process commonly proceeds via four stages: (1) adsorbate migration from the bulk solution to the adsorbent surface; (2) diffusion through the boundary layer to the surface of the adsorbent; (3) adsorption onto an active site; (4) intra-particle diffusion into the interior of the adsorbent (Aravindhan et al., 2009; Wu and Yu, 2006). In this respect, during solid- liquid sorption, either external mass transfer or intra-particle diffusion, or both, usually control the solute transfer process. The sorption rate will therefore be controlled by the slowest step, which would be either film diffusion or pore diffusion (Aravindhan et al., 2009).

The presence or absence of intra-particle diffusion can be confirmed by applying the Morris-Weber equation as described in Table 2.10. The curves of plot of q_t vs $t^{1/2}$ for both PSAC and PCAC indicated multiple diffusion steps (Wu and Yu, 2006). The first linear region with a high slope signaled a rapid external diffusion stage depicting macro-pore or interparticle diffusion, which is followed by second step of intra-particle (micropore) diffusion.

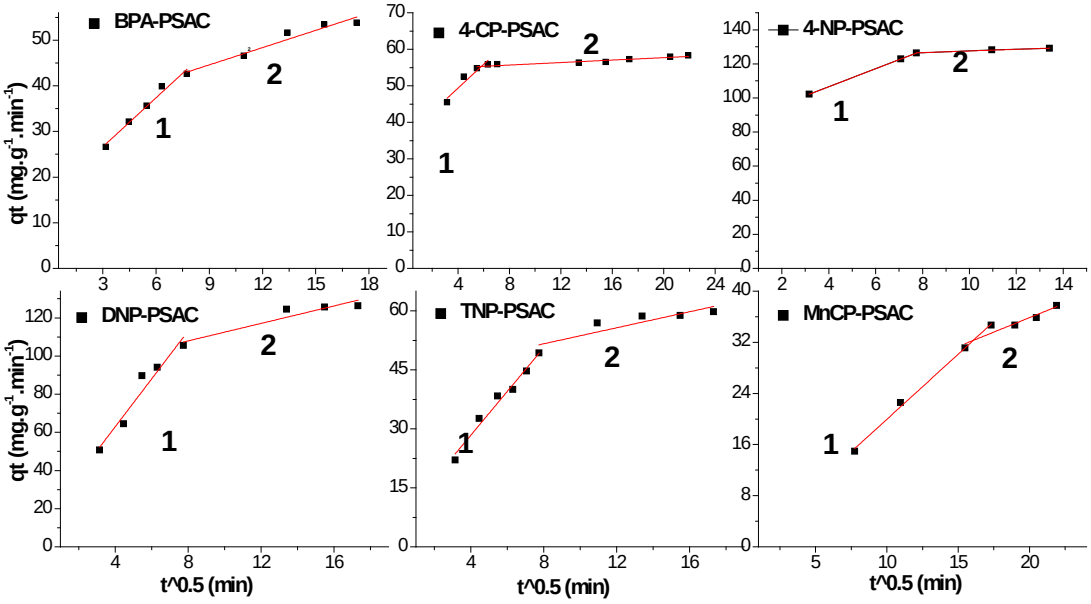

Figure 2.22a Intra-particle diffusion model linear plots for adsorption using PSAC

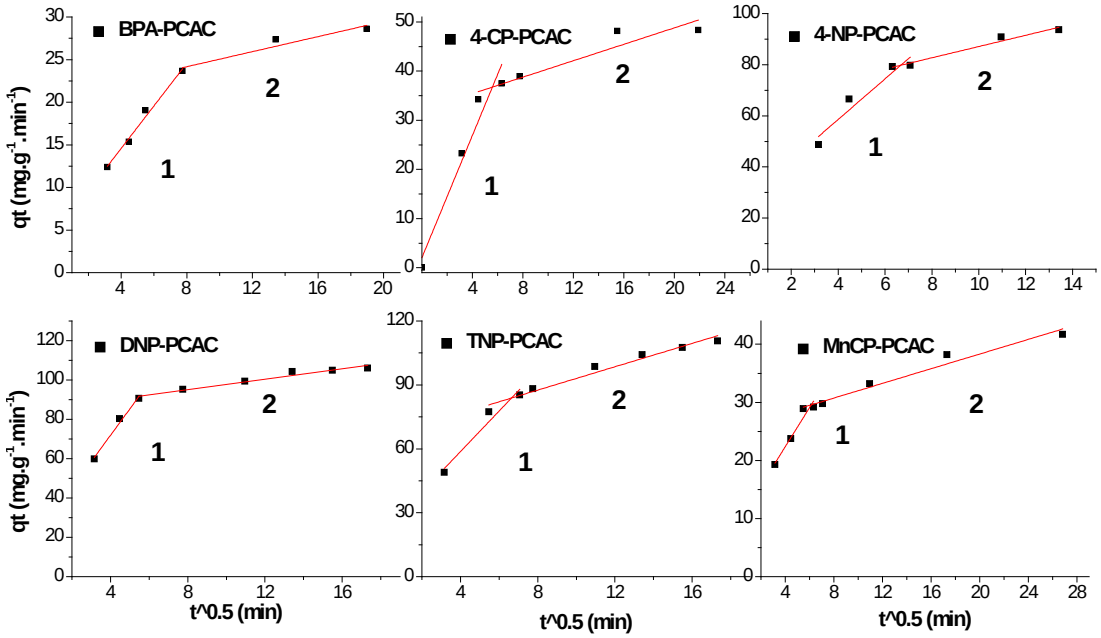

Figure 2.22b Intra-particle diffusion model linear plots for adsorption using PCAC

It was also observed that the plot did not pass through origin indicating some degree of boundary layer control and that the intra-particle diffusion is not the only rate limiting step but that other adsorption processes may also control the rate of adsorption, all of which may be operating simultaneously (Özacar and Şengil, 2005). The values of k_{IP1}, k_{IP2}, k_{LFD} and r^2 obtained from the plot are listed in Table 2.12 for PSAC and Table 2.13 for PCAC respectively.

Diffusion from the bulk liquid phase to the surface of an adsorbent may play an important role in determining the rate processes. However, the plots for LFD model did not pass through the origin despite providing good linear plots. Thus, liquid film diffusion is surmised not to be the predominant mechanism for adsorption onto PSAC and PCAC.

2.5.6 Isotherm study

The mechanism of adsorption was determined by applying isotherm models to the adsorption data obtained by varying concentration of the adsorbate at optimized conditions of pH, time and dose at room temperature. The equations and the linearized form of the different isotherm models applied are listed in Table 2.12. The applicability of isotherm models was determined based on correlation coefficient and the closeness of the calculated qe values with experimental results. The linear plots and the fits with experimental data are shown in Figures 2.23- 2.30.

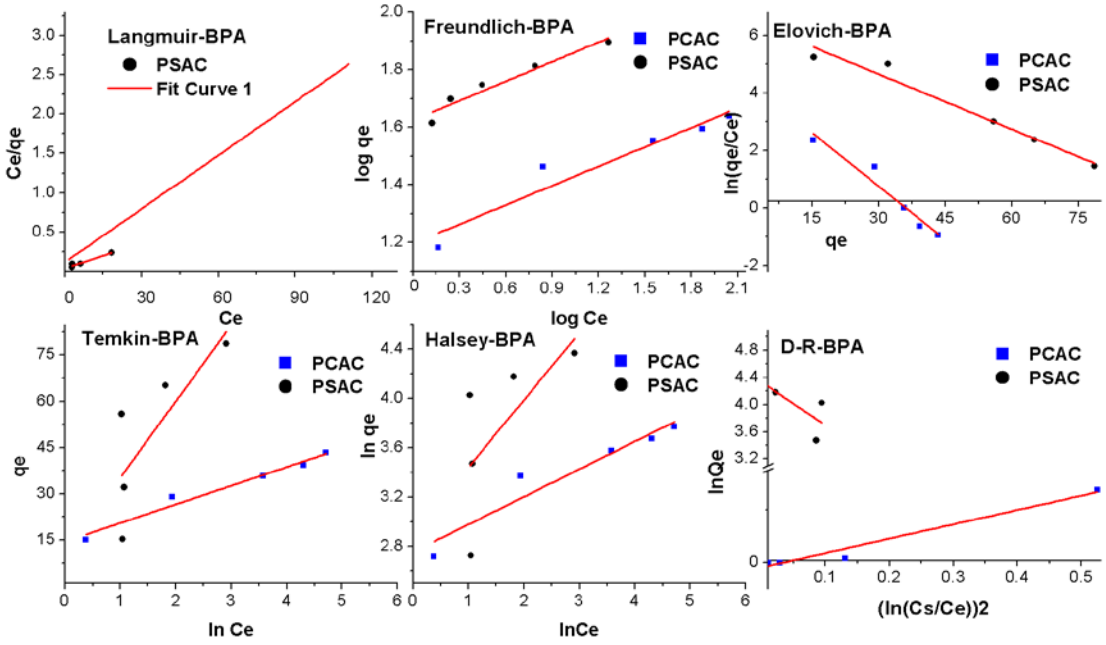

Figure 2.23 Isotherm models for BPA adsorption

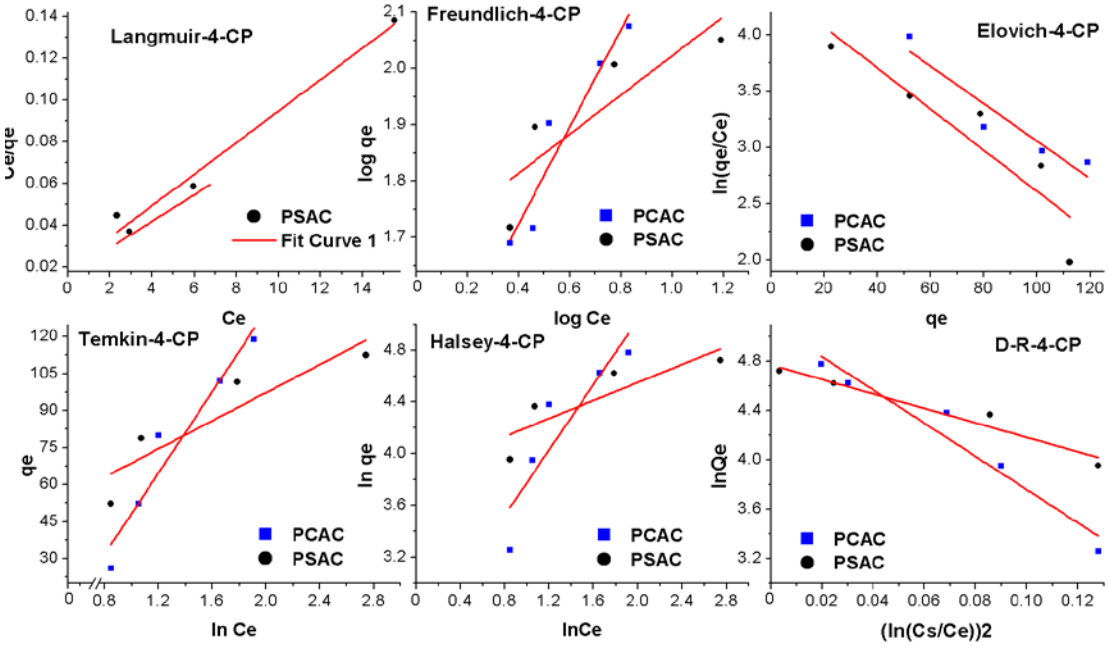

Figure 2.24 Isotherm models for 4-CP adsorption

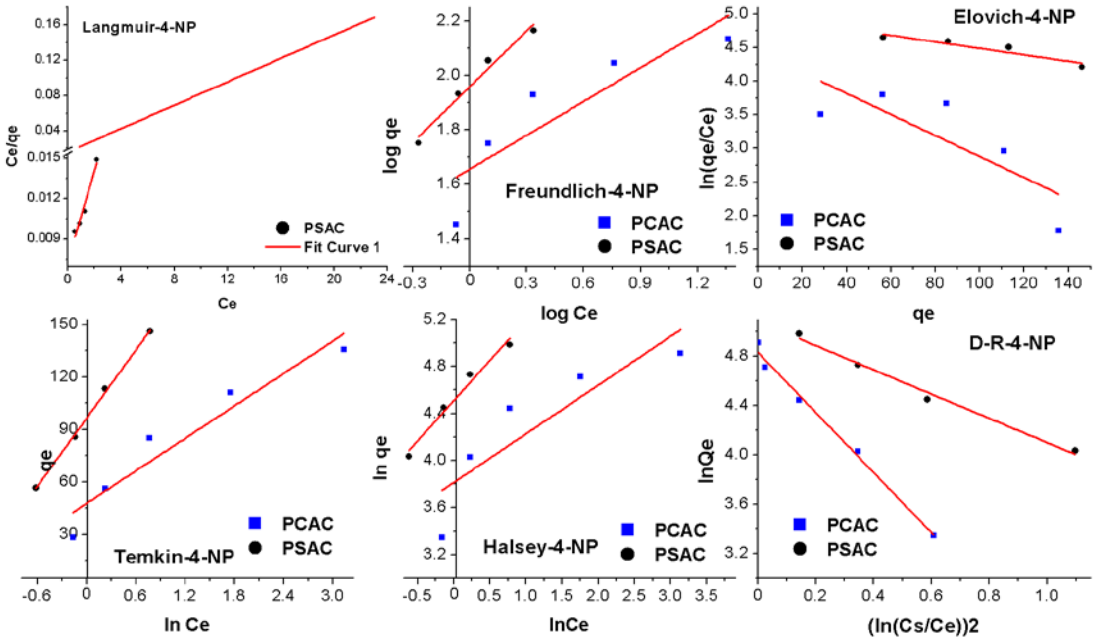

Figure 2.25 Linear plot of isotherm for 4-NP adsorption

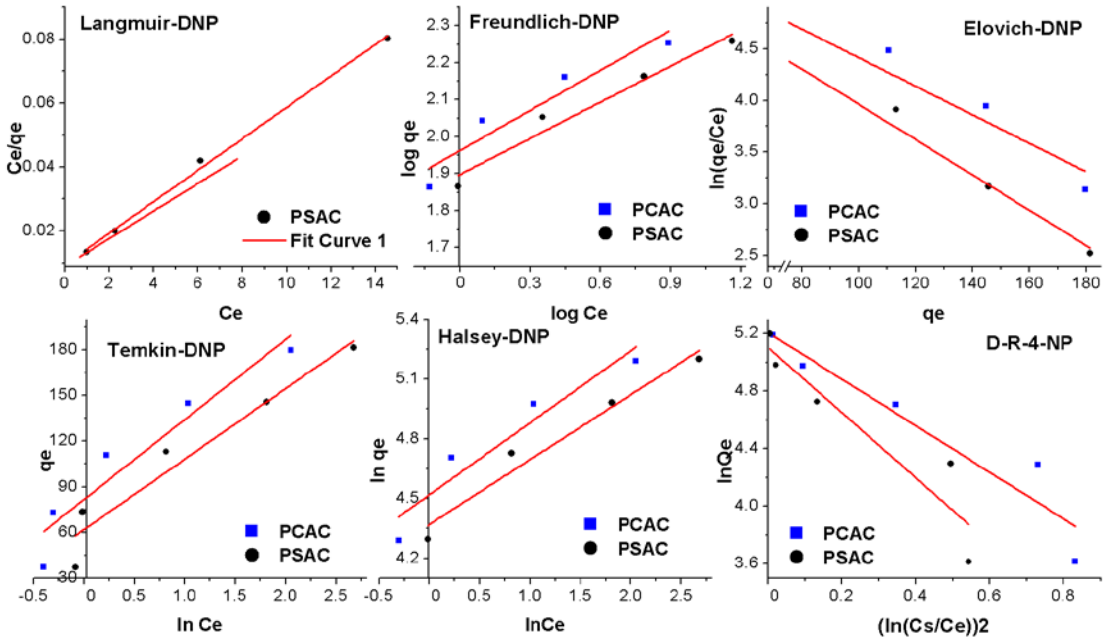

Figure 2.26 Isotherm models for DNP adsorption

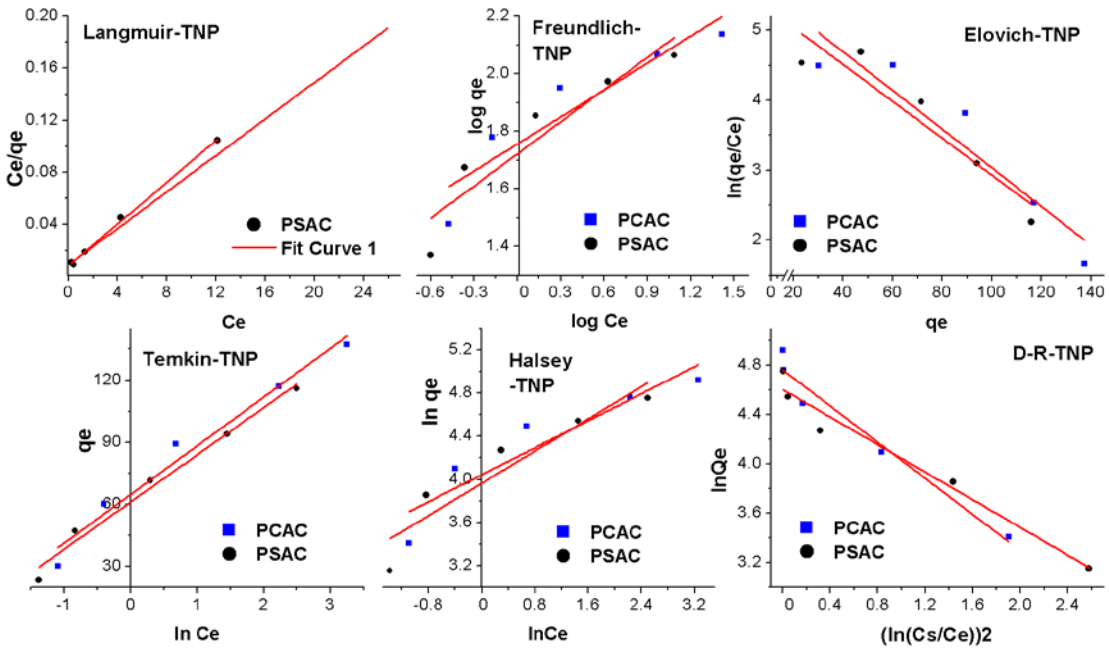

Figure 2.27 Isotherm models for TNP adsorption

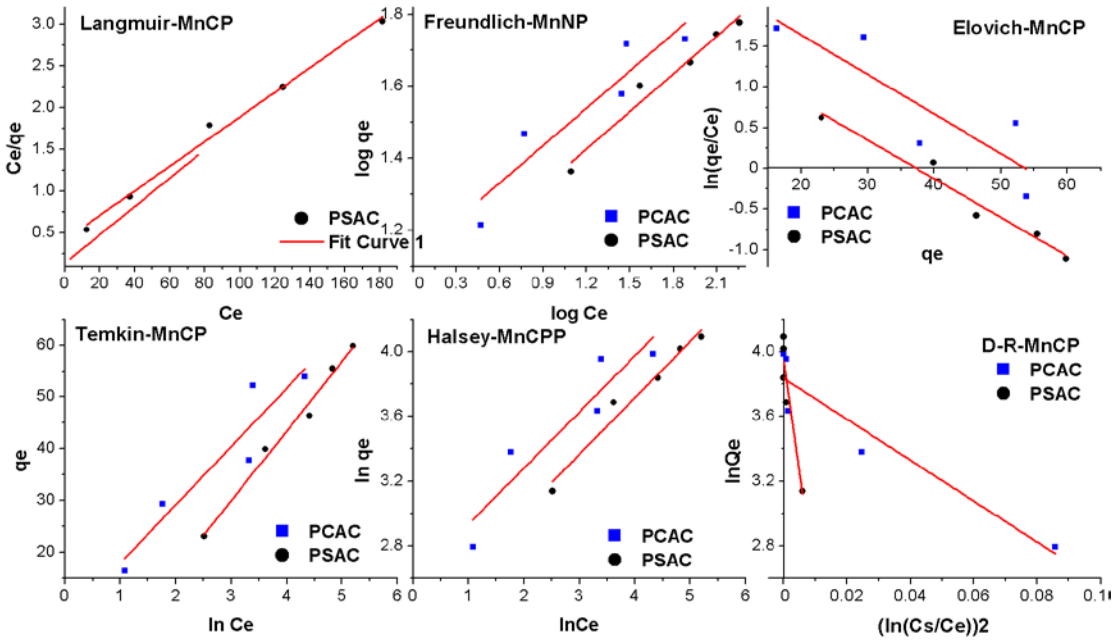

Figure 2.28 Isotherm models for MnCP adsorption

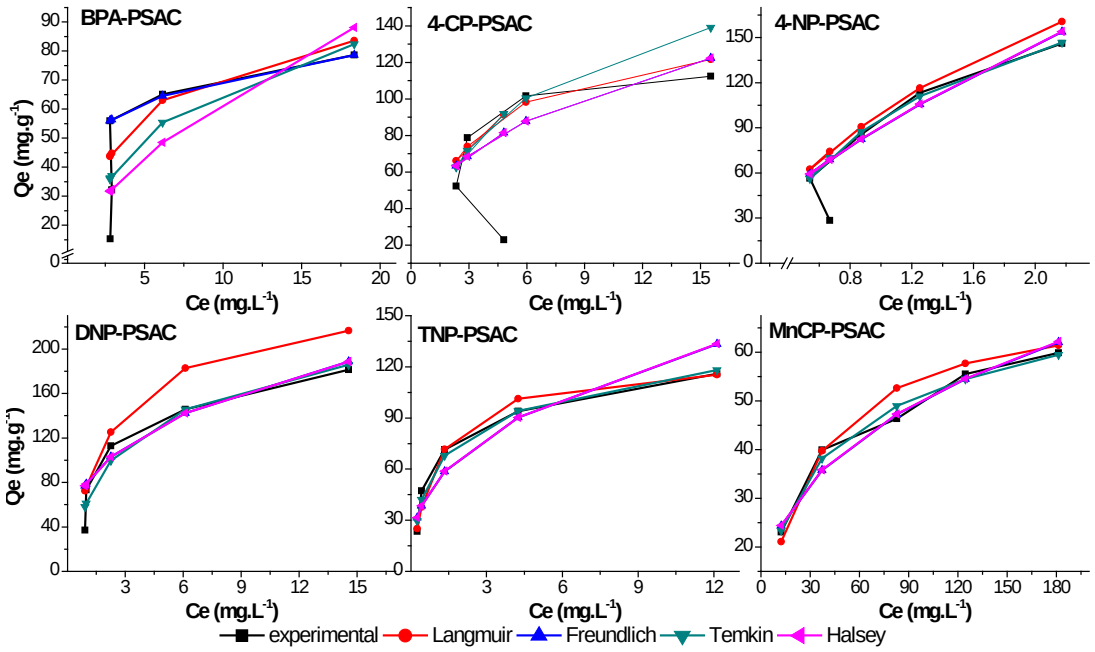

Figure 2.29 Fitting data with isotherm models using PSAC as adsorbent

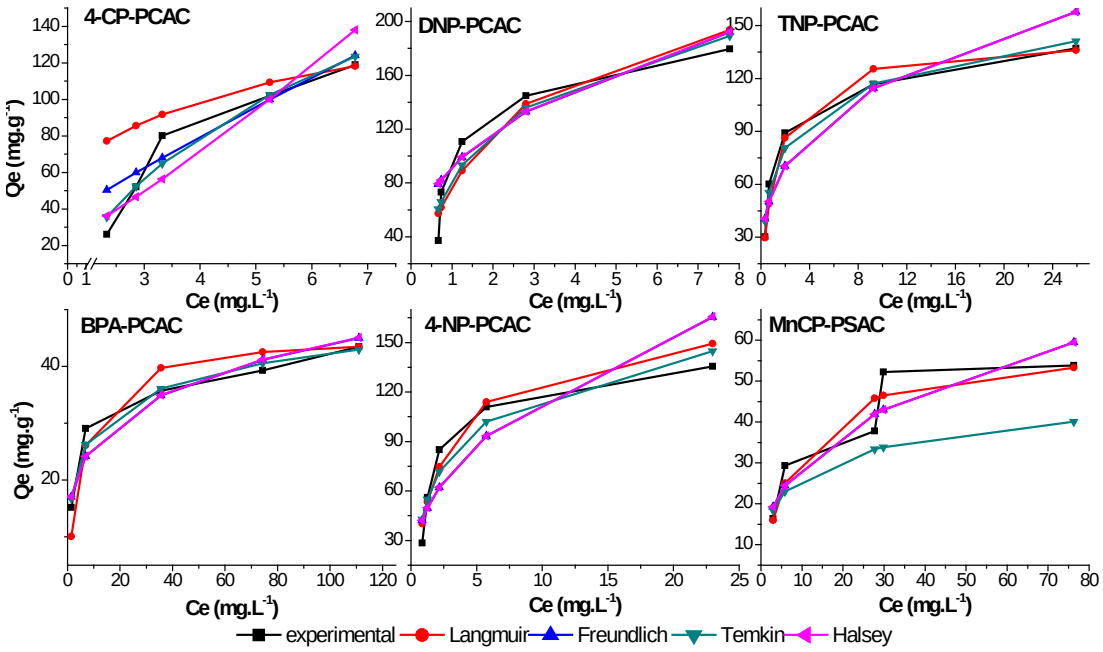

Figure 2.30 Fitting data with isotherm models using PCAC

Langmuir isotherm describes monolayer adsorption which supports chemisorption. As can be seen from Table 2.14 and 2.15, r^2 values were > 0.99 in PSAC and PCAC, and the empirical points are better represented by Langmuir plot. The isotherm constant and q_{max} which indicates maximum adsorption capacity of the adsorbents for the removal of selected pollutants obtained from the linear fit of c_e/q_e vs c_e, are listed in Tables 2.14 and 2.15 for PSAC and PCAC respectively. The maximum adsorption capacity were in order 4-NP> DNP>4-CP > TNP >BPA>MnCP for PSAC and in the order DNP >4-CP >4-NP>TNP>MnCP>BPA for PCAC respectively.

This trend is neither consistent with the polarity of these compounds: 4-NP (5,07 D) > DNP (3,3 D) > 4-CP (2.4 D) > BPA (1.41 D) TNP (1.34 D); nor solubility MnCP (100% solubility) > BPA (120 $mg.L^{-1}$) > 4-CP (24 $g.L^{-1}$) > 4-NP (16 g L-1) > TNP (12.7 $g.L^{-1}$) > DNP (2.8 $g.L^{-1}$). There are probably multiple forces affecting the sorption mechanism as discussed in section 2.6 under mechanism.

The q_m values of the adsorbates under study were found to be comparable with related literature reported adsorbents (Tables 2.16 a-f).

The Freundlich isotherm is regarded as an empirical isotherm. It indicates the surface heterogeneity of the adsorbent. Parameter n in Freundlich model is called heterogeneity factor. The exponent 1/*n* gives an indication of the favorability and capacity of the adsorbent/adsorbate system. The values of "1/n", where 1/*n* < 1;

represent favorable adsorption conditions. However based on r^2 value Freundlich isotherm was not a good fit to describe the adsorption process (Ho and McKay, 1999). Though the correlation coefficient for the Elovich plot was reasonably high the values of maximum adsorption capacity q_m was not close to the experimental adsorbed amounts at equilibrium suggesting that multilayer adsorption did not occur (Febrianto et al., 2009) for the adsorbates under study using both PSAC and PCAC.

Reasonably high correlation coefficients were obtained for PSAC using Temkin model except for BPA as adsorbate as compared to PCAC. The negative values of ΔH from positive values of adsorption energy (ΔQ) are indicative of a chemisorptive exothermic adsorption process (Hamdaoui and Naffrechoux, 2007) in both PSAC and PCAC.

Multilayer adsorption is generally discussed by the Halsey equation and was not found to fit well with the experimental data indicating that the mechanism may not involve multilayer adsorption (Halsey, 1948).

The Dubinin–Radushkevich model does not assume a homogeneous surface, like the Langmuir model. It mainly explains pore filling mechanism. The constants obtained for the D-R isotherm model i.e. k_{DR} were lower than Langmuir constant and Freundlich constants. The adsorption capacity q_{D-R} was found to be less than the Langmuir adsorption capacity. This difference in adsorption capacity could be due to different assumptions included while formulating these isotherms. The E values in the range 1–8 $kJmol^{-1}$ indicated physical adsorption. In case of BPA, 4-CP and MnCP for PSAC and PCAC, the E values were < 1 $kJmol^{-1}$.

Table 2.14 Isotherm parameters using PSAC as adsorbent

	BPA	4-CP	4-NP	DNP	TNP	MnCP
Langmuir model						
q_m ($mg.g^{-1}$)	100.0	142.86	333.33	250.0	125.0	71.43
Ka ($L.mg^{-1}$)	0.2778	0.3685	0.4286	0.4444	1.0	0.0338
r^2	0.9550	0.9820	0.9730	0.9970	0.9970	0.9920
Freundlich model						
N	5.5556	2.8818	1.4641	3.0770	2.6809	2.8736
k_F ($mg.g^{-1}$). $(L.mg^{-1})^{1/n}$	46.56	47.21	90.57	79.07	52.61	10.17
r^2	0.9990	0.7551	0.9760	0.9650	0.8820	0.9690
Elovich model						
K_E ($L.mg^{-1}$)	0.1230	0.0180	0.0040	0.0170	0.0260	0.47
q_m ($mg.g^{-1}$)	36.21	246.44	1243.0	333.18	214.12	3.7745
r^2	0.9430	0.8420	0.8890	0.9770	0.8900	0.9650
Temkin model						
B	24.67	40.32	64.98	46.31	22.78	13.44
KT ($L.mg^{-1}$)	1.5374	2.0276	4.4044	3.8071	14.69	0.4619
ΔQ ($kJ.mol^{-1}$)	102.12	62.48	38.77	54.40	110.59	187.44
ΔH ($kJ.mol^{-1}$)	-102.12	-62.48	-38.77	-54.40	-110.59	-187.44
r^2	0.6270	0.8320	0.9980	0.9390	0.9840	0.9860
Halsey model						
n_H	-1.8382	-2.8818	-1.4641	-3.0769	-2.6810	-2.8735
k_H ($mg.g^{-1}$). $(L.mg^{-1})^{1/n}$	0.0049	1.497E-05	0.0014	1.447E-06	2.424E-05	0.0012
r^2	0.4530	0.7550	0.9760	0.9650	0.8820	0.9690
D-R model						
k_{DR}	1.005E-06	9.258E-07	1.549E-07	3.571E-07	8.809E-08	2.222E-05
Q_{DR} ($mg.g^{-1}$)	76.25	118.04	161.26	165.01	99.88	52.14
r^2	0.9898	0.9580	0.9880	0.8820	0.9670	0.8940
E ($kJmol^{-1}$)	0.70545	0.73491	1.79664	1.18334	2.38250	0.15001

Table 2.15 Isotherm parameters using PCAC as adsorbent

	BPA	**4-CP**	**4-NP**	**DNP**	**TNP**	**MnCP**
Langmuir model						
q_m ($mg.g^{-1}$)	45.45	163.9	166.7	250.0	142.9	58.8
Ka ($L.mg^{-1}$)	0.1946903	0.38125	0.375	0.4444	0.7778	0.1269
r^2	0.9940	0.8340	0.9930	0.9970	0.9980	0.9770
Freundlich model						
n	4.4643	1.1848	2.4156	2.7701	3.1949	2.8902
k_F ($mg.g^{-1}$). ($L.mg^{-1}$)$^{1/n}$	15.67	24.66	45.19	91.62	57.02	13.24
r^2	0.9260	0.8770	0.7790	0.9170	0.8660	0.8770
Elovich model						
K_E ($L.mg^{-1}$)	0.1230	0.0160	0.0150	0.0130	0.0270	0.0480
q_m ($mg.g^{-1}$)	36.20	294.87	296.27	445.23	214.78	54.44
r^2	0.9430	0.9430	0.6460	0.8960	0.8890	0.7560
Temkin model						
B	6.0490	82.36	30.93	52.50	23.49	6.6560
KT ($L.mg^{-1}$)	10.99	0.6612	4.6945	4.7401	15.76	5.4125
ΔQ ($kJ.mol^{-1}$)	416.46	30.59	81.45	47.99	107.24	378.48
ΔH ($kJ.mol^{-1}$)	-416.46	-30.59	-81.45	-47.99	-107.24	-378.48
r^2	0.9730	0.6270	0.9230	0.9151	0.9731	0.9841
Halsey model						
nH	-4.4642	-0.7946	-2.4154	-2.7701	-3.1948	-2.8901
kH ($mg.g^{-1}$). ($L.mg^{-1}$)$^{1/n}$	4.60E-06	0.1353	0.0001	3.66E-06	2.456E-06	0.0006
r^2	0.9261	0.8230	0.7790	0.9171	0.8660	0.8771
D-R model						
K_{DR}	5.19E-07	2.123E-06	3.843E-07	2.55E-07	1.155E-07	1.99E-06
q_{DR} ($mg.g^{-1}$)	37.16	165.01	125.71	182.73	117.10	46.30
r^2	0.9898	0.953	0.988	0.91	0.964	0.8991
E ($kJmol^{-1}$)	0.98132	0.48535	1.14060	1.40038	2.08058	0.50129

Comparison of the study with the reported literature review.

Table 2.16a Reported ACs based adsorbent for the removal of BPA

Sr. No.	Adsorbent	Surface area ($m^2.g^{-1}$)	Q_{max} ($mg.g^{-1}$)	References
1	Activated carbon prepared from potato peels	120.35	454.6	Arampatzidou and Deliyanni, 2016
2	Activated carbon from almond shell	1216	188.9	Bautista-Toledo et al., 2005
3	(EFB-activated carbon)Palm fruit based Activated Carbon	86.62	41.98	Wirasnita et al., 2014
4	CoFe2O4/PAC composite	N/D	279.31	Li et al., 2014
5	Activated Carbon Derived from Oil Palm Empty Fruit Bunch	4.29	41.98	Wirasnita et al., 2014
6	Sugi chip	N/D	11.5	Nakanishi et al., 2002
7	Sugi sawdust	N/D	12.1	
8	Hinoki sawdust	N/D	18	
9	Esterified carboxyl Cotton	N/D	87.72	Gong et al., 2009
10	Unmodified base peat	N/D	15.97	Zhou et al., 2011
11	Modified fibric peat	N/D	29.15	
12	Graphene	N/D	182	Xu et al., 2012
13	Powdered Activated Carbon	780	178	Sui et al., 2011
14	Activated Carbon-Commercial	1225	130	Bautista-Toledo et al., 2005
15	Activated Carbon-Commercial	1084	263	
16	Activated Carbon-Almond Shell	1216	189	
17	Activated Carbon-Commercial	1777	382	Liu et al., 2009
18	Activated Carbon-Commercial	996	333	
19	Activated Carbon-Commercial	916	270	Tsai et al., 2006
20	Activated Carbon-Commercial	1060	357	
21	PSAC	604.03	100.0	Present study
22	PCAC	770.84	45.45	

N/D = Not Determined

Table 2.16b Reported ACs based adsorbent for the removal of 4-CP

Sr. No.	Adsorbent	Surface area ($m^2.g^{-1}$)	Qmax ($mg.g^{-1}$)	References
1	Agricultural Residue-based Activated Carbon	782	390	Sekirifa et al., 2013
2	Activated carbon prepared by physical method from rice husk	2681	44.64	Al-doury and Ali, 2015
3	Activated carbon prepared from date stones and palm fronds	2523	44.94	
4	Aloe vera green waste-based activated carbon	N/D	47.6	Al-doury and Ali, 2015
5	Azolla filiculoides biomass	N/D	8.24	Ali et al., 2013
6	Rice husk	N/D	44.64	Al-doury and Ali, 2015
7	Cork	N/D	93.84	Mourão et al., 2006
8	NaOH-treated CSC	N/D	54.65	Kurniawan et al., 2010
9	TiO2-treated CSC	N/D	48.42	
10	HNO3-treated CSC	N/D	23.13	
11	As-received CSC	N/D	14.88	

12	CSAC	3	72.77	Radhika and Palanivelu, 2006
13	CAC	N/D	134.01	
14	PSAC	604.03	142.86	Present study
15	PCAC	770.84	163.9	

Table 2.16c Reported ACs based adsorbent for the removal of 4-NP

Sr. No.	Adsorbent	Surface area ($m^2.g^{-1}$)	Qmax($mg.g^{-1}$)	References
1	magnetic nanoparticles (MNPs)	N/D	57.8	Mehdinia et al., 2013
2	zero-valent iron (ZVI).	N/D	72.5	Nakatsuji et al., 2015
3	Expanded Perlite	5.83	1.68	Zvezdelina et al., 2012
4	SWCNT-COOH	N/D	144.83	Moradi et al., 2012
5	SWCNTs	N/D	151.77	
6	Peat	N/D	23.39	Jaerger et al., 2015
7	MgAl-mixed oxide.	N/D	367.8	Chen et al., 2009
8	Acacia glauca sawdust	N/D	202.06	Dhorabe et al., 2016
9	olive cake based activated carbon	N/D	1.55	Abdel-Ghani et al., 2016
10	Zeolite	N/D	12.7	Varank et al., 2012
11	Bentonite	N/D	15.9	
12	PSAC	604.03	333.3	Present study
13	PCAC	770.84	166.7	

Table 2.16d Reported ACs based adsorbent for the removal of DNP

Sr. No.	Adsorbent	Surface area ($m^2.g^{-1}$)	Qmax ($mg.g^{-1}$)	References
1	yellow bentonite	N/D	3.92	Zvezdelina et al., 2012
2	Chemically treated kola nut pod	N/D	32.26	Agarry and Ogunleye, 2014
3	active carbon	2.15	277.78	Krishnan et al., 2015
4	amino functionalized imidazolium-modified silicas	605	59.81	Wang et al., 2016
5	hydrophilic molecularly imprinted polymers (MIPs)	537	138.9	Jing et al., 2014
6	PSAC	604.03	250.0	Present study
7	PCAC	770.84	250.0	

Table 2.16e Reported adsorbents for the removal of TNP

Sr. No.	Adsorbent	Surface area ($m^2.g^{-1}$)	Qmax ($mg.g^{-1}$)	References
1	Hydrotalcite	N/D	515.48	Hermosín et al., 1996
2	Amberlite IRA-67	N/D	47.16	Uslu et al., 2008
3	Hydrotalcites	N/D	160.14	Barriga et al., 2002
4	C-MCM-41	851	327.26	Sepehrian et al., 2009
5	polymeric adsorbent	400	15.0	Srivastava et al., 1995
6	Resinuous adsorbent	40	10.0	
7	Activated carbon	634	35.0	
8	Bagase fly ash	433	17.0	

9	activated carbon from almond ahell	733	74.03	Mohan et al., 2011
10	Magnetic activated carbon from almond shell	527	87.15	
11	F-400 (Calgon carbon)	N/D	327.85	
12	Activated carbon from date fruit	N/D	26.74	
13	Molybdenum ferrocynnide	25.02	52.63	
14	PSAC	604.03	125.0	Present study
15	PCAC	770.84	142.0	

Table 2.16f Reported adsorbents for the removal of MnCP

Sr. No.	Adsorbent	Surface area ($m^2.g^{-1}$)	Qmax ($mg.g^{-1}$)	References
1	Jute Fiber Carbon	N/D	71.68	Senthilkumaar et al., 2010
2	imprinted polymer	N/D	7.4	Yan et al., 2007
3	MMT-CuO	N/D	140.7	Sahithya et al., 2016
4	MMT-CuO-Ch	N/D	142.8	
5	MMT-CuO-Gg	N/D	125	
6	MMT-CuO-PLA	N/D	200	
7	PSAC	604.03	71.3	Present study
8	PCAC	770.84	58.8	

2.5.7 Thermodynamic study

The thermodynamic parameters such as change in free energy (ΔG), enthalpy (ΔH), and entropy (ΔS) for the adsorption of all six adsorbates under study using PSAC and PCAC were calculated using equations 21, 22 and 23 and are listed in Table 2.17 (a) and (b) respectively.

It was noted that the adsorption process was generally spontaneous at 303 K as indicated by the negative ΔG values for both PSAC and PCAC. The order of decreasing spontaneity at 303 K as indicated by ΔG values was DNP>4-NP>TNP>BPA>4-CP>MnCP.

The negative values of enthalpy (ΔH) suggested the adsorption was exothermic, and that the adsorption was primarily physical while the magnitude of ΔH in the range 2.1–20.9 kJ/mol indicates the heat evolved during physical adsorption (Chowdhury et al., 2011).

Further, the values of ΔS were found to be negative or very low positive values using PSAC as adsorbent which indicated a decrease of randomness at the solid–solution interface with the loading of adsorbate molecules onto the adsorbents (Chowdhury et al., 2011).

The positive values of ΔS° for BPA and TNP using PSAC as adsorbent suggested that BPA and TNP favored increased disorder and randomness at the solid–solution interface during adsorption. The randomness might be attributed to the displaced water molecules gaining more translational entropy as compared to that lost by the adsorbate molecules (BPA and TNP) during the adsorption process (Gopal and Elango, 2007).

The decrease in randomness was in the order 4-NP> MnCP >DNP>TNP>BPA> 4-CP.

Table 2.17 (a) Thermodynamic parameters for adsorption using PSAC

	Temp (°K)	**BPA**	**4-CP**	**4-NP**	**DNP**	**TNP**	**MnCP**
ΔG kJ/mole	303	-3.0879	-1.4467	-7.4781	-12.369	-3.9353	-1.507
	313	-3.0609	-1.6173	-7.4661	-12.332	-3.9012	-1.2742
	323	-3.0338	-1.788	-7.454	-12.296	-3.8672	-1.0414
	333	-3.0068	-1.9586	-7.4419	-12.26	-3.8331	-0.8087
ΔH kJ/mole		-3.9077	3.7238	-7.8439	-13.464	-4.9669	-8.5601
ΔS J/°Kmole		-0.0027	0.01706	-1.2072	-0.0036	-0.0034	-0.0233

Table 2.17 (b) Thermodynamic parameters for adsorption using PCAC

	Temperature (°K)	**BPA**	**pCP**	**pNP**	**2,4-DNP**	**2,4,6-TNP**	**MnCP**
ΔG kJ/mole	303	-4.9039	-9.2438	-6.1283	-11.653	-9.3962	-12.01
	313	-4.9048	-8.3774	-5.9505	-11.528	-10.037	-11.829
	323	-4.9058	-7.511	-5.7727	-11.404	-10.677	-11.649
	333	-4.9067	-6.6446	-5.5949	-11.279	-11.318	-11.468
ΔH kJ/mole		-4.8754	-35.496	-11.516	-15.432	10.0092	-17.483
ΔS kJ/°Kmole		0.09395	-0.0866	-17.78	-0.0125	0.06404	-18.061

2.5.8 Ionic strength study

Industrial effluent is known to contain high concentrations of salts along with pollutants, which might affect adsorption capacity of the adsorbents for the removal of pollutants. Therefore, the effect of ionic strength of the medium on the adsorption potential of PSAC and PCAC at different NaCl concentrations was investigated. It is evident from Figure 2.31 that the removal of selected pollutants was not significantly

affected even in the presence of 0.5 N NaCl. This can be attributed to the fact that adsorbate -adsorbent interactions in our study were not predominantly electrostatic.

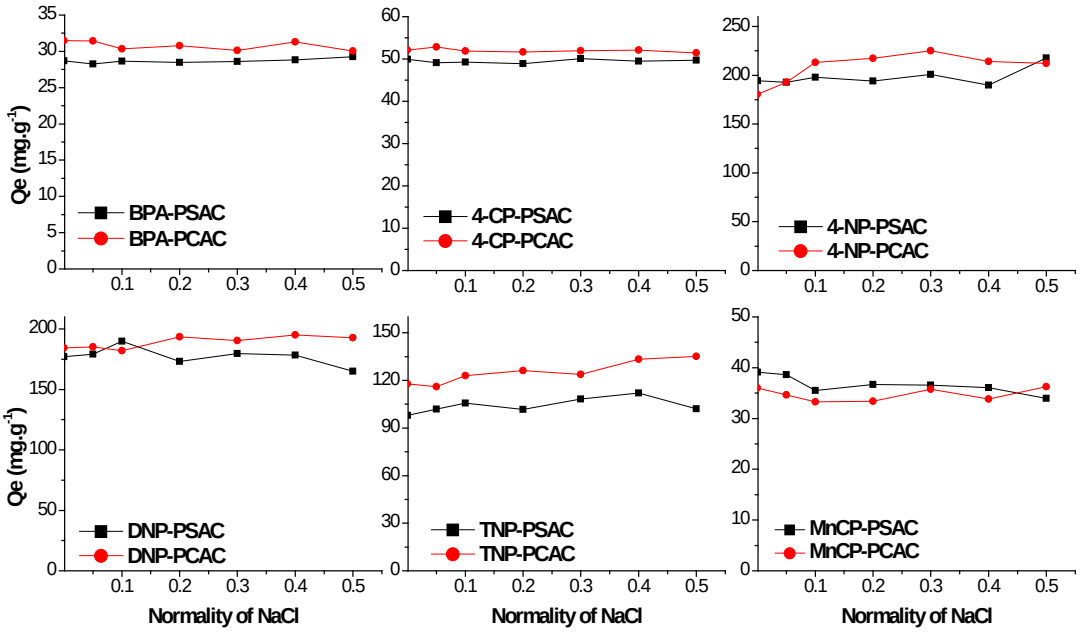

Figure 2.31 Ionic strength study for adsorption using PSAC.

2.5.9 Desorption study

Desorption study was done using different eluents like 0.1N HCl, 0.1N NaOH, Ethanol, Methanol and acetonitrile. Methanol and ethanol were observed to be better eluents. Desorption using 0.1 N HCl was observed to be moderate in case of 4-NP and DNP due to their hydrophilic nature while the recovery was < 15 % for other adsorbates under study. On the other hand 0.1 N NaOH was observed to be a better aqueous eluent as compared to 0.1 N HCl. These results support the higher adsorption in acidic condition (section 2.5.1) as compared to alkaline conditions due to less electrostatic interaction in case of alkaline medium. Organic solvents proved to be better eluents as compared to both acidic and basic eluents. Recovery was in order Acetonitrile < Ethanol ≤ Methanol. Thus methanol was selected as desorption solvent. It can be seen from Figures 2.32 and 2.33 that the recovery and reusability of adsorbent was effective up to three cycles and also the eluent can also be reused after distillation, suggesting that the use of the adsorbents could prove economical.

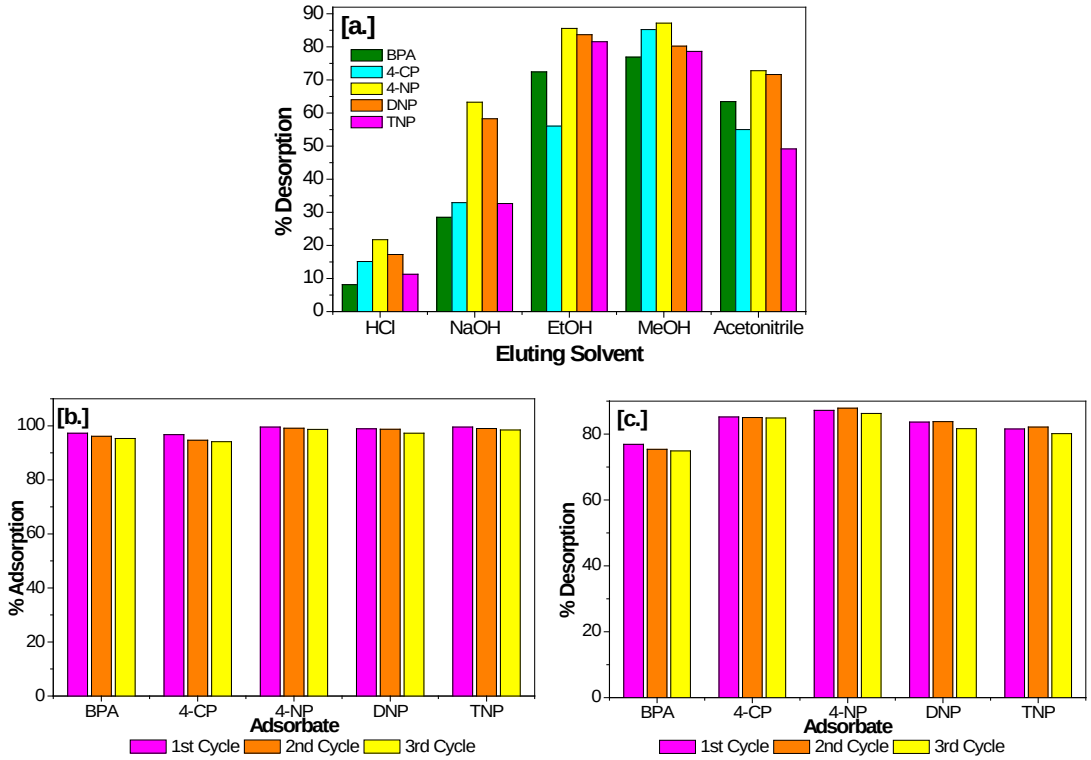

Figure 2.32 Recovery study of adsorbent-PSAC

(a.) selection of eluting solvent (b.) % Adsorption (c.) % Desorption

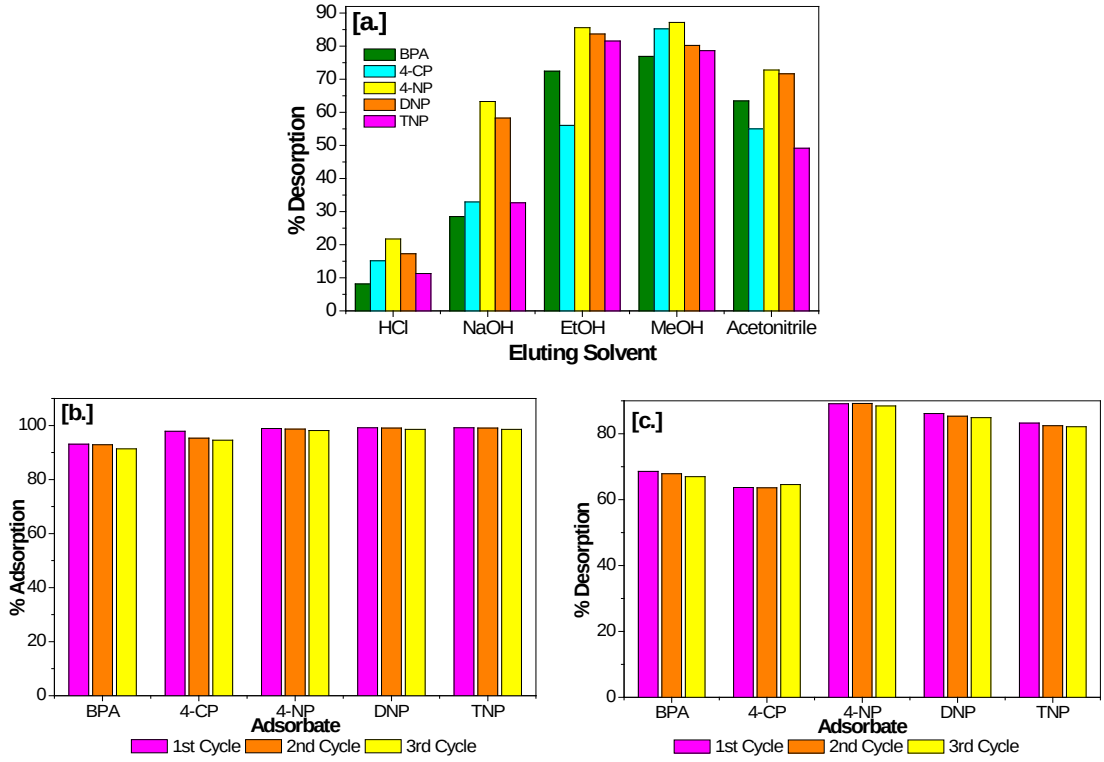

Figure 2.33 Recovery study of adsorbent-PCAC

(a.) selection of eluting solvent (b.) % Adsorption (c.) % Desorption

2.5.10 Adsorbate IR Spectral Analysis

There are more peaks in the spectrum taken after adsorption of phenols and monocrotophos with increased transmittance and further presence of peaks arising from phenol and monocrotophos molecules indicate their adsorption from aqueous solution by PSAC and PCAC. The characteristic peaks of the adsorbates under study seen in the spectra are summarised in tables 2.18 (a-e)

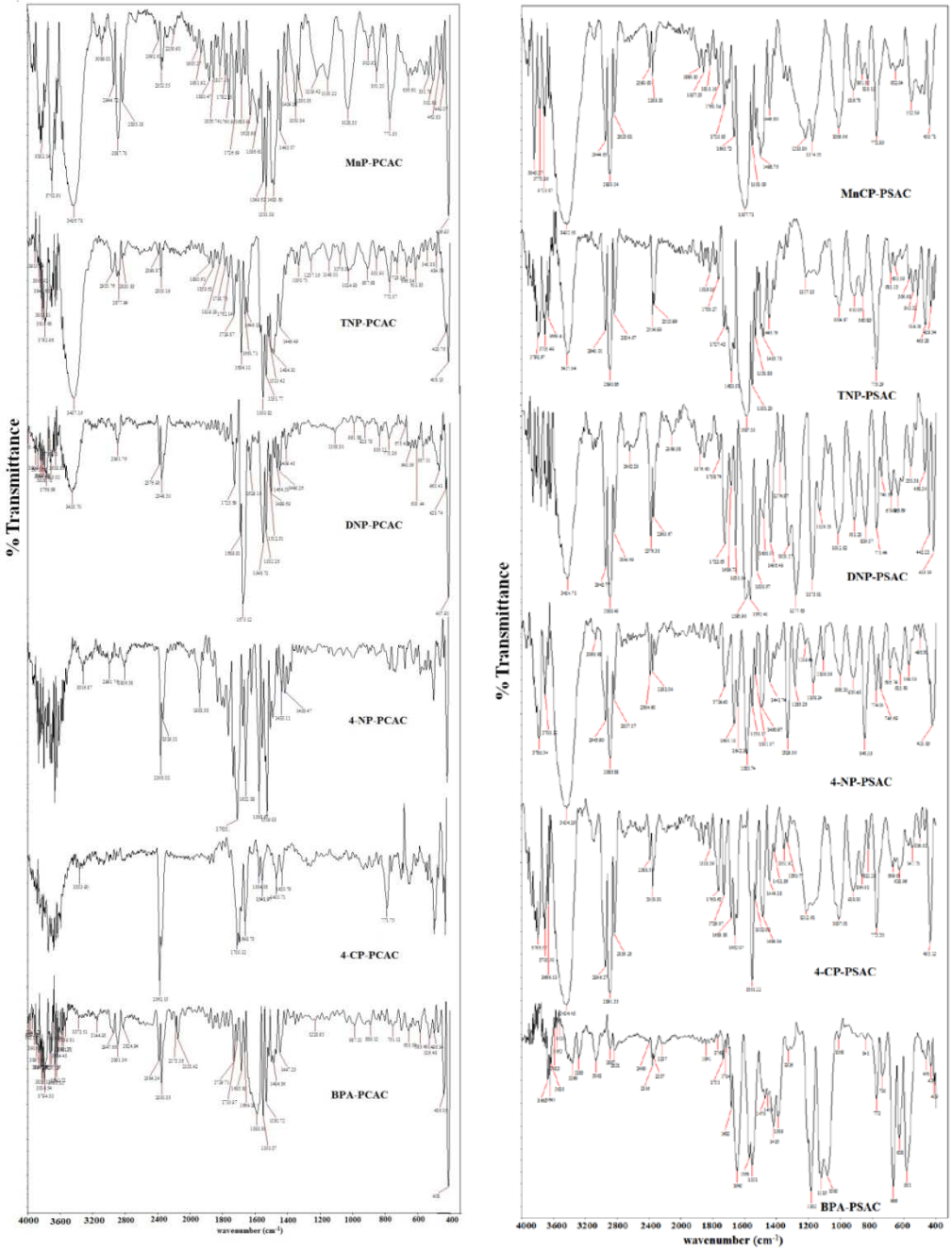

Figure 2.34 FTIR spectra of Adsorbents after adsorption study

The C−H stretching peaks appear at 3100 to 2800 cm^{-1} in the spectrum taken after adsorption of all the model pollutants under study. The peak appearing at 1380-1420 cm^{-1} indicates the existence of phenolic structure, and the peaks at 800 and 750 cm^{-1} in the fingerprint area indicate the presence of an aromatic structure, O–H out-of-plane bending and out of plane C-H bending of ring C-H vibrations (Gundogdu et al., 2012; Stuart, 2004) DNP, TNP and MnCP indicate hydrogen bonding to the adsorbents which is very weak in 4NP, 4CP and BPA.

Table 2.18a Characteristics peaks observed for TNP

Sr. No.	**Frequencies (cm^{-1})**	**Assignment** (Stuart, 2004; Xiao-Hong and Xian-Zhou, 2011)
1	1484, 1515, 1531, 1550	asymmetric stretching of NO_2
2	1257, 1330, 1318	symmetric stretching of NO_2
3	3437	O–H stretching
4	723	O–H out-of-plane bending
5	2800-3100	C−H stretching
6	1339	peak due to phenolic –OH

Table 2.18b Characteristics peaks observed for BPA

Sr. No.	**Frequencies (cm^{-1})**	**Assignment** (Stuart, 2004)
1	3373	O–H stretching
2	3044	C-H stretch aromatic
3	2947	C-H stretch aromatic
4	1530	O-H bending
5	1484, 1447	C-H bending
6	1228	C-O bending
7	2800-3100	C−H stretching
8	1338	peak due to phenolic –OH

Table 2.18c Characteristics peaks observed for 4-CP

Sr. No.	**Frequencies (cm^{-1})**	**Assignment** (Stuart, 2004)
1	3353	O–H stretching
2	1564, 1541, 1590, 1455	C-H bending
3	1420	C-H stretch aromatic
4	1090	C-H bending
5	772	C-Cl stretching
6	2800-3100	C−H stretching
7	1335	peak due to phenolic –OH

Table 2.18d Characteristics peaks observed for 4-NP

Sr. No.	Frequencies (cm^{-1})	Assignment (Chiș, 2004; Stuart, 2004)
1	3316	O–H stretching
2	2991	C-H bending
3	1610, 1590	-C=C stretching
4	1499, 1340	NO_2 group asymmetric
5	750	para substituted benzene
6	2800-3100	C−H stretching
7	1339	peak due to phenolic –OH

Table 2.18e Characteristics peaks observed of DNP

Sr. No.	Frequencies (cm^{-1})	Assignment (Stuart, 2004; Yadav RA, 2015)
1	3453	O–H stretching
2	1582	asymmetric NO_2
3	1512	C-O stretching
4	1409	C-O-H bending
5	1108	symmetric NO_2
6	2800-3100	C−H stretching
7	1334	peak due to phenolic –OH

Table 2.18f Characteristics peaks observed of MnCP

Sr. No.	Frequencies (cm^{-1})	Assignment (Bhalerao and Puranik, 2009; Furniss et al., 1992; Stuart, 2004; Zhu et al., 2006)
1	3618, 3543	N–H groups stretching
2	1665	O=CN-H
3	1483, 1445	N-H deformation
4	918, 749	aliphatic phosphate groups
5	1218	P=O stretching
6	1443	C=C deformation
7	1174, 1009	P-O-C asymmetric and symmetric stretching
8	1597	protonated secondary amino group
9	2800-3100	C−H stretching

2.6 Mechanism

The adsorbates under study interact with the functional group present on carbon surface by different mechanisms. The carbonyl, and oxygen groups which are present on the carbon(as evidenced by IR and XPS) may act as electron donor and interact with the aromatic rings of adsorbates (phenols) which may act as electron acceptors a

typical "donor–acceptor mechanism" (Mattson and Mark, 1971). Further π–π interactions between electrons in phenols and aromatic rings of the carbon basal planes may also contributes to uptake of phenols onto PSAC and PCAC (Coughlin et al., 1968; Liu et al., 2009). Several researchers have reported that π-π interactions were responsible for adsorption of phenols and chlorophenols in neutral and ionic forms on PSAC and PCAC (Diaz-Flores et al., 2006; Li et al., 2009).

Another possible interaction could be hydrogen bonding between the OH groups, amino and phosphate groups of adsorbates with the carboxyl and phenolic groups of carbons. In the case of nitrophenol the electron density in the aromatic ring is decreased because of the -NO_2 group in 4-nitrophenol in comparison to other phenols under study. Further, the functional groups in 4 NP are at para position, making it more susceptible to adsorption by π–π interactions.

Considering the adsorption process of TNP, at ~pH 2.0 the surface of PSAC would be positively charged while PCAC upto pH 3.5. At pH 2 TNP would exist as triphenoxide to some extent leading to electrostatic interactions between TNP and PSAC as well as PSAC. At highr pH conditions PSAC would have negative surface charge and PCAC would become less positive while TNP would further exist predominantly as triphenoxide anion. So the electostatic attractions would become minimal. However there is only 12% decerease in adsorption at higher pH conditions for PSAC while in the case of PCAC the decrease was around 17% with change in pH from 2 to 3 after which the adsorption performance was relatively constant with pH. Further TNP which is a strong acid can protonate basic sites of PSAC and PCAC and the TNP anion could then be attracted electrostatically to the positive protonated sites. The other interactions of TNP with PSAC and PCAC could be π–π interactions as well as hydrogen bonding interactions between –COOH and –OH surface functionalities with the nitro group oxygen's (H-bond acceptors) and the acidic –OH (H-bond donor) of TNP and also dipole–dipole attractions (Figure 2.34).

The optimum pH for uptake of 4-CP was at neutral pH, in which 4-CP is in the nonionic form (pKa= 9.38) and thus the adsorption must be governed by non-electrostatic interactions between the solute molecule and sorbent surface, i.e., the π–π interactions between the solute aromatic ring and the adsorbent as well as hydrogen bonding

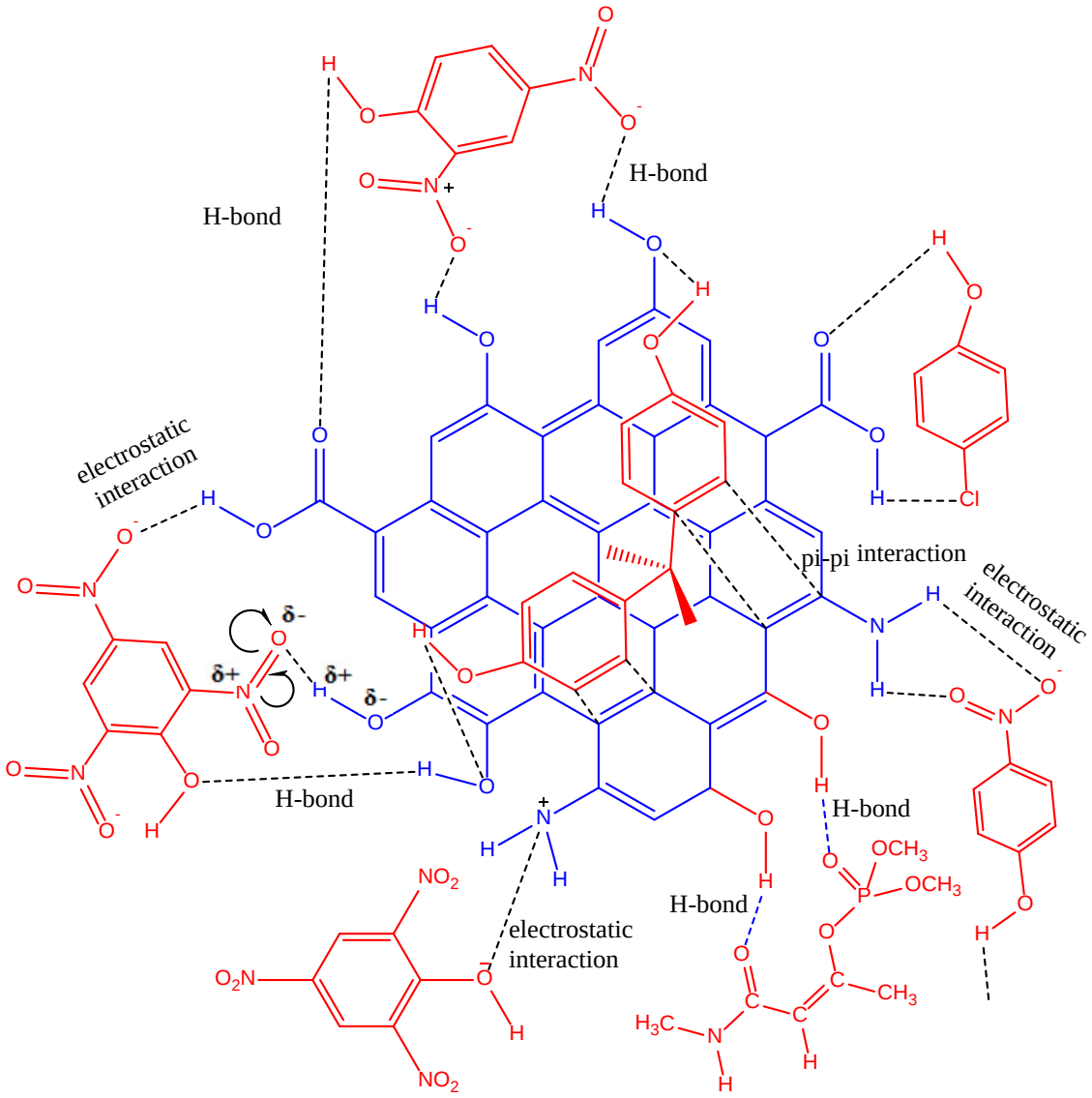

Figure 2.35 proposed mechanism for the interaction between adsorbent and pollutants

The strong electronegativity of Cl atom in chlorophenol decreases the electron density of benzene ring and makes chlorophenol a π–electron acceptor. The π–π interaction will be enhanced by the decrease in electron density of benzene ring as in the case of nitrophenols (Ding et al., 2016).

On the other hand polar groups on the AC surface could bind water molecules and facilitate formation of denser water molecule clusters, and thus facilitate hydrogen bonding in monocrotophos (Peng et al., 2016). Adsorption of monocrotophos on PCAC is less than in PSAC.

2.7 Conclusions

Four activated carbons (SPAC, PSAC, PCAC and PAC) using a combination of physical and chemical activation methods have been fabricated from palm shell powder. The prepared carbons where characterized using different analytical techniques. The XRD of the ACs showed amorphous nature, PSAC and PCAC exhibited better adsorption capacity as compared to SPAC and PCAC for removal of BPA, 4-CP, 4-NP, DNP, TNP and MnCP studied as model pollutants. The optimized adsorption parameters were studied for understanding kinetics, isotherm and thermodynamics of adsorption. The most suitable kinetics followed was pseudo-second order and elovich model. The isotherm followed was Langmuir. The thermodynamic study showed the spontaneous behavior of adsorption. Apart from van der waals forces and electrostatic interaction, H-bonding and π-π interaction were found to be responsible for the adsorption. The adsorption capacities were found to be comparable/ higher as compared to literature reported adsorbents for the model pollutants under study.

2.8 References:

Abdel-Ghani, N.T., Rawash, E.S.A., El-Chaghaby, G.A., 2016. Equilibrium and kinetic study for the adsorption of p-nitrophenol from wastewater using olive cake based activated carbon. Glob. J. Environ. Sci. Manag. 2, 11–18. doi:10.7508/gjesm.2016.01.002

Agarry, S., Ogunleye, O., 2014. Chemically treated kola nut pod as low-cost natural adsorbent for the removal of 2,4-dinitrophenol from synthetic wastewater: Batch equilibrium, kinetic, and thermodynamic modelling studies. Turkish J. Eng. Environ. Sci. 38, 11–40. doi:10.3906/muh-1304-24

Ahmaruzzaman, M., Gayatri, S.L., 2011. Activated neem leaf: A novel adsorbent for the removal of phenol, 4-nitrophenol, and 4-chlorophenol from aqueous solutions. J. Chem. Eng. Data 56, 3004–3016. doi:10.1021/je100937r

Al-doury, M.M.I., Ali, S.S., 2015. Removal of Phenol and Parachlorophenol from Synthetic Wastewater Using Prepared Activated Carbon from Agricultural Wastes. Int. J. Sustain. Green Energy 4, 92–101. doi:10.11648/j.ijrse.20150403.14

Ali, M., Balarak, D., Mahdavi, Y., 2013. Application of Azolla for 2, 4, 6-Trichlorophenol (TCP) Removal from Aqueous Solutions. Arch. Hyg. Sci. 2, 143–149.

Altintig, E., Kirkil, S., 2016. Preparation and properties of Ag-coated activated carbon nanocomposites produced from wild chestnut shell by $ZnCl_2$ activation. J. Taiwan Inst. Chem. Eng. 63, 180–188. doi:http://dx.doi.org/10.1016/j.jtice.2016.02.032

An, D., Westerhoff, P., Zheng, M., Wu, M., Yang, Y., Chiu, C.-A., 2015. UV-activated persulfate oxidation and regeneration of NOM-Saturated granular activated carbon. Water Res. 73, 304–310. doi:http://dx.doi.org/10.1016/j.watres.2015.01.040

Angın, D., Altintig, E., Köse, T.E., 2013. Influence of process parameters on the

surface and chemical properties of activated carbon obtained from biochar by chemical activation. Bioresour. Technol. 148, 542–549. doi:http://dx.doi.org/10.1016/j.biortech.2013.08.164

Antonio-Cisneros, C.M., Elizalde-González, M.P., 2010. Characterization of Manihot residues and preparation of activated carbon. Biomass and Bioenergy 34, 389–395. doi:http://dx.doi.org/10.1016/j.biombioe.2009.12.001

Arami-Niya, A., Daud, W.M.A.W., Mjalli, F.S., 2010. Using granular activated carbon prepared from oil palm shell by $ZnCl_2$ and physical activation for methane adsorption. J. Anal. Appl. Pyrolysis 89, 197–203. doi:http://dx.doi.org/10.1016/j.jaap.2010.08.006

Arampatzidou, A.C., Deliyanni, E.A., 2016. Comparison of activation media and pyrolysis temperature for activated carbons development by pyrolysis of potato peels for effective adsorption of endocrine disruptor bisphenol-A. J. Colloid Interface Sci. 466, 101–112. doi:http://dx.doi.org/10.1016/j.jcis.2015.12.003

Aravindhan, R., Rao, J.R., Nair, B.U., 2009. Application of a chemically modified green macro alga as a biosorbent for phenol removal. J. Environ. Manage. 90, 1877–1883. doi:http://dx.doi.org/10.1016/j.jenvman.2008.12.005

Aroua, M.K., Leong, S.P.P., Teo, L.Y., Yin, C.Y., Daud, W.M.A.W., 2008. Real-time determination of kinetics of adsorption of lead(II) onto palm shell-based activated carbon using ion selective electrode. Bioresour. Technol. 99, 5786–5792. doi:http://dx.doi.org/10.1016/j.biortech.2007.10.010

Aworn, A., Thiravetyan, P., Nakbanpote, W., 2009. Preparation of CO_2 activated carbon from corncob for monoethylene glycol adsorption. Colloids Surfaces A Physicochem. Eng. Asp. 333, 19–25. doi:http://dx.doi.org/10.1016/j.colsurfa.2008.09.021

Aworn, A., Thiravetyan, P., Nakbanpote, W., 2008. Preparation and characteristics of agricultural waste activated carbon by physical activation having micro- and mesopores. J. Anal. Appl. Pyrolysis 82, 279–285. doi:http://dx.doi.org/10.1016/j.jaap.2008.04.007

Bağda, E., Erşan, M., Bağda, E., 2013. Investigation of adsorptive removal of tetracycline with sponge like, Rosa canina gall extract modified, polyacrylamide cryogels. J. Environ. Chem. Eng. 1, 1079–1084. doi:http://dx.doi.org/10.1016/j.jece.2013.08.024

Barriga, C., Gaitan, M., Pavlovic, I., Ulibarri, M.A., Hermosin, M.C., Cornejo, J., 2002. Hydrotalcites as sorbent for 2,4,6-trinitrophenol: influence of the layer composition and interlayer anion. J. Mater. Chem. 12, 1027–1034. doi:10.1039/B107979B

Bautista-Toledo, I., Ferro-Garcia, M.A., Rivera-Utrilla, J., Moreno-Castilla, C., Vegas Fernandez, F.J., 2005. Bisphenol A removal from water by activated carbon. Effects of carbon characteristics and solution chemistry. Environ. Sci. Technol. 39, 6246–6250.

Bello, O.S., Adegoke, K.A., Akinyunni, O.O., 2015. Preparation and characterization of a novel adsorbent from *Moringa oleifera* leaf. Appl. Water Sci. 1–11. doi:10.1007/s13201-015-0345-4

Belyaeva, O. V, Krasnova, T.A., Semenova, S.A., 2011. Effect of modification of granulated activated carbons with ozone on their properties. Russ. J. Appl. Chem. 84, 597–601. doi:10.1134/S1070427211040070

Bhalerao, T.S., Puranik, P.R., 2009. Microbial degradation of monocrotophos by Aspergillus oryzae. Int. Biodeterior. Biodegradation 63, 503–508. doi:http://dx.doi.org/10.1016/j.ibiod.2008.11.011

Bhatnagar, A., Hogland, W., Marques, M., Sillanpää, M., 2013. An overview of the modification methods of activated carbon for its water treatment applications. Chem. Eng. J. 219, 499–511. doi:http://dx.doi.org/10.1016/j.cej.2012.12.038

Boehm, H.P., 1994. Some aspects of the surface chemistry of carbon blacks and other carbons. Carbon N. Y. 32, 759–769. doi:http://dx.doi.org/10.1016/0008-6223(94)90031-0

Bonarowska, M., Raróg-Pilecka, W., Karpiński, Z., 2011. The use of active carbon

pretreated at 2173 K as a support for palladium catalysts for hydrodechlorination reactions. Catal. Today 169, 223–231. doi:http://dx.doi.org/10.1016/j.cattod.2010.12.039

Bouchelta, C., Medjram, M.S., Bertrand, O., Bellat, J.-P., 2008. Preparation and characterization of activated carbon from date stones by physical activation with steam. J. Anal. Appl. Pyrolysis 82, 70–77. doi:http://dx.doi.org/10.1016/j.jaap.2007.12.009

Bouchelta, C., Medjram, M.S., Zoubida, M., Chekkat, F.A., Ramdane, N., Bellat, J.-P., 2012. Effects of pyrolysis conditions on the porous structure development of date pits activated carbon. J. Anal. Appl. Pyrolysis 94, 215–222. doi:http://dx.doi.org/10.1016/j.jaap.2011.12.014

Boyd, G.E., Adamson, A.W., Myers, L.S.J., 1947. The exchange adsorption of ions from aqueous solutions by organic zeolites; kinetics. J. Am. Chem. Soc. 69, 2836–2848.

Budinova, T., Ekinci, E., Yardim, F., Grimm, A., Björnbom, E., Minkova, V., Goranova, M., 2006. Characterization and application of activated carbon produced by H_3PO_4 and water vapor activation. Fuel Process. Technol. 87, 899–905. doi:http://dx.doi.org/10.1016/j.fuproc.2006.06.005

Cabal, B., Budinova, T., Ania, C.O., Tsyntsarski, B., Parra, J.B., Petrova, B., 2009. Adsorption of naphthalene from aqueous solution on activated carbons obtained from bean pods. J. Hazard. Mater. 161, 1150–1156. doi:http://dx.doi.org/10.1016/j.jhazmat.2008.04.108

Campbell, Q.P., Bunt, J.R., Kasaini, H., Kruger, D.J., 2012. The preparation of activated carbon from South African coal. J. South. African Inst. Min. Metall. 112, 37–44.

Chen, S., Xu, Z.P., Zhang, Q., Lu, G.Q.M., Hao, Z.P., Liu, S., 2009. Studies on adsorption of phenol and 4-nitrophenol on MgAl-mixed oxide derived from MgAl-layered double hydroxide. Sep. Purif. Technol. 67, 194–200. doi:http://dx.doi.org/10.1016/j.seppur.2009.03.016

Cheng, C., Liu, H., Dai, P., Shen, X., Zhang, J., Zhao, T., Zhu, Z., 2016. Microwave-assisted preparation and characterization of mesoporous activated carbon from mushroom roots by phytic acid ($C_6H_{18}O_{24}P_6$) activation. J. Taiwan Inst. Chem. Eng. 67, 532–537. doi:http://dx.doi.org/10.1016/j.jtice.2016.08.032

Chin, H.C., 1981. Preparation and characterization of carbon-sulfur surface compounds. Carbon N. Y. 19, 175–186. doi:http://dx.doi.org/10.1016/0008-6223(81)90040-3

Chiș, V., 2004. Molecular and vibrational structure of 2,4-dinitrophenol: FT-IR, FT-Raman and quantum chemical calculations. Chem. Phys. 300, 1–11. doi:http://dx.doi.org/10.1016/j.chemphys.2004.01.003

Chiu, C.-A., Hristovski, K., Huling, S., Westerhoff, P., 2013. In-situ regeneration of saturated granular activated carbon by an iron oxide nanocatalyst. Water Res. 47, 1596–1603. doi:http://dx.doi.org/10.1016/j.watres.2012.12.021

Chowdhury, S., Chakraborty, S., Saha, P., 2011. Biosorption of Basic Green 4 from aqueous solution by *Ananas comosus* (pineapple) leaf powder. Colloids Surf. B. Biointerfaces 84, 520–527. doi:10.1016/j.colsurfb.2011.02.009

Chowdhury, Z.Z., Hamid, S.B.A., Das, R., Hasan, M.R., Zain, S.M., Khalid, K., Uddin, M.N., 2013. Preparation of carbonaceous adsorbents from lignocellulosic biomass and their use in removal of contaminants from aqueous solution. BioResources 8, 6523–6555.

Cimino, R., Cychosz, K.A., Thommes, M., Neimark, A. V, 2013. Experimental and theoretical studies of scanning adsorption–desorption isotherms. Colloids Surfaces A Physicochem. Eng. Asp. 437, 76–89. doi:http://dx.doi.org/10.1016/j.colsurfa.2013.03.025

Coughlin, R.W., Ezra, F.S., Tan, R.N., 1968. Influence of chemisorbed oxygen in adsorption onto carbon from aqueous solution. J. Colloid Interface Sci. 28, 386–396. doi:10.1016/0021-9797(68)90069-6

Delamar, M., Désarmot, G., Fagebaume, O., Hitmi, R., Pinsonc, J., Savéant, J.-M.,

1997. Modification of carbon fiber surfaces by electrochemical reduction of aryl diazonium salts: Application to carbon epoxy composites. Carbon N. Y. 35, 801–807. doi:http://dx.doi.org/10.1016/S0008-6223(97)00010-9

Demiral, H., Demiral, İ., Karabacakoğlu, B., Tümsek, F., 2011. Production of activated carbon from olive bagasse by physical activation. Chem. Eng. Res. Des. 89, 206–213. doi:http://dx.doi.org/10.1016/j.cherd.2010.05.005

Dhorabe, P.T., Lataye, D.H., Ingole, R.S., 2016. Removal of 4-nitrophenol from aqueous solution by adsorption onto activated carbon prepared from *Acacia glauca* sawdust. Water Sci. Technol. 73, 955–966. doi:10.2166/wst.2015.575

Diaz-Flores, P.E., Leyva-Ramos, R., Guerrero-Coronado, R.M., Mendoza-Barron, J., 2006. Adsorption of Pentachlorophenol from Aqueous Solution onto Activated Carbon Fiber. Ind. Eng. Chem. Res. 45, 330–336. doi:10.1021/ie050507o

Ding, H., Li, X., Wang, J., Zhang, X., Chen, C., 2016. Adsorption of chlorophenols from aqueous solutions by pristine and surface functionalized single-walled carbon nanotubes. J. Environ. Sci. 43, 187–198. doi:http://dx.doi.org/10.1016/j.jes.2015.09.004

Dubinin, M.M., Radushkevich, L. V., 1947. Equation of the Characteristic Curve of Activated Charcoal. Proc. Acad. Sci. USSR 55, 331–333.

Elovich, S.Y., Larionov, O.G., 1962. Theory of adsorption from nonelectrolyte solutions on solid adsorbents. Bull. Acad. Sci. USSR, Div. Chem. Sci. 11, 191–197. doi:10.1007/BF00908016

Esfandiari, A., Kaghazchi, T., Soleimani, M., 2012. Preparation and evaluation of activated carbons obtained by physical activation of polyethyleneterephthalate (PET) wastes. J. Taiwan Inst. Chem. Eng. 43, 631–637. doi:http://dx.doi.org/10.1016/j.jtice.2012.02.002

Febrianto, J., Kosasih, A.N., Sunarso, J., Ju, Y.-H., Indraswati, N., Ismadji, S., 2009. Equilibrium and kinetic studies in adsorption of heavy metals using biosorbent: A summary of recent studies. J. Hazard. Mater. 162, 616–645.

doi:http://dx.doi.org/10.1016/j.jhazmat.2008.06.042

Foroushani, F.T., Tavanai, H., Hosseini, F.A., 2016. An investigation on the effect of $KMnO_4$ on the pore characteristics of pistachio nut shell based activated carbon. Microporous Mesoporous Mater. 230, 39–48. doi:http://dx.doi.org/10.1016/j.micromeso.2016.04.030

Freundlich, H.M.F., 1906. Over the Adsorption in Solution. J. Phys. Chem. 57, 385–471.

Fu, K., Yue, Q., Gao, B., Sun, Y., Zhu, L., 2013. Preparation, characterization and application of lignin-based activated carbon from black liquor lignin by steam activation. Chem. Eng. J. 228, 1074–1082. doi:http://dx.doi.org/10.1016/j.cej.2013.05.028

Furniss, B.S., Smith, G.P.W., Hannaford, A.J., Tatchell, A.R., 1992. Textbook of Practical Organic Chemistry 5th ed.

Gao, H., Chen, J., Zhang, Y., Zhou, X., 2016. Sulfate radicals induced degradation of Triclosan in thermally activated persulfate system. Chem. Eng. J. 306, 522–530. doi:http://dx.doi.org/10.1016/j.cej.2016.07.080

Gao, Y., Xu, S., Ortaboy, S., Kan, Y., Yue, Q., Gao, B., 2016. Preparation of well-developed mesoporous activated carbon with high yield by ammonium polyphosphate activation. J. Taiwan Inst. Chem. Eng. 66, 394–399. doi:http://dx.doi.org/10.1016/j.jtice.2016.06.037

García, A.B., Martínez-Alonso, A., y Leon, C.A.L., Tascón, J.M.D., 1998. Modification of the surface properties of an activated carbon by oxygen plasma treatment. Fuel 77, 613–624. doi:http://dx.doi.org/10.1016/S0016-2361(97)00111-7

Ghauch, A., Tuqan, A.M., Kibbi, N., 2012. Ibuprofen removal by heated persulfate in aqueous solution: A kinetics study. Chem. Eng. J. 197, 483–492. doi:http://dx.doi.org/10.1016/j.cej.2012.05.051

Gong, R., Liang, J., Chen, J., Huang, F., 2009. Removal of bisphenol A from aqueous solution by hydrophobic sorption of hemimicelles. Int. J. Environ. Sci. & Technol. 6, 539–544. doi:10.1007/BF03326093

Gopal, V., Elango, K.P., 2007. Kinetic and thermodynamic investigations of adsorption of fluoride onto activated Aloe vera carbon. J. Indian Chem. Soc. 84, 1114–1118.

Gundogdu, A., Duran, C., Senturk, H.B., Soylak, M., Ozdes, D., Serencam, H., Imamoglu, M., 2012. Adsorption of Phenol from Aqueous Solution on a Low-Cost Activated Carbon Produced from Tea Industry Waste: Equilibrium, Kinetic, and Thermodynamic Study. J. Chem. Eng. Data 57, 2733–2743. doi:10.1021/je300597u

Guo, J., Xu, W.S., Chen, Y.L., Lua, A.C., 2005. Adsorption of NH3 onto activated carbon prepared from palm shells impregnated with H_2SO_4. J. Colloid Interface Sci. 281, 285–290. doi:10.1016/j.jcis.2004.08.101

Guo, Y., Rockstraw, D.A., 2007. Physicochemical properties of carbons prepared from pecan shell by phosphoric acid activation. Bioresour. Technol. 98, 1513–1521. doi:http://dx.doi.org/10.1016/j.biortech.2006.06.027

Gupta, S. Sen, Bhattacharyya, K.G., 2006. Adsorption of Ni(II) on clays. J. Colloid Interface Sci. 295, 21–32. doi:http://dx.doi.org/10.1016/j.jcis.2005.07.073

Halsey, G., 1948. Physical Adsorption on Non-Uniform Surfaces. J. Chem. Phys. 16, 931–937. doi:10.1063/1.1746689

Hamdaoui, O., Naffrechoux, E., 2007. Modeling of adsorption isotherms of phenol and chlorophenols onto granular activated carbon: Part I. Two-parameter models and equations allowing determination of thermodynamic parameters. J. Hazard. Mater. 147, 381–394. doi:http://dx.doi.org/10.1016/j.jhazmat.2007.01.021

Hermosín, M.C., Pavlovic, I., Ulibarri, M.A., Cornejo, J., 1996. Hydrotalcite as sorbent for trinitrophenol: Sorption capacity and mechanism. Water Res. 30, 171–177. doi:http://dx.doi.org/10.1016/0043-1354(95)00088-3

Hesas, R.H., Daud, W.M.A.W., Sahu, J.N., Arami-Niya, A., 2013. The effects of a microwave heating method on the production of activated carbon from agricultural waste: A review. J. Anal. Appl. Pyrolysis 100, 1–11. doi:http://dx.doi.org/10.1016/j.jaap.2012.12.019

Hirunpraditkoon, S., Tunthong, N., Ruangchai, A., Nuithitikul, K., 2011. Adsorption Capacities of Activated Carbons Prepared from Bamboo by KOH Activation. World Acad. Sci. Eng. Technol. 5, 591–595.

Ho, Y.-S., 2006. Review of second-order models for adsorption systems. J. Hazard. Mater. 136, 681–689. doi:http://dx.doi.org/10.1016/j.jhazmat.2005.12.043

Ho, Y.S., Mckay, G., 1998. The kinetics of sorption of basic dyes from aqueous solution by sphagnum moss peat. Can. J. Chem. Eng. 76, 822–827. doi:10.1002/cjce.5450760419

Ho, Y.S., McKay, G., 1999. Comparative sorption kinetic studies of dye and aromatic compounds onto fly ash. J. Environ. Sci. Heal. Part A 34, 1179–1204. doi:10.1080/10934529909376889

Huang, K.-C., Couttenye, R.A., Hoag, G.E., 2002. Kinetics of heat-assisted persulfate oxidation of methyl tert-butyl ether (MTBE). Chemosphere 49, 413–420. doi:http://dx.doi.org/10.1016/S0045-6535(02)00330-2

Huling, S.G., Jones, P.K., Lee, T.R., 2007. Iron Optimization for Fenton-Driven Oxidation of MTBE-Spent Granular Activated Carbon. Environ. Sci. Technol. 41, 4090–4096. doi:10.1021/es062666k

Huling, S.G., Kan, E., Wingo, C., 2009. Fenton-driven regeneration of MTBE-spent granular activated carbon—Effects of particle size and iron amendment procedures. Appl. Catal. B Environ. 89, 651–658. doi:http://dx.doi.org/10.1016/j.apcatb.2009.02.002

Huling, S.G., Ko, S., Park, S., Kan, E., 2011. Persulfate oxidation of MTBE- and chloroform-spent granular activated carbon. J. Hazard. Mater. 192, 1484–1490. doi:10.1016/j.jhazmat.2011.06.070

Hutson, A., Ko, S., Huling, S.G., 2012. Persulfate oxidation regeneration of granular activated carbon: reversible impacts on sorption behavior. Chemosphere 89, 1218–1223. doi:10.1016/j.chemosphere.2012.07.040

Jaerger, S., dos Santos, A., Fernandes, A.N., Almeida, C.A.P., 2015. Removal of p-Nitrophenol from Aqueous Solution Using Brazilian Peat: Kinetic and Thermodynamic Studies. Water, Air & Soil Pollut. 226, 236. doi:10.1007/s11270-015-2500-9

Jain, A., Balasubramanian, R., Srinivasan, M.P., 2016. Hydrothermal conversion of biomass waste to activated carbon with high porosity: A review. Chem. Eng. J. 283, 789–805. doi:http://dx.doi.org/10.1016/j.cej.2015.08.014

Jaouadi, M., Hbaieb, S., Guedidi, H., Reinert, L., Amdouni, N., Duclaux, L., 2016. Preparation and characterization of carbons from β-cyclodextrin dehydration and from olive pomace activation and their application for boron adsorption. J. Saudi Chem. Soc. doi:http://dx.doi.org/10.1016/j.jscs.2016.01.001

Jing, T., Wang, J., Liu, M., Zhou, Y., Zhou, Y., Mei, S., 2014. Highly effective removal of 2,4-dinitrophenolic from surface water and wastewater samples using hydrophilic molecularly imprinted polymers. Environ. Sci. Pollut. Res. Int. 21, 1153–1162. doi:10.1007/s11356-013-2007-0

Juan, Y., Ke-Qiang, Q., 2009. Preparation of activated carbon by chemical activation under vacuum. Environ. Sci. Technol. 43, 3385–3390.

Jung, S.-H., Kim, J.-S., 2014. Production of biochars by intermediate pyrolysis and activated carbons from oak by three activation methods using CO_2. J. Anal. Appl. Pyrolysis 107, 116–122. doi:http://dx.doi.org/10.1016/j.jaap.2014.02.011

Karthikeyan, S., Sivakumar, P., 2012. The Effect of Activating Agents on the Activated Carbon Prepared from *Feronia limonia* (L .) Swingle (Wood Apple) Shell. J. Environ. Nanotechnol. 1, 5–12. doi:10.13074/jent.2012.10.121009

Kilpimaa, S., Runtti, H., Kangas, T., Lassi, U., Kuokkanen, T., 2015. Physical activation of carbon residue from biomass gasification: Novel sorbent for the

removal of phosphates and nitrates from aqueous solution. J. Ind. Eng. Chem. 21, 1354–1364. doi:http://dx.doi.org/10.1016/j.jiec.2014.06.006

Kong, J., Yue, Q., Huang, L., Gao, Y., Sun, Y., Gao, B., Li, Q., Wang, Y., 2013. Preparation, characterization and evaluation of adsorptive properties of leather waste based activated carbon via physical and chemical activation. Chem. Eng. J. 221, 62–71. doi:http://dx.doi.org/10.1016/j.cej.2013.02.021

Krishnan, K.A., Suresh, S.S., Arya, S., Sreejalekshmi, K.G., 2015. Adsorptive removal of 2,4-dinitrophenol using active carbon: kinetic and equilibrium modeling at solid–liquid interface. Desalin. Water Treat. 54, 1850–1861. doi:10.1080/19443994.2014.890548

Kumar, A., Jena, H.M., 2016. Removal of methylene blue and phenol onto prepared activated carbon from Fox nutshell by chemical activation in batch and fixed-bed column. J. Clean. Prod. 137, 1246–1259. doi:http://dx.doi.org/10.1016/j.jclepro.2016.07.177

Kurniawan, T.A., Waihung, L., Repo, E., Sillanpää, M.E.T., 2010. Removal of 4-chlorophenol from contaminated water using coconut shell waste pretreated with chemical agents. J. Chem. Technol. Biotechnol. 85, 1616–1627. doi:10.1002/jctb.2473

Kushwaha, S., Sreelatha, G., Padmaja, P., 2011. Evaluation of Acid-Treated Palm Shell Powder for Its Effectiveness in the Adsorption of Organophosphorus Pesticides: Isotherm, Kinetics, and Thermodynamics. J. Chem. Eng. Data 56, 2407–2415. doi:10.1021/je1013334

Lagergren, S., 1898. About the Theory of so Called Adsorption of Soluble Substances, Kungliga Svenska Vetenskapsakademiens Handlingar. K. Sven. Vetenskapsakademiens Handl. 24, 1–39.

Langmuir, I., 1916. The Constitution and Fundamental Properties of Solids and Liquids. Part I. Solids. J. Am. Chem. Soc. 38, 2221–2295. doi:10.1021/ja02268a002

Li, J.-M., Meng, X.-G., Hu, C.-W., Du, J., 2009. Adsorption of phenol, p-chlorophenol and p-nitrophenol onto functional chitosan. Bioresour. Technol. 100, 1168–1173. doi:http://dx.doi.org/10.1016/j.biortech.2008.09.015

Li, M., Wu, S.C., Peng, Y.-H., Shih, Y., 2016. Adsorption of volatile organic vapors by activated carbon derived from rice husk under various humidity conditions and its statistical evaluation by linear solvation energy relationships. Sep. Purif. Technol. 170, 102–108. doi:http://dx.doi.org/10.1016/j.seppur.2016.06.029

Li, Z., Gondal, M.A., Yamani, Z.H., 2014. Preparation of magnetic separable $CoFe_2O_4$/PAC composite and the adsorption of bisphenol A from aqueous solution. J. Saudi Chem. Soc. 18, 208–213. doi:http://dx.doi.org/10.1016/j.jscs.2011.06.012

Liang, C., Lin, Y.-T., Shin, W.-H., 2009. Persulfate regeneration of trichloroethylene spent activated carbon. J. Hazard. Mater. 168, 187–192. doi:http://dx.doi.org/10.1016/j.jhazmat.2009.02.006

Lillo-Ródenas, M.A., Cazorla-Amorós, D., Linares-Solano, A., 2003. Understanding chemical reactions between carbons and NaOH and KOH: An insight into the chemical activation mechanism. Carbon N. Y. 41, 267–275. doi:http://dx.doi.org/10.1016/S0008-6223(02)00279-8

Liou, T.-H., 2010. Development of mesoporous structure and high adsorption capacity of biomass-based activated carbon by phosphoric acid and zinc chloride activation. Chem. Eng. J. 158, 129–142. doi:http://dx.doi.org/10.1016/j.cej.2009.12.016

Liu, G., Ma, J., Li, X., Qin, Q., 2009. Adsorption of bisphenol A from aqueous solution onto activated carbons with different modification treatments. J. Hazard. Mater. 164, 1275–1280. doi:http://dx.doi.org/10.1016/j.jhazmat.2008.09.038

Liu, H., Dai, P., Zhang, J., Zhang, C., Bao, N., Cheng, C., Ren, L., 2013a. Preparation and evaluation of activated carbons from lotus stalk with trimethyl phosphate and tributyl phosphate activation for lead removal. Chem. Eng. J. 228, 425–434. doi:http://dx.doi.org/10.1016/j.cej.2013.04.117

Liu, H., Gao, Q., Dai, P., Zhang, J., Zhang, C., Bao, N., 2013b. Preparation and characterization of activated carbon from lotus stalk with guanidine phosphate activation: Sorption of Cd(II). J. Anal. Appl. Pyrolysis 102, 7–15. doi:http://dx.doi.org/10.1016/j.jaap.2013.04.010

López, G.P., Castner, D.G., Ratner, B.D., 1991. XPSO 1s binding energies for polymers containing hydroxyl, ether, ketone and ester groups. Surf. Interface Anal. 17, 267–272. doi:10.1002/sia.740170508

Lowell, S., Shields, J.E., Thomas, M.A., Thommes, M., 2004. No Characterization of Porous Solids and Powders: Surface Area, Pore Size and Density Title.

Lozano-Castelló, D., Lillo-Ródenas, M.A., Cazorla-Amorós, D., Linares-Solano, A., 2001. Preparation of activated carbons from Spanish anthracite: I. Activation by {KOH}. Carbon N. Y. 39, 741–749. doi:http://dx.doi.org/10.1016/S0008-6223(00)00185-8

Lua, A.C., Guo, J., 2001. Microporous Oil-Palm-Shell Activated Carbon Prepared by Physical Activation for Gas-Phase Adsorption. Langmuir 17, 7112–7117. doi:10.1021/la010290c

Manoj, B., Kunjomana, A.G., 2012. Study of stacking structure of amorphous carbon by X-ray diffraction technique. Int. J. Electrochem. Sci. 7, 3127–3134.

Marsh, H., Rodriguez-Reinoso, F., 2006. Activated Carbon, in: Elsevier Science & Technology Books. pp. 401–462.

Marzbali, M.H., Esmaieli, M., Abolghasemi, H., Marzbali, M.H., 2016. Tetracycline adsorption by H_3PO_4-activated carbon produced from apricot nut shells: A batch study. Process Saf. Environ. Prot. 102, 700–709. doi:http://dx.doi.org/10.1016/j.psep.2016.05.025

Matos, J., Nahas, C., Rojas, L., Rosales, M., 2011. Synthesis and characterization of activated carbon from sawdust of Algarroba wood. 1. Physical activation and pyrolysis. J. Hazard. Mater. 196, 360–369. doi:http://dx.doi.org/10.1016/j.jhazmat.2011.09.046

Mattson, J.S., Mark, H.B., 1971. Activated Carbon: Surface Chemistry and Adsorption from Solution, M. Dekker.

Mazlan, M.A.F., Uemura, Y., Yusup, S., Elhassan, F., Uddin, A., Hiwada, A., Demiya, M., 2016. Activated Carbon from Rubber Wood Sawdust by Carbon Dioxide Activation. Procedia Eng. 148, 530–537. doi:http://dx.doi.org/10.1016/j.proeng.2016.06.549

Mehdinia, A., Baradaran Kayyal, T., Jabbari, A., Aziz-Zanjani, M.O., Ziaei, E., 2013. Magnetic molecularly imprinted nanoparticles based on grafting polymerization for selective detection of 4-nitrophenol in aqueous samples. J. Chromatogr. A 1283, 82–88. doi:10.1016/j.chroma.2013.01.093

Menéndez-Díaz, J.A., Martín-Gullón, I., 2006. Chapter 1 Types of carbon adsorbents and their production, Interface Science and Technology. doi:10.1016/S1573-4285(06)80010-4

Mérel, P., Tabbal, M., Chaker, M., Moisa, S., Margot, J., 1998. Direct evaluation of the sp3 content in diamond-like-carbon films by XPS. Appl. Surf. Sci. 136, 105–110. doi:http://dx.doi.org/10.1016/S0169-4332(98)00319-5

Mewada, A., Pandey, S., Shinde, S., Mishra, N., Oza, G., Thakur, M., Sharon, M., Sharon, M., 2013. Green synthesis of biocompatible carbon dots using aqueous extract of *Trapa bispinosa* peel. Mater. Sci. Eng. C 33, 2914–2917. doi:http://dx.doi.org/10.1016/j.msec.2013.03.018

Mohan, D., Sarswat, A., Singh, V.K., Alexandre-Franco, M., Jr., C.U.P., 2011. Development of magnetic activated carbon from almond shells for trinitrophenol removal from water. Chem. Eng. J. 172, 1111–1125. doi:http://dx.doi.org/10.1016/j.cej.2011.06.054

Monsalvo, V.M., Mohedano, A.F., Rodriguez, J.J., 2011. Activated carbons from sewage sludge: Application to aqueous-phase adsorption of 4-chlorophenol. Desalination 277, 377–382. doi:http://dx.doi.org/10.1016/j.desal.2011.04.059

Moradi, O., Yari, M., Moaveni, P., Norouzi, M., 2012. Removal of p-nitrophenol and

Naphthalene from Petrochemical Wastewater Using SWCNTs and SWCNT-COOH Surfaces. Fullerenes, Nanotub. Carbon Nanostructures 20, 85–98. doi:10.1080/1536383X.2010.533309

Moreno-Castilla, C., Ferro-Garcia, M.A., Joly, J.P., Bautista-Toledo, I., Carrasco-Marin, F., Rivera-Utrilla, J., 1995. Activated Carbon Surface Modifications by Nitric Acid, Hydrogen Peroxide, and Ammonium Peroxydisulfate Treatments. Langmuir 11, 4386–4392. doi:10.1021/la00011a035

Mourão, P.A.M., Carrott, P.J.M., Carrott, M.M.L.R., 2006. Application of different equations to adsorption isotherms of phenolic compounds on activated carbons prepared from cork. Carbon N. Y. 44, 2422–2429. doi:http://dx.doi.org/10.1016/j.carbon.2006.05.015

Muniandy, L., Adam, F., Mohamed, A.R., Ng, E.-P., 2014. The synthesis and characterization of high purity mixed microporous/mesoporous activated carbon from rice husk using chemical activation with NaOH and KOH. Microporous Mesoporous Mater. 197, 316–323. doi:http://dx.doi.org/10.1016/j.micromeso.2014.06.020

Nakanishi, A., Tamai, M., Kawasaki, N., Nakamura, T., Tanada, S., 2002. Adsorption Characteristics of Bisphenol A onto Carbonaceous Materials Produced from Wood Chips as Organic Waste. J. Colloid Interface Sci. 252, 393–396. doi:http://dx.doi.org/10.1006/jcis.2002.8387

Nakatsuji, Y., Salehi, Z., Kawase, Y., 2015. Mechanisms for removal of p-nitrophenol from aqueous solution using zero-valent iron. J. Environ. Manage. 152, 183–191. doi:http://dx.doi.org/10.1016/j.jenvman.2015.01.012

Nowicki, P., Kazmierczak, J., Pietrzak, R., 2015. Comparison of physicochemical and sorption properties of activated carbons prepared by physical and chemical activation of cherry stones. Powder Technol. 269, 312–319. doi:http://dx.doi.org/10.1016/j.powtec.2014.09.023

Oleszczuk, P., Ćwikła-Bundyra, W., Bogusz, A., Skwarek, E., Ok, Y.S., 2016. Characterization of nanoparticles of biochars from different biomass. J. Anal.

Appl. Pyrolysis 121, 165–172. doi:http://dx.doi.org/10.1016/j.jaap.2016.07.017

Olivares-Marín, M., Fernández-González, C., Macías-García, A., Gómez-Serrano, V., 2012. Preparation of activated carbon from cherry stones by physical activation in air. Influence of the chemical carbonisation with H_2SO_4. J. Anal. Appl. Pyrolysis 94, 131–137. doi:http://dx.doi.org/10.1016/j.jaap.2011.11.019

Olivares-Marín, M., Fernández-González, C., Macías-García, A., Gómez-Serrano, V., 2007. Porous Structure of Activated Carbon Prepared from Cherry Stones by Chemical Activation with Phosphoric Acid. Energy & Fuels 21, 2942–2949. doi:10.1021/ef060652u

Örkün, Y., Karatepe, N., Yavuz, R., 2012. Influence of temperature and impregnation ratio of H_3PO_4 on the production of activated carbon from hazelnut shell. Acta Phys. Pol. A 121, 277–280.

Otake, Y., Jenkins, R.G., 1993. Characterization of oxygen-containing surface complexes created on a microporous carbon by air and nitric acid treatment. Carbon N. Y. 31, 109–121. doi:http://dx.doi.org/10.1016/0008-6223(93)90163-5

Özacar, M., Şengil, İ.A., 2005. A kinetic study of metal complex dye sorption onto pine sawdust. Process Biochem. 40, 565–572. doi:http://dx.doi.org/10.1016/j.procbio.2004.01.032

Ozdemir, I., Şahin, M., Orhan, R., Erdem, M., 2014. Preparation and characterization of activated carbon from grape stalk by zinc chloride activation. Fuel Process. Technol. 125, 200–206. doi:http://dx.doi.org/10.1016/j.fuproc.2014.04.002

Passe-Coutrin, N., Altenor, S., Cossement, D., Jean-Marius, C., Gaspard, S., 2008. Comparison of parameters calculated from the BET and Freundlich isotherms obtained by nitrogen adsorption on activated carbons: A new method for calculating the specific surface area. Microporous Mesoporous Mater. 111, 517–522. doi:http://dx.doi.org/10.1016/j.micromeso.2007.08.032

Peng, L., Wang, L., Hu, X., Wu, P., Wang, X., Huang, C., Wang, X., Deng, D., 2016. Ultrasound assisted, thermally activated persulfate oxidation of coal tar

DNAPLs. J. Hazard. Mater. 318, 497–506. doi:10.1016/j.jhazmat.2016.07.014

Peng, P., Lang, Y.-H., Wang, X.-M., 2016. Adsorption behavior and mechanism of pentachlorophenol on reed biochars: pH effect, pyrolysis temperature, hydrochloric acid treatment and isotherms. Ecol. Eng. 90, 225–233. doi:http://dx.doi.org/10.1016/j.ecoleng.2016.01.039

Radhika, M., Palanivelu, K., 2006. Adsorptive removal of chlorophenols from aqueous solution by low cost adsorbent--Kinetics and isotherm analysis. J. Hazard. Mater. 138, 116–124. doi:10.1016/j.jhazmat.2006.05.045

Rambabu, N., Azargohar, R., Dalai, A.K., Adjaye, J., 2013. Evaluation and comparison of enrichment efficiency of physical/chemical activations and functionalized activated carbons derived from fluid petroleum coke for environmental applications. Fuel Process. Technol. 106, 501–510. doi:http://dx.doi.org/10.1016/j.fuproc.2012.09.019

Romero-Anaya, A.J., Lillo-Ródenas, M.A., de Lecea, C.S.-M., Linares-Solano, A., 2012. Hydrothermal and conventional H_3PO_4 activation of two natural bio-fibers. Carbon N. Y. 50, 3158–3169. doi:http://dx.doi.org/10.1016/j.carbon.2011.10.031

Rudzinski, W., Panczyk, T., 2002. The Langmuirian Adsorption Kinetics Revised: A Farewell to the XXth Century Theories? Adsorption 8, 23–34. doi:10.1023/A:1015214406179

Şahin, Ö., Saka, C., 2013. Preparation and characterization of activated carbon from acorn shell by physical activation with H_2O–CO_2 in two-step pretreatment. Bioresour. Technol. 136, 163–168. doi:http://dx.doi.org/10.1016/j.biortech.2013.02.074

Sahithya, K., Das, D., Das, N., 2016. Adsorptive removal of monocrotophos from aqueous solution using biopolymer modified montmorillonite–CuO composites: Equilibrium, kinetic and thermodynamic studies. Process Saf. Environ. Prot. 99, 43–54. doi:http://dx.doi.org/10.1016/j.psep.2015.10.009

Saka, C., 2012. BET, TG–DTG, FT-IR, SEM, iodine number analysis and

preparation of activated carbon from acorn shell by chemical activation with $ZnCl_2$. J. Anal. Appl. Pyrolysis 95, 21–24. doi:http://dx.doi.org/10.1016/j.jaap.2011.12.020

Sekirifa, M.L., Hadj-Mahammed, M., Pallier, S., Baameur, L., Richard, D., Al-Dujaili, A.H., 2013. Preparation and characterization of an activated carbon from a date stones variety by physical activation with carbon dioxide. J. Anal. Appl. Pyrolysis 99, 155–160. doi:http://dx.doi.org/10.1016/j.jaap.2012.10.007

Selvaraju, G., Bakar, N.K.A., 2017. Production of a new industrially viable green-activated carbon from Artocarpus integer fruit processing waste and evaluation of its chemical, morphological and adsorption properties. J. Clean. Prod. 141, 989–999. doi:http://dx.doi.org/10.1016/j.jclepro.2016.09.056

Senthilkumaar, S., Krishna, S., Kalaamani, P., Subburamaan, C. V., Subramaniam, N.G., 2010. Adsorption of organophosphorous pesticide from aqueous solution using “waste” jute fiber carbon. Mod. Appl. Sci. 4, 67–83.

Sepehrian, H., Fasihi, J., Khayatzadeh Mahani, M., 2009. Adsorption Behavior Studies of Picric Acid on Mesoporous MCM-41. Ind. Eng. Chem. Res. 48, 6772–6775. doi:10.1021/ie801716k

Shahkarami, S., Dalai, A.K., Soltan, J., 2016. Enhanced CO_2 Adsorption Using MgO-Impregnated Activated Carbon: Impact of Preparation Techniques. Ind. Eng. Chem. Res. 55, 5955–5964. doi:10.1021/acs.iecr.5b04824

Shamsuddin, M.S., Yusoff, N.R.N., Sulaiman, M.A., 2016. Synthesis and Characterization of Activated Carbon Produced from Kenaf Core Fiber Using H_3PO_4 Activation. Procedia Chem. 19, 558–565. doi:http://dx.doi.org/10.1016/j.proche.2016.03.053

Shin, S., Jang, J., Yoon, S.-H., Mochida, I., 1997. A study on the effect of heat treatment on functional groups of pitch based activated carbon fiber using FTIR. Carbon N. Y. 35, 1739–1743. doi:http://dx.doi.org/10.1016/S0008-6223(97)00132-2

Shoaib, M., Al-Swaidan, H.M., 2015. Optimization and characterization of sliced activated carbon prepared from date palm tree fronds by physical activation. Biomass and Bioenergy 73, 124–134. doi:http://dx.doi.org/10.1016/j.biombioe.2014.12.016

Silva, A.R., Freire, C., de Castro, B., Freitas, M.M.A., Figueiredo, J.L., 2001. Anchoring of a nickel(II) Schiff base complex onto activated carbon mediated by cyanuric chloride. Microporous Mesoporous Mater. 46, 211–221. doi:http://dx.doi.org/10.1016/S1387-1811(01)00297-9

Singh, C.K., Sahu, J.N., Mahalik, K.K., Mohanty, C.R., Mohan, B.R., Meikap, B.C., 2008. Studies on the removal of Pb(II) from wastewater by activated carbon developed from Tamarind wood activated with sulphuric acid. J. Hazard. Mater. 153, 221–228. doi:http://dx.doi.org/10.1016/j.jhazmat.2007.08.043

Song, T., Liao, J., Xiao, J., Shen, L., 2015. Effect of micropore and mesopore structure on CO_2 adsorption by activated carbons from biomass. New Carbon Mater. 30, 156–166. doi:http://dx.doi.org/10.1016/S1872-5805(15)60181-0

Srivastava, S.K., Gupta, V.K., Johri, N., Mohan, D., 1995. bagasse fly ash- A sugar industry waste material. Indian J. Chem. Tech. 2, 333–336.

Stuart, B., 2004. Infrared spectroscopy: fundamentals and applications, John Wiley & Sons: West Sussex. doi:10.1002/0470011149

Sui, Q., Huang, J., Liu, Y., Chang, X., Ji, G., Deng, S., Xie, T., Yu, G., 2011. Rapid removal of bisphenol A on highly ordered mesoporous carbon. J. Environ. Sci. (China) 23, 177–182.

Sun, K., Jiang, chun J., 2010. Preparation and characterization of activated carbon from rubber-seed shell by physical activation with steam. Biomass and Bioenergy 34, 539–544. doi:http://dx.doi.org/10.1016/j.biombioe.2009.12.020

Sun, Y., Li, H., Li, G., Gao, B., Yue, Q., Li, X., 2016. Characterization and ciprofloxacin adsorption properties of activated carbons prepared from biomass wastes by H_3PO_4 activation. Bioresour. Technol. 217, 239–244.

doi:http://dx.doi.org/10.1016/j.biortech.2016.03.047

Sun, Y., Yue, Q., Gao, B., Wang, Y., Gao, Y., Li, Q., 2013. Preparation of highly developed mesoporous activated carbon by $H_4P_2O_7$ activation and its adsorption behavior for oxytetracycline. Powder Technol. 249, 54–62. doi:http://dx.doi.org/10.1016/j.powtec.2013.07.029

Tam, M.S., Antal, M.J., 1999. Preparation of Activated Carbons from Macadamia Nut Shell and Coconut Shell by Air Activation. Ind. Eng. Chem. Res. 38, 4268–4276. doi:10.1021/ie990346m

Tang, L., Li, L., Chen, R., Wang, C., Ma, W., Ma, X., 2016. Adsorption of acetone and isopropanol on organic acid modified activated carbons. J. Environ. Chem. Eng. 4, 2045–2051. doi:http://dx.doi.org/10.1016/j.jece.2016.03.031

Tang, Y., Liu, Q., Chen, F., 2012. Preparation and characterization of activated carbon from waste ramulus mori. Chem. Eng. J. 203, 19–24. doi:http://dx.doi.org/10.1016/j.cej.2012.07.007

Temkiin, M., Pyzhev, V., 1939. Kinetics of the Synthesis of Ammonia on Promoted Iron Catalysts. Jour. Phys. Chem. (U.S.S.R.) 13, 851–867.

Teng, H., Hsieh, C., 1999. Activation Energy for Oxygen Chemisorption on Carbon at Low Temperatures 292–297.

Thommes, M., 2010. Physical Adsorption Characterization of Nanoporous Materials. Chemie Ing. Tech. 82, 1059–1073. doi:10.1002/cite.201000064

Tian, Z., Qiu, Y., Zhou, J., Zhao, X., Cai, J., 2016. The direct carbonization of algae biomass to hierarchical porous carbons and CO_2 adsorption properties. Mater. Lett. 180, 162–165. doi:http://dx.doi.org/10.1016/j.matlet.2016.05.169

Tsai, W.-T., Lai, C.-W., Su, T.-Y., 2006. Adsorption of bisphenol-A from aqueous solution onto minerals and carbon adsorbents. J. Hazard. Mater. 134, 169–175. doi:http://dx.doi.org/10.1016/j.jhazmat.2005.10.055

Tsitonaki, A., Petri, B., Crimi, M., Mosbæk, H., Siegrist, R.L., Bjerg, P.L., 2010. In

Situ Chemical Oxidation of Contaminated Soil and Groundwater Using Persulfate: A Review. Crit. Rev. Environ. Sci. Technol. 40, 55–91. doi:10.1080/10643380802039303

Tsubouchi, N., Nishio, M., Mochizuki, Y., 2016. Role of nitrogen in pore development in activated carbon prepared by potassium carbonate activation of lignin. Appl. Surf. Sci. 371, 301–306. doi:http://dx.doi.org/10.1016/j.apsusc.2016.02.200

Tzvetkov, G., Mihaylova, S., Stoitchkova, K., Tzvetkov, P., Spassov, T., 2016. Mechanochemical and chemical activation of lignocellulosic material to prepare powdered activated carbons for adsorption applications. Powder Technol. 299, 41–50. doi:http://dx.doi.org/10.1016/j.powtec.2016.05.033

Uslu, A., Faaij, A.P.C., Bergman, P.C.A., 2008. Pre-treatment technologies, and their effect on international bioenergy supply chain logistics. Techno-economic evaluation of torrefaction, fast pyrolysis and pelletisation. Energy 33, 1206–1223. doi:http://dx.doi.org/10.1016/j.energy.2008.03.007

Valix, M., Cheung, W.H., McKay, G., 2004. Preparation of activated carbon using low temperature carbonisation and physical activation of high ash raw bagasse for acid dye adsorption. Chemosphere 56, 493–501. doi:http://dx.doi.org/10.1016/j.chemosphere.2004.04.004

Valizadeh, S., Younesi, H., Bahramifar, N., 2016. Highly mesoporous K_2CO_3 and KOH/activated carbon for SDBS removal from water samples: Batch and fixed-bed column adsorption process. Environ. Nanotechnology, Monit. Manag. 6, 1–13. doi:http://dx.doi.org/10.1016/j.enmm.2016.06.005

Varank, G., Demir, A., Yetilmezsoy, K., Top, S., Sekman, E., Bilgili, M.S., 2012. Removal of 4-nitrophenol from aqueous solution by natural low-cost adsorbents. Indian J. Chem. Technol. 19, 7–25.

Vasu, A.E., 2008. Surface Modification of Activated Carbon for Enhancement of Nickel(II) Adsorption 5, 973–4945. doi:10.1155/2008/610503

W. J. Weber, Morris, J.C., 1963. Kinetics of Adsorption on Carbon from Solution. J. Sanit. Eng. Div. 83, 31–59.

Waldemer, R.H., Tratnyek, P.G., Johnson, R.L., Nurmi, J.T., 2007. Oxidation of Chlorinated Ethenes by Heat-Activated Persulfate: Kinetics and Products. Environ. Sci. Technol. 41, 1010–1015. doi:10.1021/es062237m

Wang, J., Wu, F., Wang, M., Qiu, N., Liang, Y., Fang, S., 2010. Preparation of activated carbon from a renewable agricultural residue of pruning mulberry shoot. Afr J Biotechnol 9, 2762–2767. doi:10.5897/AJB09.1421

Wang, Z., Ye, C., Wang, H., 2016. Preparation of amino functionalized imidazolium-modified silicas by different coupling agents for removal of 2,4-dinitrophenol from aqueous solutions. Int. J. Environ. Sci. Technol. 13, 113–124. doi:10.1007/s13762-015-0827-9

Wirasnita, R., Hadibarata, T., Yusoff, A.R.M., Yusop, Z., 2014. Removal of Bisphenol A from Aqueous Solution by Activated Carbon Derived from Oil Palm Empty Fruit Bunch. Water, Air Soil Pollut. 225, 2148. doi:10.1007/s11270-014-2148-x

Wollbrink, A., Volgmann, K., Koch, J., Kanthasamy, K., Tegenkamp, C., Li, Y., Richter, H., Kämnitz, S., Steinbach, F., Feldhoff, A., Caro, J., 2016. Amorphous, turbostratic and crystalline carbon membranes with hydrogen selectivity. Carbon N. Y. 106, 93–105. doi:http://dx.doi.org/10.1016/j.carbon.2016.04.062

Wu, J., Yu, H.-Q., 2006. Biosorption of 2,4-dichlorophenol from aqueous solution by Phanerochaete chrysosporium biomass: Isotherms, kinetics and thermodynamics. J. Hazard. Mater. 137, 498–508. doi:http://dx.doi.org/10.1016/j.jhazmat.2006.02.026

Xiao-Hong, L., Xian-Zhou, Z., 2011. Vibrational spectroscopy investigation using ab initio and density functional theory analysis on the structure of 2,4,6-trinitrophenol. Comput. Theor. Chem. 963, 34–39. doi:http://dx.doi.org/10.1016/j.comptc.2010.09.005

Xu, J., Chen, L., Qu, H., Jiao, Y., Xie, J., Xing, G., 2014. Preparation and characterization of activated carbon from reedy grass leaves by chemical activation with H_3PO_4. Appl. Surf. Sci. 320, 674–680. doi:http://dx.doi.org/10.1016/j.apsusc.2014.08.178

Xu, J., Wang, L., Zhu, Y., 2012. Decontamination of bisphenol A from aqueous solution by graphene adsorption. Langmuir 28, 8418–8425. doi:10.1021/la301476p

Yadav RA, D. V, 2015. Experimental IR and Raman Spectroscopy and DFT Methods Based Material Characterization and Data Analysis of 2- Nitrophenol. Biochem. Pharmacol. Open Access 4. doi:10.4172/2167-0501.1000183

Yan, S., Fang, Y., Yao, W., Gao, Z., 2007. Characterization and quality assessment of binding properties of the monocrotophos molecularly imprinted microspheres prepared by precipitation polymerization in toluene. Polym. Eng. Sci. 47, 1302–1308. doi:10.1002/pen.20806

Yang, J., Qiu, K., 2011. Experimental Design To Optimize the Preparation of Activated Carbons from Herb Residues by Vacuum and Traditional $ZnCl_2$ Chemical Activation. Ind. Eng. Chem. Res. 50, 4057–4064. doi:10.1021/ie101531p

Yorgun, S., Yıldız, D., 2015. Preparation and characterization of activated carbons from Paulownia wood by chemical activation with H_3PO_4. J. Taiwan Inst. Chem. Eng. 53, 122–131. doi:http://dx.doi.org/10.1016/j.jtice.2015.02.032

Zhou, Y., Chen, L., Lu, P., Tang, X., Lu, J., 2011. Removal of bisphenol A from aqueous solution using modified fibric peat as a novel biosorbent. Sep. Purif. Technol. 81, 184–190. doi:http://dx.doi.org/10.1016/j.seppur.2011.07.026

Zhu, X., Cai, J., Yang, J., Su, Q., Gao, Y., 2006. Films coated with molecular imprinted polymers for the selective stir bar sorption extraction of monocrotophos. J. Chromatogr. A 1131, 37–44. doi:10.1016/j.chroma.2006.07.041

Zhu, Y., Gao, J., Li, Y., Sun, F., Gao, J., Wu, S., Qin, Y., 2012. Preparation of activated carbons for SO_2 adsorption by CO_2 and steam activation. J. Taiwan Inst. Chem. Eng. 43, 112–119. doi:http://dx.doi.org/10.1016/j.jtice.2011.06.009

Zhu, Z., Li, A., Yan, L., Liu, F., Zhang, Q., 2007. Preparation and characterization of highly mesoporous spherical activated carbons from divinylbenzene-derived polymer by $ZnCl_2$ activation. J. Colloid Interface Sci. 316, 628–634. doi:http://dx.doi.org/10.1016/j.jcis.2007.09.016

Zvezdelina, Y., Bogdana, K., Georgieva, N., 2012. Macedonian Journal of Chemistry and Chemical Engineering,. Maced. J. Chem. Chem. Eng. 31, 101–114.